MICROCLIMATIC CONDITIONS AT THE EXTERNAL SURFACE OF BUILDING ENVELOPES

MIKKEL KRISTIAN KRAGH

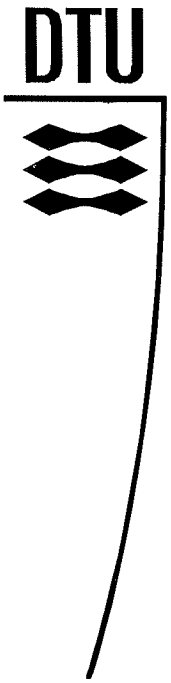

REPORT
R-027
1998

ISSN 1396-4011
ISBN 87-7877-028-9

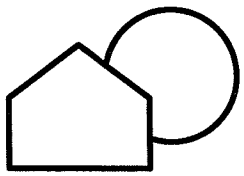

DEPARTMENT OF BUILDINGS AND ENERGY
TECHNICAL UNIVERSITY OF DENMARK

MICROCLIMATIC CONDITIONS AT THE EXTERNAL SURFACE OF BUILDING ENVELOPES

Mikkel Kristian Kragh. 1998. Report R-027.
Department of Buildings and Energy. Technical University of Denmark

N.	*Chapter*	*Page*	*Line*		*Correction*
1	Summary	iv	21	'precipitation'	should read 'evaporation'
2	2. Microclimate	24		T_{sky} formula: t_{dp} given in [K]	t_{dp} should be given in [°C]
3		25		'Lund'-formulae	Reference: Höglund, Ingemar. 1973. Metod för beräkning af extreme yttemperaturer hos isolerade ytterkonstruktioner. Statens Institut for Byggnads-forskning, Rapport R6: 1973. Stockholm. Sweden.
4		30-32		precipitation/driving rain intensities given in '[mm]'	should be given in [mm/h]
5	5. Full-scale ...	45	11	'Offset ...'	should be disregarded
6	7. Long-wave...			'Lund'-formulae	as above (3)
7				'Berdahl'-formula	should be disregarded - the application is dubious and the plot is erroneous.
8	8. Window ...	100	10	ΔT	should read ΔT_a
9		121	16-17	h_c	should read h_{c+rad}
10			18	'convective film coeff.'	should read 'radiation and convection film coefficient'
11	9. Meteorological ...	134		Table 9.2	Reference: Helbo Andersen, A. 1997. Slagregnspåvirkning af klimaskærmskonstruktioner. Department of Buildings and Energy. Technical University of Denmark.
12	Nomenclature	141		r_h and r_v given in [mm]	should be given in [mm/h]

MICROCLIMATIC CONDITIONS AT THE EXTERNAL SURFACE OF BUILDING ENVELOPES

PH.D. DISSERTATION BY

MIKKEL KRISTIAN KRAGH

PREFACE

The present dissertation concludes the Ph.D.-work entitled *Microclimatic Conditions at the External Surface of Building Envelopes*, carried out between August 1995 and August 1998. The project deals with the conversion from meteorological data to local conditions in a given position on a building envelope. The project is the first of its kind at the Department of Buildings and Energy, and represents as such a pilot study, hopefully continued by subsequent activities.

The topic is both comprehensive and complex. The approach itself thus becomes an essential issue. Methodological problems are discussed, as the identification of the methodological problems is an absolute prerequisite to a scientific approach.

The literature survey and the creation of a network in terms of contacts in external research environments have been time consuming. After the introductory phase, measurement activities were planned and financial support was applied for. As the literature study, the evaluation of potential areas of interest and the design and planning of measurements were the main aim, the measurement results obtained in the course of the project should be conceived as preliminary, and the activities should be continued after conclusion of the present project. As the subject is the climate around buildings, seasonal variations should be included in future studies.

Acknowledgements

Two private funds have granted the project with financial support for the realization of the measurement set-up, namely *Fabrikant P.A. Fiskers Fond*, and *Martha og Paul Kerrn-Jespersens Fond*. Without this support, the experimental part of the work would not have been possible.

I wish to thank the members of the Microclimate Group, *Fabien J.R. van Mook*, Eindhoven University of Technology, and *Anneli Högberg*, Chalmers University of Technology, for the fruitful exchange of ideas and results during the past two years.

I also wish to thank my supervisor, *Professor Svend Svendsen, Ph.D.*, who managed to find the time for a discussion, whenever it was needed.

Thanks to my dear friend *Niels Casper Andersen*, a truly pleasant and educated interlocutor.

Finally, I wish to express my heartfelt gratitude to my lovely wife *Claudia* for her admirable patience and support.

Lyngby, August 1998

Mikkel Kristian Kragh

Structure of the dissertation

The thesis is divided into five parts:

PART I / Chapters 1, 2 and 3 / B A C K G R O U N D. The project is described, the motivation for the research and the microclimate is defined in relation to both building physics research and applications. The method is discussed in a philosophical perspective, as identifying methodological problems, and defining the method itself, are considered quintessential issues.

PART II / Chapter 4 / A N A L Y S I S. A fundamental introduction to the component microclimatic factors. Air temperature, air humidity, solar radiation and air velocity are briefly described for completeness, whilst driving rain and long-wave radiation are described in more detail. Convective heat transfer and surface coefficients are treated, although they are not microclimatic factors, merely resulting from combinations of such factors. They are included as they are important in relation to transfer of heat and moisture at the surface of the building envelope, and as they are related to the case studies of the project.

PART III / Chapters 5, 6, 7, 8 and 9 / M E T H O D. Selected subject are investigated in the form of case studies. Driving rain measurement is the main area of interest, including development of measurement equipment. Long-wave irradiation is measured and compared with empirical formulae from the literature. Window convection heat transfer is another main area of interest. Nocturnal convective heat transfer from a double pane glazing is studied and measurement principles are discussed. Finally, a compilation of meteorological data for hygrothermal simulations, including estimation of driving rain, is described.

PART IV / Chapter 10 / F I N D I N G S. A brief summary of main conclusions in the dissertation.

PART V / Appendices I, II and III / A P P E N D I C E S. Auxiliary notes. System error estimation in relation to the window convection measurements, design notes on an apparatus for external convection measurement, formulae for conversion of relative humidity and dry-bulb temperature into dew point temperature.

Keywords *Building physics; Microclimate; Methodology; Driving rain; Driving rain collector; Window convection heat transfer; Long-wave radiation; Climatic input for hygrothermal calculations; Recommendations for future studies.*

DEPARTMENT OF BUILDINGS AND ENERGY • TECHNICAL UNIVERSITY OF DENMARK • DK - 2800 LYNGBY

SUMMARY

The present dissertation concludes the Ph.D.-project *Microclimatic Conditions at the External Surface of Building Envelopes*, carried out at the Department of Buildings and Energy between August 1995 and August 1998.

The focus on the energy consumption perspectives has resulted in the developing of thermally well-insulating building components. Moisture in constructions may cause failure and unsatisfactory performance. Innovation of building components has lead to hitherto unknown problems caused by moisture in the constructions. One major objective of the current research is to establish models of the coupled heat and moisture transfer in order to develop construction types with satisfactory performance and long service life/durability. Such models depend on descriptions of the ambient climate, used as input for hygrothermal simulations.

Hygrothermal simulations are usually based on use of the Design Reference Year, yielding one typical year of hourly weather data. However, whilst such data are recorded at a meteorological weather station, moisture critical situations may result from very local conditions, for instance in a particularly exposed position on a given building.

In a building physical perspective, the (exterior) microclimate is defined as the conditions affecting transfer of heat and moisture in the immediate vicinity of the external surface of the building envelope. The microclimate results from a combination of meteorological factors and local characteristics.

The microclimatic parameters are the following:

- Temperature
- Humidity
- Long-wave radiation
- Solar radiation corrected for shading objects
- Driving rain
- Air velocity

The complex subject, and the project itself, are discussed in a philosophical context, and methodological problems are identified. In particular, the problems pertaining to the processes of preparation and interpretation are discussed - the preparation process being the delimitation of a well-defined object of a given investigation. The combination of complex climatic phenomena and the need for information, in terms of applicable guidelines, dictates a pragmatic approach, which, as a matter of fact, is also the case for engineering science in general. Adoption of parameter definitions, and assumptions regarding the relative significance of parameters, may to some extent predetermine the outcome of the research. Such assumptions and parameter definitions should thus be introduced consciously and with possible consequences in mind.

It has been necessary to focus on selected topics owing to both time frame and financial limits. Analysis of the needs, in terms of input for hygrothermal calculations, has lead to the choice of three main areas of interest, namely:

- Driving rain
- Long-wave radiation
- Window convection heat transfer

A full-scale microclimate measurement set-up has been established for measurement of driving rain, precipitation, long-wave irradiation, air temperature, air humidity as well as wind speed and wind direction. Measurements of window convection heat transfer has been carried out as a nocturnal series of short duration.

Driving rain
One of the main tasks has been to investigate and develop methods of measuring driving rain on buildings. A traditional driving rain collector (DRC), consisting of a tray mounted onto a vertical building surface, and drained to a commercially available pluviometer, has been produced. In order to improve the performance of the collector, a new design has been developed. A collector plate equipped with a self-siphoning reservoir is suspended from a load cell, thus permitting detection of droplets staying on the collector. Moreover, a net with a mesh size of 1 mm is fixed inside the collector tray in order to minimize reflection of the impinging droplets by dispersion. The new design is referred to as the *load cell DRC*.

The data processing has not yet been fully developed; the load cell output is logged as 10-second instantaneous values, giving the cumulative driving rain load. The driving rain loads are subsequently estimated on the basis of 10-minute averages.

Evaporation from the collectors is detected by the load cell DRC, even in periods of high ambient air humidity in connection with precipitation events. It is expected, that precipitation may also progress during precipitation, leading to underestimation of the driving rain load.

The traditional DRC and the novel load cell DRC were mounted side-by-side for comparative studies. Preliminary results indicate that the load cell DRC detects substantially more driving rain than the traditional one. During the measurement series, the traditional DRC detected approximately 60 per cent of the driving rain detected by means of the load cell DRC. The discrepancy is ascribed to evaporation from the traditional collector. Three different DRC designs are currently being tested side-by-side on the facade of a high-rise building at Eindhoven University of Technology.

The spatial distribution over a three storey, west facing gable has been found to be in agreement with the qualitative guidelines of present standards. Along the upper edge of the three storey gable, the catch ratios were found to be up to twice the catch ratio found around the centre. The data material is yet too limited to yield a basis for quantitative comparison. As present standards are based on results obtained by means of traditional driving rain collectors, findings regarding evaporation from the collectors, and subsequent underestimation, may lead to future reconsideration of the guidelines.

An introductory study of Computational Fluid Dynamics (CFD) has been carried out in order to assess the methods of estimating driving rain, and identify potential pittfalls. Computational fluid dynamics methods represent an interesting alternative to costly wind tunnel testing of air flow around buildings. During recent years, methods of simulating driving rain have been developed, but the work is still at a relatively early stage. Depending on the specific CFD code, grid generation is cumbersome, and in some cases even impossible. Increasing computer capacity, and the developing of gradually more advanced codes, are facilitating the solving of

still more complex problems - the true difficulty remains the validation of the results. The models and the results are difficult to validate - both in terms of driving rain and air flow. The fact that programs are continuously developed, and user interfaces are improved, should not divert attention from the fact that the problem under consideration is a complicated fluid dynamics task. Assumptions regarding boundary conditions are quintessential, and design of computational grid will affect the results. Future applications may comprise calculation of driving rain catch ratios, depending on weather type, local features, building geometry and position on a given building. For validation of such routines there is a pronounced need for comprehensive driving rain measurements, and methods of comparing results obtained with different types of driving rain collectors.

Long-wave radiation
Short duration measurements of long-wave irradiation have been carried out from horizontal and vertical surfaces, in order to compare with selected empirical formulae from the literature. The atmospheric component of the irradiation clearly constitutes the most uncertain part of the estimation of incident long-wave radiation. This is reflected in large discrepancies between the measured and the theoretically determined values. The determination is more accurate for vertical than for horizontal surfaces, as the atmospheric component becomes less significant. The best fit to the measured data was achieved by means of Cole's formulae for long-wave radiation incident upon inclined building surfaces. The common assumption of the surroundings acting as a black-body radiator at ambient air temperature appears to yield an adequate approximation under the considered conditions - particularly considering the uncertainty of the atmospheric component. The long-wave data of the design reference year can be used, keeping the uncertainty in mind. The ground component can be calculated, assuming the surroundings to act as a black-body radiator at ambient air temperature. However, whenever possible, the incident long-wave radiation should be measured - preferably by means of a precision pyrgeometer.

Window convection heat transfer
The improved thermal performance of windows results in lower external surface temperatures on the window pane, and consequently in condensation risk. In terms of energy calculations, the convection heat loss is not considered significant. A more detailed description of the complex phenomena is, however, a prerequisite for the establishing of applicable models for assessment of condensation risk.

Consequently, night-time measurements were carried out on a north facing window pane. The convective film coefficient was found to depend closely on wind direction. The convective heat transfer coefficient determined in calm weather situations was found to have values between the results found for internal surfaces and external surfaces with no wind. This implies that the design guidelines overestimate the convective heat transfer, which appears reasonable for energy calculations, but is not adequate for assessment of condensation risk and condensation duration. Such calculations should be based on more detailed measures, or possibly underestimation.

Observation of in situ low-ε window panes mounted in different positions would yield valuable information in terms of characterizing situations with formation of condensation. Such a set-up should comprise measurement of reference surface temperatures employing a number of thermocouples, temperature differences by means of a number of thermopiles (possibly a Mayer ladder technique) and long-wave irradiation by means of a precision pyrgeometer. Moreover, general climate parameters such as wind, ambient air temperature and humidity as well as long-wave sky radiation should be recorded.

Meteorological data for hygrothermal simulations
Three years of meteorological data have been compiled in the format of the Danish Design Reference Year (DRY). The material is referred to as Meteorological Test Reference Case, Copenhagen (METREC), and the specific years are 1991, 1992 and 1993. The files provide a basis for hygrothermal calculations with climatic situations differing from those of the DRY. Precipitation is given as hourly values as opposed to the 3 hour values of the DRY. The data can be combined with the guidelines for estimation of driving rain as given in the British standard BS 8104, in order to include driving rain data in hygrothermal simulations.

Recommendations for future activities
In general, there is a pronounced need for a better understanding of the microclimatic conditions at the external surface of buildings envelopes. Driving rain data are needed for the validation of theoretical estimation of driving rain loads. The driving rain measurement technique has to be developed in order to establish a basis for exchange of results, and the relation between reference precipitation and meteorological precipitation should be investigated.

Driving rain
- Comparative testing of DRC types
- Studies of evaporation during rain
- Long duration measurements - preferably in more locations and more orientations
- Checking of reference precipitation measurement
- CFD estimation of driving rain

Long-wave radiation
- Simultaneous pyrgeometer measurement from vertical and horizontal surfaces

Window convection heat transfer and condensation phenomena
- In situ measurements on low-ε windows, encompassing observation of condensation and precision measurement of long-wave irradiation. Long duration measurements allowing for observation of seasonal variations

The complex convection phenomena at the external surface of the building envelope should be investigated in order to provide information for the modelling of condensation phenomena.

RESUMÉ

Nærværende afhandling er konklusionen på et Ph.D.-projekt med den danske titel *Mikroklimatiske forhold ved ydersiden af klimaskærmkonstruktioner*, gennemført over en treårig periode mellem august 1995 og august 1998 ved Institut for Bygninger og Energi, Danmarks Tekniske Universitet.

Der har gennem en årrække været fokuseret på vigtigheden af energirigtige bygningskonstruktioner. Dette har ført til udvikling af termisk velisolerende bygningskomponenter og bygningstyper. Fugt i bygningskonstruktioner kan give anledning til en række skader og/eller utilfredsstillende ydeevne. Et væsentligt interesseområde for forskningen på bygningsområdet er etablering af modeller af koblet fugt- og varmetransport med henblik på udvikling af konstruktionsprincipper og -typer med tilfredsstillende ydeevne og lang levetid. Sådanne modeller afhænger af beskrivelser af det omgivende klima som inddata til hygrotermisk simulering af bygninger og bygningsdele.

Hygrotermisk simulering er typisk baseret på anvendelse af et referenceår (fx. det danske Design Reference Year, DRY, udviklet ved IBE), som giver vejrdata på timedata for et typisk dansk år. Sådanne data er observeret under meteorologiske standardbetingelser, medens fugtmæssigt kritiske situationer typisk er resultat af helt lokale påvirkninger, som eksempelvis kan optræde i den mest udsatte position på en given bygning.

I bygningsfysisk sammenhæng er det (udvendige) mikroklima defineret som de klimatiske forhold, som har betydning for fugt- og varmetransport ved ydersiden af klimaskærmen. Klimaskærmen betegner helt generelt adskillelsen mellem klimaet inde og ude, uden at specificere type af bygningsdel. Mikroklimaet fremkommer af meteorologiske (globale) påvirkninger og lokale forhold såsom topologi, lægivere, bygningsgeometri og position på en given bygning.

De mikroklimatiske parametre er følgende:

- Temperatur
- Fugtighed
- Langbølget stråling
- Solstråling korrigeret for skygger
- Slagregn
- Lufthastighed

Emnets kompleksitet, og projektet i sig selv, er diskuteret i et videnskabsteoretisk perspektiv, og metodologiske problemer er identificeret. I særdeleshed problemerne i forbindelse med præparationsprocessen er diskuteret (her betegner præparationsprocessen afgrænsningen af genstanden for en undersøgelse, i form af parameteridentificering). Kombinationen af komplekse klimatiske fænomener, og behovet for retningslinier til brug i praksis, dikterer en pragmatisk metodik, som det i øvrigt gælder for ingeniørvidenskaben i almindelighed. Introduktion af parameterdefinitioner og antagelser med hensyn til de enkelte parametres betydning kan influere på de opnåede resultater. Sådanne antagelser og parameterdefinitioner må således foretages kritisk og i bevidsthed om mulige konsekvenser af de foretagne valg.

Det har været nødvendigt at udvælge emner for nærmere studier af hensyn til tidsramme og økonomi. På baggrund af en behovsanalyse, navnligt med fokus på behovet for data til brug for hygrotermisk simulering, er tre hovedområder udvalgt:

- Slagregn
- Langbølget stråling
- Konvektiv varmetransport fra vinduer

En mikroklima-målestation i fuld skala er etableret til måling af slagregn, nedbør, langbølget stråling, lufttemperatur, luftfugtighed samt vindhastighed og -retning. Måling af det konvektive varmetab fra ydersiden af en termorude er gennemført som en serie nat-målinger af kortere varighed.

Slagregn
En af de væsentligste opgaver i projekter har været at studere og udvikle metoder til måling af slagregn mod bygninger. En traditionel slagregnsopsamler er fremstillet. Opsamleren består af en opsamlerbakke monteret på en lodret ydermur og drænet til en kommerciel nedbørsopsamler. Med henblik på at forbedre måleteknikken er et nyt design blevet udviklet: En opsamlerbakke inklusive reservoir er ophængt i en vejecelle. Vejecellen registrerer systemets samlede vægt, og giver således mulighed for at registrere dråber som bliver hængende på opsamlerbakken. Desuden er der i opsamlerbakken monteret et net, således at regndråberne spredes ved kollision med opsamleren. Reflektion fra opsamleren bliver således reduceret. Den nye type slagregnsopsamler betegnes *vejecelle DRC* (engelsk: load cell driving rain collector), eller *vejecelle-opsamler.*

Databehandlingen af signalet fra den nye opsamler er endnu ikke færdigudviklet. Vejecellens signal bliver lagret som 10-sekunders øjebliksværdier for den kumulative slagregnsmængde. Slagregnsmængderne er herefter estimeret på basis af 10-minutters middelværdier.

Den nye type slagregnsopsamler registrerer fordampning fra opsamlerbakken, selv i perioder med høj luftfugtighed i forbindelse med nedbørshændelser. Det må forventes, at fordampning ligeledes finder sted under selve nedbørsforløbet, med underestimering af slagregnsmængderne til følge.

Den traditionelle slagregnsopsamler og vejecelle-opsamleren er monteret side-om-side for sammenligning. Foreløbige resultater tyder på at vejecelle-opsamleren registrerer væsentligt mere slagregn end den traditionelle opsamler. Over den betragtede måleserie registrerede den traditionelle opsamler 60 procent af slagregnsmængden registreret med vejecelle-opsamleren. Forskellen tilskrives fordampning fra den traditionelle opsamler. Tre alternative opsamler-principper bliver i øjeblikket afprøvet side-om-side på facaden af en høj bygning på Eindhoven University of Technology.

Den rumlige distribution af slagregnen over den betragtede tre etagers, vestvendte gavl, har vist sig at stemme kvalitativt overens med retningslinierne i de eksisterende standarder. Langs gavlens overkant registreres op til dobbelt så store mængder slagregn som omkring gavlens midte. Datamaterialet er endnu ikke tilstrækkeligt til kvantitativ sammenligning med standarderne. Eventuel underbygning af resultaterne med hensyn til fordampning og følgende underestimering, kan føre til revidering af fremtidige standarder, da de eksisterende standarder er etableret på grundlag af resultater opnået med slagregnsopsamlere af den traditionelle type.

Et indledende studium af Computational Fluid Dynamics (CFD) er gennemført med henblik på vurdering af metoder til estimering af slagregn mod bygninger, og identificering af eventuelle problemer. Som middel til modellering af luftstrømninger omkring bygninger udgør CFD-metoder et interessant og relativt nyt alternativ til vindtunnelforsøg, som er forbundet med relativt store omkostninger. Gennem de seneste år er udvikling af metoder til simulering af slagregn mod bygninger blevet indledt. Net-generering (inddeling af beregningsdomænet i celler) er besværligt og tidskrævende - afhængigt af den enkelte CFD-kode. I visse tilfælde viser net-genereringen sig endog umulig. Stigende computer-kapacitet, og udvikling af stadigt mere avancerede koder, giver mulighed for løsning af stadigt mere komplekse problemer. Det væsentligste problem er validering af de opnåede resultater. Modellerne og resultaterne er vanskelige at validere - både med hensyn til slagregn og luftstrømning. Dét, at modellerne bliver videreudviklet, og brugerfladen bliver lettere tilgængelig, må imidlertid ikke aflede opmærksomheden fra, at sådan modellering er et kompliceret fluid dynamisk problem. Antagelser med hensyn til randbetingelser er essentielle, og udformning af net kan influere resultaterne. Fremtidige anvendelser kan omfatte generering af slagregnskoefficienter, afhængige af vejrtype, lokale karakteristika, bygningsgeometri og position på en given bygning. Til brug for validering af sådanne beregninger behøves omfattende slagregnsmålinger, samt metoder til sammenligning af resultater opnåede med forskellige opsamlertyper.

Langbølget stråling

Måling af langbølget stråling er gennemført som serier af kort varighed fra vandret og lodret til brug for sammenligning med empiriske beregningsudtryk fra litteraturen. Himmelstrålingsdelen udgør den mest usikre del af estimeringen af den langbølgede indstråling. Dette kommer til udtryk i store afvigelser mellem de målte og de beregnede værdier. Der er bedre overensstemmelse for lodrette flader, hvor himmelstrålingsdelen får mindsket betydning. Den bedste tilnærmelse til de målte data er opnået ved brug af Coles formler for langbølget stråling mod hældende flader. Den almindelige antagelse, at omgivelserne kan tilnærmes som et sort legeme ved lufttemperatur, resulterer i acceptable tilnærmelser under de aktuelle forhold - specielt når usikkerheden på himmelstrålingen tages i betragtning. Referenceåret, DRY, indeholder data for himmelstråling, som kan anvendes når blot usikkerheden erindres; strålingsudveksling med omgivelserne kan beregnes udfra antagelsen om, at omgivelserne betragtes som 'sorte' og har luftens temperatur. Det skal dog bemærkes, at den langbølgede indstråling, om muligt, altid bør måles - og helst ved brug af et præcisions-pyrgeometer.

Konvektiv varmetransport fra vinduer

Vinduers/ruders forbedrede ydeevne i termisk henseende resulterer i lavere temperaturer på den udvendige overflade af glasset. De lavere temperaturer har i visse tilfælde ført til udvendig kondensdannelse, hvilket af brugeren opleves som utilfredsstillende. Det konvektive varmetab fra ydersiden af en velisoleret klimaskærm, for eksempel et velisolerende vindue, har ikke stor betydning i energimæssig sammenhæng. Imidlertid er der brug for en mere detaljeret beskrivelse af de komplekse varmetransportfænomener ved ydersiden af ruder til brug for vurdering af kondensrisiko og varighed af kondensforekomst.

Der er gennemført gennemført nat-målinger på et nordvendt vindue. Den konvektive varmeovergangskoefficient afhænger tydeligt af vindretningen. Den konvektive varmetransport i roligt vejr (størst kondensrisiko) er bestemt til at have værdier mellem resultaterne for indvendige overflader og for udvendige overflader uden vind. Dette indikerer, at foreskrifterne overestimerer den konvektive varmetransport, hvilket også forekommer rimeligt i forbindelse med energimæssige beregninger. I forbindelse med vurdering af kondensrisiko og varighed af kondensdannelse, er en sådan, relativt grov, beskrivelse imidlertid ikke tilstrækkelig. Sådanne

beregninger skal baseres på mere detaljerede modeller, subsidiært underestimering af konvektionen.

Observering af in situ lavenergi-ruder, monteret i forskellige positioner, ville kunne bidrage med værdifuld information til karakterisering af situationer med kondensdannelse. En sådan opstilling bør omfatte måling af reference-overfladetemperatur ved anvendelse af et antal termoelementer, temperaturforskelle ved anvendelse af et antal termosøjler (eventuelt ved brug af en *Mayer ladder* metode) og langbølget indstråling ved brug af et præcisions-pyrgeometer. Opstillingerne bør desuden suppleres af referencemålinger omfattende vind, lufttemperatur og luftfugtighed samt himmelstråling.

Meteorologiske test reference data
Tre års meteorologiske data er samlet i DRY-format. Materialet betegnes Meteorological Test Reference Case, Copenhagen (METREC), og de tre konkrete år er 1991, 1992, 1993. Filerne udgør et grundlag for hygrotermisk simulering med klimasituationer som afviger fra situationerne i DRY. Nedbør er givet som timeværdier, i modsætning til 3-timers værdierne i DRY. Disse data kan kombineres med retningslinierne i den britiske standard BS 8104 med henblik på at inddrage slagregnsbelastning i hygrotermiske simuleringer.

Anbefaling af fremtidige aktiviteter på området
I almindelighed er der et udtalt behov for bedre forståelse af de mikroklimatiske forhold ved ydersiden af klimaskærmkonstruktioner. Der er brug for slagregnsdata til brug for validering af metoder til estimering af slagregnspåvirkninger. Teknikken til måling af slagregn må udvikles med henblik på at etablere en standard for udveksling af resultater. Desuden bør forholdet mellem reference-nedbør og nedbør observeret under meteorologiske forhold undersøges yderligere.

Slagregn
- Sammenlignende afprøvning af opsamlertyper
- Undersøgelse af fordampning i forbindelse med nedbør
- Langtidsmåling af slagregn af hensyn til sæsonvariationer
  - helst flere steder og flere orienteringer
- Studie af reference-nedbør i forhold til normal nedbør
- CFD metoder til estimering af slagregn

Langbølget stråling
- Samtidig måling af indstråling mod vandret og lodret (varierende omgivelser)

Konvektiv varmetransport fra vinduer
- In situ målinger på lavenergi-vinduer omfattende observering af kondens og præcisionsmåling af langbølget indstråling. Langtidsmåling af hensyn til sæsonvariationer.

De komplekse fænomener ved den udvendige overflade af klimaskærmen bør studeres, med henblik på at tilvejebringe beskrivelser af forhold af betydning for kondensdannelse.

CONTENTS

Chapter 1

BACKGROUND

The project
The present report concludes a Ph.D.-project, carried out at the Department of Buildings and Energy between August 1995 and August 1998. The department has a long tradition in calculation of energy and moisture transfer in buildings, and in compiling weather data for energy calculations. The Ph.D. work is a pilot study, in the sense that it is the department's first project specifically treating the *microclimate* around building envelopes. The aim is to identify potential areas of future research, to discuss measurement principles and to carry out case studies of selected parameters.

Building physics
The building physical research is focused on hygrothermal behaviour of buildings. Energy and moisture aspects are studied in order to gain understanding of fundamental physical phenomena - knowledge which will lead to improvement of construction principles. Optimization of performance, and the development of novel types of constructions, depend closely on the available engineering tools, which again depend on the ability to model the problems under consideration.

The buildings are studied with focus on two main areas of interest:

- Durability
- Performance (energy consumption, functionality, comfort, aesthetics)

Although in different perspectives, coupled heat and moisture transfer is essential in both of these areas.

For years, the energy consumption perspectives have been in focus, leading to awareness and the developing of thermally well-insulating building components. Innovation of building components has also lead to new types of problems caused by moisture in the constructions. One major objective of current research is to establish models of coupled heat and moisture transfer in order to develop construction types with satisfactory performance and long service life/durability.

Detailed models of coupled heat and moisture transfer in constructions have been developed - facilitated by increasing computer capacity. Such models are typically based on use of weather data in the shape of a Design Reference Year, yielding exterior climatic boundary conditions. The use of weather data in this form generally leads to satisfactory estimation in terms of energy calculations and assessment of indoor thermal comfort.

The durability of the building envelope, and the performance during the service life of a building envelope, depends closely on moisture conditions. The problems caused by moisture in constructions include structural damage, reduction of thermal insulation, health risk/detrimental effects and aesthetic decay.

Microclimate
For the purpose of hygrothermal simulations, there is a pronounced need for a more detailed description of the climatic conditions in the immediate vicinity of the external surface of the building envelope - in this context referred to as the *microclimate*.

> *A climatic situation leading to moisture problems or unsatisfactory performance of the building envelope will usually be due to very local conditions.*

The Design Reference Year yields *meteorological data*, observed at a meteorological station and valid for a relatively large area, e.g. Copenhagen. The microclimate is a result of both the meteorological weather and local characteristics such as topography, obstacles, building geometry and position on a specific building.

> ***Microclimate definition***
> *In the context of the present study, the microclimate is defined as the conditions affecting transfer of heat and moisture in the immediate vicinity of the external surface of the building envelope. In more general terms, the microclimate is pertaining to a limited area of considerable uniformity in terms of climatic conditions, differing from the conditions of its enveloping macroclimate, owing to local climatic factors such as exposure.*

The microclimatic parameters are:

- Temperature
- Humidity
- Long-wave radiation
- Solar radiation corrected for shading objects
- Driving rain
- Air velocity

The microclimate is studied in a building physical perspective, i.e. the parameters are defined on the basis of heat and moisture balances at the external surface of the building envelope. The heat and moisture transfer through the building envelope is not considered, and architectonic and durability aspects are not treated directly.

Two important examples of building physical problems in need for microclimatic input are *driving rain* as a moisture source and *external condensation* on thermally well-insulating windows.

External condensation on window panes is an example of a phenomenon, which is experienced as products with still better thermal performance are introduced. To be able to understand the fundamental mechanisms, and subsequently establish models for the estimating of condensation risk, a more detailed description of the microclimatic conditions is needed.

Another sparsely described, microclimatic issue is the rain impinging on the surface of building envelopes. The driving rain is an important moisture source in climates such as the Danish, with frequent rain and wind. Wetting of the building envelope can result in problems pertaining to durability and performance. There is a need for guidelines regarding the driving rain loads, if models of combined heat and moisture transfer are to approximate the behaviour of constructions in moisture critical situations more accurately.

Scope

The issue is comprehensive, in the sense that it has affinities to virtually every aspect of building physics. The intrinsic complexity of the microclimatic phenomena constitutes another challenge. As the work is defined as a Ph.D. study, and furthermore aims at establishing a branch of research at the department, a general discussion of method and methodological problems has been given priority. The complex nature of the problem, and the identified need for information for the applications, dictate a pragmatic approach in terms of experimental work. The objective is to establish an introduction to the microclimatic issue, identifying future areas of research and gaining experience regarding measurement principles.

It has been necessary to leave out certain aspects of the problem. The selection of topics has been based on the need for knowledge as well as the given time frame and financial situation. Aspects regarding solar radiation have not been included in the studies; The existing expertise at the department, and the comprehensive research in the area, make other areas more relevant in a microclimatic context. Wind flow around built structures is not studied explicitly either, but is related to the studies of convection heat transfer and driving rain.

Focus on driving rain as the knowledge is limited and guidelines are needed. Sparse measurement data are available and more data are needed for calibration of simulation techniques and validation of existing methods.

Focus on convection heat transfer because of the problems with external condensation on well-insulating window panes. These windows have been developed in order to save energy, but the external condensation yields an obstacle to the application.

Focus on long-wave radiation being a significant quantity in night-time situations, which represent the highest condensation risk.

In recognition of the complex nature of the problem, and the given framework of the project, the issues are addressed in the form of case studies. The objective is to both acquire knowledge of the parameters (quantitatively and qualitatively) and to investigate measurement techniques and equipment.

Chapter 2

METHODOLOGICAL PROBLEMS

Project definition
In the following, methodological questions pertaining to the present project are discussed.

In this context, the term *Microclimate* is related to buildings and signifies the building physical conditions *in the immediate vicinity of the external surface of the building envelope*, resulting from interaction between meteorological weather situations and local features.

The project is of the *discovery* type. As there is no simple way of generating hypotheses, the chosen methods will usually result from tradition, intuition and financial as well as practicable possibilities. The extent and nature of the present project are the results of several factors, mainly: tradition at the institute and in the scientific community in general, time frame, economy and co-ordination with other research activities.

The overall objective is to establish general guidelines for the applications. These cannot be produced on the basis of the results of this project alone, but the results will form a basis for evaluation of the parameters, as well as a basis for the testing of existing methods.

The project should be seen as a pilot project, aiming at identifying potential areas of future work. As the measurements have been conducted over a limited period of time, it should also be stressed, that it is important to continue the measurements after the conclusion of this work.

The aim of the present project is to describe the influence of the microclimatic conditions on the heat and moisture transfer at the exterior of the building envelope. The very complex nature of the problem raises a series of methodological issues; some regarding data acquisition, some regarding the conversion of the acquired information into knowledge of governing mechanisms. In this chapter, a number of these issues are addressed.

Not many answers are given; yet, the identification and explicit formulation of the fundamental problems, combined with specific findings of the case studies, may serve as reference points for further studies of the phenomena.

Cognitive objective
As mentioned above, the aim of the project is to obtain general guidelines for the conversion of meteorological data into specific conditions at a given building. The objective is to find methods of modifying weather data, establishing a realistic input for simulations with a greater extent of nuance, by taking local features into consideration. The project will provide information for this process, whereas generally applicable guidelines will demand a further elaboration of the research in this field.

The fundamental conflict is the wish for *acceptable* approximations based on knowledge of the applications versus the intrinsic complexity of the climate and the limitations of attainable accuracy. The degree of detail of possible guidelines must yield significant differentiation of exposure, yet without pretending absolute accuracy. Clearly, absolute accuracy is inconsistent with the nature of the climate itself.

The cognitive objective of the project is *Applicability*; This is characteristic of the Engineering Science as a whole. Operation is based on pragmatic values as opposed to epistemic[1] values; method and objective are determined on account of efficiency, safety, simplicity (measurement, calculation), economy and validity. In this context, it is fully acceptable to introduce *quasi objects* - objects serving to describe problems and thus make solutions possible. Examples of such entities are *Equivalent Sky Temperature* and *Airfield Driving Rain*; these are not actual physical entities but describe specific conditions in an appropriate way. Also the categorizations of topography and surroundings are instances of such artificial entities.

Ontology[2]

Since the field is relatively new, and which moreover must be categorized as a hybrid of several existing disciplines, no definite ontology exists in the area of microclimate within the tradition of Building Physics; The project is of the discovery type, i.e. no general theory exists in the field. The intrinsic complexity of the studied phenomena means that solutions are sought applying a variety of disciplines. The ontology is created from the existing theoretical apparatus, as represented by meteorology, heat and moisture transfer theory, material science and fluid dynamics.

The work is carried out towards applicable design guidelines and is thus engineering science as opposed to the 'pure' natural sciences. The discovery process is taking place simultaneously from several angles. The approaches are of a similar character throughout the research environment, although differences appear regarding specifics of both design of experiments and interpretation of results. Considering the activity of the different research groups as a whole, the discovery process is generally expected to converge towards a common cognition in terms of empirical expressions and other measures.

Parameter identification

The project deals with issues significant to transfer of heat and moisture at the external surface of the building envelope. In reality, primarily vertical surfaces towards air are considered, whilst characteristic differences compared with inclined surfaces and surfaces towards soil are outlined. The conditions in the immediate vicinity of the surface are studied, while the influence of the surroundings is evaluated on the basis of case studies and a survey of the literature.

The parameter identification is initially adopted from the building physics and hygrothermal calculations. As discussed in the following, identification of the parameters constitutes an important part of the formulation of the problem and the objects to be studied. Traditionally, the coupled heat and moisture transfer is calculated on the basis of the following parameters:

- Temperature of the ambient air
- Humidity of the ambient air (relative humidity or dew point)
- Solar irradiance corrected for shading objects
- Long-wave irradiance from sky and surroundings
- Air velocity
- Driving rain

[1] Epistemic: Pertaining to knowledge; the objective is to expand the cognition in search for *truth*.

[2] Ontology: The theory of *being*. Ontology is the general theory of what there is [Mautner, 1997]. In this context, the concept is adopted in the sense of an *organized system of terminology*.

These parameters constitute parts of the heat and moisture balances at the exterior surface of the building envelope, and result from interaction between the meteorological climate and local features. When considering simulation of the behaviour of the building envelope, this set of parameters is virtually standard. Later in this section, and throughout the rest of the report, this definition will be subject to discussion. As described in the following, a parameter like driving rain could very well be split into several separate parameters; The choice of representation thus implies presumptions as to the significance of the specific parameters, and may to some extent predetermine the outcome of the research.

Preparation process: Research Object - Model Object

E X A M P L E I : One current area of interest within the Building Physics is the convection heat transfer at the external surface of window panes. There is a need for a more detailed description of the convection heat transfer, in order to estimate condensation risk on the external surface of modern, well-insulating window panes. In this context, the *Research Object* can be described as the *convective heat transfer at the external surface of window panes*. These general terms include all realistic combinations of building geometry, positioning on the building, window pane type and meteorological conditions. In order to obtain a clear and manageable model, the parameters are defined, and parameters assumed insignificant are neglected. The parameter definition is based on theoretical considerations and previous experience. The energy balance is defined in terms of heat flux through the window pane, radiation exchange with surroundings and convection. The phenomena may be studied full-scale by measurements in one or more set-ups. Such a set-up could comprise one window in a given location. The set-up thus constitutes an instance of all window types in all locations. The problem can be further simplified by eliminating one or more parameters. As an example, the solar radiation can be eliminated by nocturnal measurements. The process described above, is called the *Preparation Process* and the result is a *Model Object*. In this context, the *Model Object* is defined as a *given window* (with a well-defined thermal resistance) in a *given location*, at *night-time* (no solar radiation) and the energy balance is based on three factors: *heat flux through the window pane*, *radiation exchange* with surroundings (long-wave) and, finally, *convection*.

In the present work, the main objective is to investigate microclimatic parameters influencing the transfer of heat and moisture. Thus, the problem is defined on the basis of moisture and heat balances at the exterior of the building envelope. The Research Object is precisely these balances and their boundaries in abstract/schematic form.

In the Philosophy of Science, concepts like Research Object and Model Object are defined and discussed on a rather abstract level; When examples are applied, these have usually been picked from the fundamental research. It is not unproblematic to apply such distinct definitions to a project like the present one, in which the objective is in fact to measure, or rather to attempt to measure, *something resembling the reality in its full complexity*. In the following, the preparation process is commented in relation to the present project, the applied models are identified and it is found that the most important aspect of the work is a conscious introduction of assumptions and parameter definitions.

In principle, meteorology and material properties are not considered - these are considered as known boundary conditions in this context. The proposed building is an instance of every conceivable geometry in any location, although limited to the area of Denmark.

In general terms, the Research Object can be described as *Heat and moisture transfer at the exterior of the building envelope as a function of all parameters and governing factors*. The

project deals with the interrelationship between microclimate and hygrothermal conditions at the surface of the building - Including microclimate as a result of interaction between local features and meteorological situations.

The Research Object is subject to a preparation process depending on the purpose of the specific model. The result of this preparation is a Model Object. In the context of the present project, four different types of Model Objects are employed according to the specific tasks.

I Full-scale measurement: Selected measurement positions, given local conditions
II Simulation: Limitations in detailing, simplified boundary conditions
III Common Task of the Microclimate Group: Common problem, different approaches
IV Possible development of algorithms for the applications: Correlations, *rules-of-thumb*

These models all implement different parameters and different generalizations. Each model is modified according to demands like simplicity and achievable degree of detail. With regard to the choice of model, Jakobsen and Petersen [1997] state the following:

(...) the perhaps most important part of scientific work consists in establishing conceptual models in which problems under investigation can be represented in a way that makes solutions possible.

A fundamental demand of a good model is that it can represent 'the reality', allowing problems to be solved or handled in a constructive manner. In addition, the same authors state that theory is a prerequisite for preparation of the Research Object, and for the Research Object to be an adequate representation of 'the reality'. Hence, there will be an interaction between defining a model and the possible development of a theoretical apparatus.

The distinction, as described above, is to some extent in disagreement with the definitions as proposed by Jakobsen and Petersen [1997].

(...) research objects are not only objects as they appear to us unaffected as part of the environment. They are delimited and modified in such a way that they can be regarded as instances of abstract generic objects. Such abstract generic objects are called model objects. Consequently, a research object is an entity which can be viewed as an instance of a model object. Model objects are abstract conceptual entities, and they are the proper targets of scientific theories.

In this sense, the Model Object of the project would consist of a schematic representation of the microclimate between the combined heat and moisture transfer and surroundings, building geometry etc. Thus, the Research Object would consist of specific parameters as recorded at the proposed building.

As already stated, it is not of great consequence which of the above terminologies is chosen, as far as division into objects is concerned - the preparation process will essentially be the same. It is important that this preparation process is performed consciously and well-founded for the work to be *scientific* as opposed to part of *other cognitive activities*.

Underdetermination[3]

The microclimate and the attempt to model or describe it, is a complex matter. Alone the factors pertaining to the physical boundaries, such as building geometry, material properties and surroundings, yield numerous permutations, therefore situations, to be considered. In addition, the global/meteorological climate varies in an almost chaotic fashion. Hence, in the light of these aspects, even full-scale measurements will always represent specific cases, which under no circumstances dictate universal rules. Possible empirical correlations will always be underdetermined in a pronounced way. Having recognized this situation, the challenge remains to design the experiments so as to yield a *sufficiently* precise measure of relevant correlations and magnitudes for the selected cases. Cases must be representative to the widest possible extent. Overall, the underdetermination of the measurements can be divided into three dimensions:

I Space
II Time
III Precision

In the following, the three aspects are introduced briefly.

I. Space

It is not possible to measure 'reality' in all of its complexity. A limited part of 'reality' is recorded by means of a number of sensors available to the project. A further limitation is the ability to actually mount the sensors physically. The parameter variation will thus be recorded in few, selected positions. The spatial distribution of the parameters will be described discretely in a limited number of positions, although the spatial distribution is essential in a microclimatic context.

II. Time

Clearly, the duration of the measurement series is limited, and during the series, the parameters are recorded with a certain temporal resolution. The chosen resolution can be based on different considerations, typically computer capacity and estimation of the parameter variations.

III. Precision

Finally, the precision of the measurement is limited. The precision of the sensor is essential; Greater precision can be achieved by means of more costly equipment, leading to necessary compromise. In addition, every measurement set-up will influence the situation being measured, and thus potentially introduce errors.

Pertaining to the precision aspect is the whole discussion regarding the influence of the surrounding environment on the measured quantities. Does a recorded quantity owe to the effect of the surroundings? - an effect otherwise being presumed insignificant - or is it due to the operation of measuring devices constructed on the basis of theoretical considerations and thus predetermining results? The latter aspect of the problem is known as the *Experimental Recourse*[4].

[3] Underdetermination: Different theories using different theoretical concepts, but both well supported empirically, are said to be *underdetermined by the empirical evidence*, and the same applies to theories that are mutually incompatible but fit all the available evidence [Mautner, 1997].

[4] Experimental Recourse: A theory gives a prediction; The prediction is tested by means of an experiment, which is calibrated by employing the original theory. In this way, convergence will be obtained, if this is the intention.

Interpretation
In order to describe the variation of the individual parameters as functions of relevant factors, disturbance of local conditions and influences of other parameters are reduced as far as possible.

EXAMPLE II: When measuring the convective heat transfer, the influence of radiation is minimized in order to attain significant convection quantities. The desired effect is obtained by choosing a test plate with a) low solar absorptivity, b) low long-wave emissivity and c) the test plate is supplied with an electrical effect to increase the surface temperature, and thus the heat loss from the surface. These three measures will all, to some extent, make the test plate differ from the surface of a *normal* building envelope surface.

EXAMPLE III: Driving rain is usually thought of as only one parameter - the intensity of rain impinging on the external surface of the building envelope. In preparation for studies of humidity related issues, a further differentiation might appear to be relevant. Thus, one could operate with both intensity, drop-size distribution and duration as well as the nature of the events over time. Such a degree of detail is demanding in terms of equipment and data processing, but would make more thorough analyses possible. In this context, trivial problems pertaining to measuring equipment become significant. Since resources are always limited, the measurements are carried out in few, selected positions on a surface with a given orientation and a given exposure. Apart from this, the set-up itself will influence the results to some extent; partly because the draining from the collector takes place with a certain delay and with a certain threshold value, partly because the conditions at the proposed surface and in its immediate vicinity are changed owing to the presence of the equipment. This leads to the classic discussion of measurements and the validity of results obtained from an object representing the reality. The fact that the parameters have been defined prior to designing the experiment, and the fact that the measurements will always have a finite accuracy and be valid for a limited range of conditions, may turn out to predetermine the outcome to some degree.

In the context of the present study, laboratory activities are limited to small tests of the devices during the design phase. The innovative part of the project consists mainly in development of equipment, which is tested in a controlled environment.

Laboratory experiments are characterized by the ability to control and manipulate the different loads in surroundings which are well-known and well-defined. When regarding a topic as complex as the microclimate, individual aspects can be isolated and studied in the laboratory. Parameter studies in general, and elimination of error sources in particular, are made possible in specially designed set-ups. The problem in relation to this matter consists in the translation of the achieved results into meaningful statements about the reality from which the set-up is virtually isolated.

Traditionally, scaled experiments in wind tunnel facilities have been an efficient way to model and describe wind environment around built structures. Moreover, in the course of recent years, wind tunnel facilities have been developed for full-scale microclimate modelling, employing control of practically all climate parameters. However, the use of such facilities is inevitably associated with substantial costs, and has not been practicable within the framework of the present project.

To a great extent, alternative, potential methods will be assessed by employing abductive methods[5], i.e. choice of the best solution on the basis of certain, more precisely specified criteria. Besides, *Experimental Parameter Variation* will be performed within the framework of a given hypothesis, e.g. when adjusting methods of calculation to fit results obtained experimentally or by simulation. It should be noted that, in this context, the aim is empirical correlations suitable for engineering purposes as opposed to exact expressions, in recognition of the intrinsic complexity of the matter. A fundamental aspect of the work is the demarcation and hereby the definition of its scope of validity. An important part of this process is the exclusion of all other factors.

Demarcation[6]

The influence of the surroundings is evaluated by use of theory as well as implicit and tacit assumptions. When performing simulations, the surroundings are sought modelled, and the model is subject to sensitivity analysis. Moreover, existing results and calculation algorithms are compared with the registered data. Note that the surroundings and their effects are given by choice of location for the measuring station. The significance of the surroundings, on the other hand, is an object of evaluation and interpretation. Strictly speaking, consistency between data material and theoretical structure is not an adequate basis for validation. Such consistency may be due to part hypotheses and assumptions which tacitly form parts of the theoretical basis.

Data material is always being interpreted. E X A M P L E I V : The wind and the airflow around a building geometry will typically have a turbulent character. By choice of log-frequency, and possibly averaging, an interpretation will be made implicitly. This way, assumptions regarding the significance of the chosen representation will form the basis for, and to some extent characterize, the data material. Analogue considerations will apply to the other parameters, though most significantly when regarding *rapidly* varying quantities. Similar problems occur in connection with simulations. Choice of time step length, a most basic operation, may affect the possible solutions. The sometimes tacitly introduced presumptions express a degree of predetermination, betraying the intended objectivity. As these aspects cannot be avoided, an important part of the demarcation consists in the analysis of these problems, namely by clarifying the mechanisms and adopting a conscious and systematic approach when introducing suppositions and parameter definitions.

A fundamental aspect of the demarcation criteria is that the measurements are not over-interpreted. Clearly, the case studies of the project will contribute with valuable information regarding magnitudes of specific quantities and possible improvements of measuring devices and suchlike; The findings will provide information for the discovery process - Provided that the experiments are designed with possible effects of suppositions and parameter identification in mind.

Generalization

When is a sufficient foundation for generalization obtained? Regardless of the extent of the measurement activities, underdetermination will be distinct. The evidence is limited in comparison with the endless possibilities of variation as offered by the numerous parameters. In theory, the induction problem - the finite evidence - is usually dealt with by probability calculus. Thus, the evaluation is based on statistical methods.

---

[5] Scientifically useful abduction is *Inference to the Best Explanation*. The general form of such an inference is: (1) D is a collection of data; (2) H (a hypothesis) would, if true, explain D; (3) no other hypothesis can explain D as well as H does. (4) Therefore, H is probably true [Mautner, 1997].

[6] Demarcation designates the fixing of a boundary or dividing line. In this context, the *demarcation criteria* defines the demands of *science* as opposed to *other cognitive activity*.

Extrapolation cannot be accepted on the present basis as presented in this project, but the specific results will serve to test and corroborate, or possibly falsify[7], existing models and existing methods of calculation. In a field such as the present, the correspondence between the theoretical structure and the reality must have a pragmatic form. The objective is not to define universal rules, merely useful, functional correlations providing improved approximations, when compared with the methods applied hitherto.

[7] Falsification: refutation; showing that a hypothesis is false [Mautner, 1997].

Chapter 3

BUILDING PHYSICS AND MICROCLIMATE

General

The conditions at the external surface of the building envelope result from an interaction between the properties of the building itself and the ambient climate. In a building physical context, the conditions are described in terms of heat and moisture balances. Usually, the objective is to investigate the moisture or the heat flux through a given construction. In this chapter, a brief introduction to microclimatic aspects of building physics is given. Four examples and a presentation of moisture problems define the microclimate in a the building physical context.

Typically, weather data for hygrothermal calculations are either measured data, acquired in connection with an experimental set-up, or standard meteorological parameters, as given in a design reference year. The weather data given in the design reference year describe typical meteorological conditions. If the heat and moisture transfer through a building envelope is to be modelled in detail, it is crucial to convert such global data into microclimatic conditions in the immediate vicinity of the building envelope.

Good architectural design, satisfactory building physical performance and long service life of a building all depend upon realistic and reliable climatic data, allowing for a qualified design process. The following examples illustrate the need for descriptions of microclimatic conditions in relation to building physical problems. The task of the present project, and subsequent research activities, is to provide information enabling researchers, developers, engineers and architects to assess the exposure of a given construction.

E X A M P L E I : Solar data material is usually given as irradiance (beam and diffuse) on a horizontal surface. In order to determine solar data for a given surface with given surroundings and a given orientation, the data are modified by means of geometrical formulae to account for orientation and shading objects (near and far). Moreover the reflectivity of the surroundings can be accounted for. This way, the global (or meteorological) data are converted into microclimatic input for hygrothermal calculations.

E X A M P L E I I : Air flow around buildings is a more complicated issue. The meteorological wind observations are carried out in a height of 10 metres over open terrain, whereas the wind in built areas is highly influenced by obstacles such as buildings. In the tradition of structural engineering, guidelines have been developed regarding the pressure distribution over building geometries as a function of wind loads. Such distributions can be determined by full-scale measurement, scaled modelling in wind tunnel or by means of *Computational Fluid Dynamics* (CFD). Such guidelines, however, are not adequate for estimation of air flow in connection with calculation of convection heat transfer from the building envelope. Current design guidelines incorporate simplified formulae in recognition of the complexity of the problem. These design guidelines either yield a fixed value for the convective heat transfer coefficient, or express the coefficient as a function of the wind speed, regarding neither wind direction and building geometry, nor the position on the geometry. For calculations of energy consumption, this type of pragmatic, approximative approach is found to be adequately accurate. When considering the heat loss through a normal well-insulated construction, the contribution of the surface resistance to the total thermal resistance is usually insignificant. However, the air flow

around a given structure will be important with respect to the progress of condensation and drying processes. For detailed calculation of energy transfer, for instance at the external surface of window panes, the guidelines are no longer satisfactory.

EXAMPLE III: Energy-conscious design of windows has lead to instances of external window condensation. From a building physical point of view, external condensation does not represent a serious problem, but the performance of the window may not satisfy the user. In order to assess the condensation risk, calculation of energy transfer at the external surface of well-insulating windows has thus become an issue.

EXAMPLE IV: Driving rain is defined as rain which is carried along by the wind so that it impinges onto vertical surfaces. Driving rain is depending on the meteorological parameters wind speed and precipitation, but the spatial distribution of driving rain on a given building surface depends closely on local factors such as the geometry of the surroundings and the wind direction relative to the considered surface. Rough guidelines for the calculating of driving rain loads exist, but measurement results are sparse, and there is a pronounced need for a better understanding of the governing mechanisms. Qualitatively, it can be said, that the highest intensities of driving rain are observed along the edges of a given surface, and in particular at the upper corners of the geometry. The highest driving rain intensities occur during spells of relatively short duration, leading to demands in terms of temporal resolution of the measured data.

Full-scale, model-study, simulation

Microclimate, being the result of complex interaction between numerous factors, is intrinsically a local phenomenon. The findings of full-scale microclimatic measurements are consequently valid for a certain area or a certain building geometry.

As the microclimate is distinguished precisely by the interaction between building and climatic factors, it is necessary to base most studies on in situ experiments. Selected parameters can be studied in laboratory set-ups, or by means of computer-based simulation.

Wind-tunnel testing is an efficient way of conducting studies of wind flow around built structures. Characteristic velocity, topological factors and local shape factors can be tested in a wind tunnel employing a model of the buildings and terrain. However, such measurements are related with substantial cost.

Computational fluid dynamics is a relatively new measure for simulation of air flows about geometries. Still more complex problems can be modelled as computer capacity increases. As commercially available CFD programs can handle increasingly complex tasks, one of the most important remaining problems consists in determining correct boundary conditions for a specific case, for instance when simulating the details of a building. The complex wind and pressure fields around a building make it difficult to choose the right input data for the boundaries.

Moisture problems

In recent years, attention has been directed towards building failures caused by moisture. In the present work, these problems are not studied, but they are the main reason for the wish for microclimatic information. The microclimatic moisture sources can be described as

- Humidity of ambient air
- Soil humidity

- Driving rain

Soil conditions are not considered in the present project.

Rain penetration is an important moisture source. The expression also covers situations where the water is not forced all the way through the building envelope. Penetration of wind-driven rain into the building envelope leads to wetting, or even saturation, of porous materials by rainwater. In extreme cases, the result may even be dampness on inner surfaces. Wind pressure does not affect wetting of porous materials significantly, but is the main reason for leakage through cracks and joints.

In the small pores of porous materials (with diameters measured in micrometers), water is absorbed and transported by capillary forces which are much greater than the pressures exerted by the wind. Thus, the pressure of the wind does not influence the rate of flow of moisture through most brick walls. The capillary forces decrease as the diameter of a pore or crack increases, and when a hole is about 0.1 mm or more across, the wind pressure may be more than the capillary forces [Lacy, 1977].

Undesired consequences of high humidity [after Nevander and Elmarsson, 1994]

- Moisture cracks and other aesthetic effects such as soiling of facades
- Deterioration due to
  - frost damage (masonry/rendering)
  - salt decomposition
  - corrosion (concrete reinforcement)
  - rot and other biological activity
  - chemical processes
- Health risks (detrimental effects) and odour nuisance by
  - mould
  - emissions from materials
- Increased energy consumption
  - reduced thermal insulation
  - evaporation
- Reduced durability
- Dimensional changes

Wetting of the building envelope leads to higher thermal conductivity. Consequently, heat losses are increased, while more heat has to be used to evaporate the moisture. Apart from the hygrothermal aspects, driving rain may cause cosmetic surface effects such as run-off staining.

Frost damage occurs when there is sufficient water entrained in pores to disrupt the material on freezing. The necessary conditions therefore include wetting tending towards saturation shortly before freezing. Temperatures just below zero may not freeze water in small spaces, and the temperature in the material may remain higher than air temperature. For this reason, the number of zero transitions (air temperature passing through 0°C) is not likely to give an accurate indication of the number of freeze thaw cycles in the material (although for some purposes it may suffice as a means of ranking frost resistance). A typical frost damage is detachment of rendering due to frost action. Water sufficient to cause disruption on freezing accumulates at the wall/render interface, and an expanding *ice lens* mechanism can develop during extended cold spells.

At the surface of the building envelope, the evaporation rate depends upon the humidity of the ambient air, the air flow (convection of both heat and moisture), heat flux from interior as well as incident solar and long-wave radiation. Building materials are usually only saturated for short periods of time. Most of the time, the evaporation of water takes place at a rate which is determined by the resistance to flow of water, or of water vapour, through the pores of the material, rather than by the microclimatic conditions. Lacy [1977] states that the drying of walls seems influenced mainly by the frequency and duration of the dry spells between periods of driving rain, rather than by the actual weather during the dry spells.

Constructive measures
Performance and durability can be improved by choice of materials, construction detailing and architectural features. The component design process can be optimized if the climatic factors are described, allowing for the assessing of the exposure of different parts of a given building. Further knowledge of the microclimatic conditions at the external surface of the building envelope is a means for further detailing of hygrothermal simulation, thus permitting the developing of buildings with improved performance.

Microclimatic data can be used as input for hygrothermal simulations, enabling researchers and practitioners to assess alternative construction principles, and to develop novel construction types.

Quantification of the parameters, both in terms of maximum exposure and temporal variation, will provide a basis for the developing of test routines, such as tightness tests.

More qualitative descriptions, such as coefficients for the spatial driving rain distribution over a building geometry, yield information regarding the demands to the various components of the building envelope, depending on the exposure of the specific position. For instance, it may not be necessary to design the whole building envelope with respect to maximum driving rain loads, which are only experienced in certain positions.

A more detailed knowledge of the heat transfer processes at the external surface of window panes, will make studies of external condensation phenomena possible.

With increasing computer capacity, complex problems can be modelled by means of computational fluid dynamics. Current research aims at modelling driving rain distributions on the building envelope. CFD tools can be used to model air flow around a building as a function of roughness parameters and wind profile. Particle tracking can subsequently provide information regarding the trajectories of the rain droplets within the air flow. This type of method constitutes a relatively new way of conducting parameter variations. However, these methods need to be calibrated or corroborated on the basis of in situ measurements.

Chapter 4

MICROCLIMATE

The preceding chapters gave a general introduction to both the project, the methodological problems and the relation between building physics and microclimate. In the present chapter, the component factors are treated individually. Some of the parameters are mentioned briefly for completeness; these parameters are air temperature, air humidity, solar radiation and air velocity. Long-wave radiation and driving rain are described more thoroughly, as they are the subjects of case studies in subsequent chapters. The specific subjects are studied because of their explicitly microclimatic nature, and due to a need for knowledge of the subjects within the applications. The chapter is concluded with a brief description of convection heat transfer and surface coefficients; These are not microclimatic phenomena, but as they are essential to the description of the conditions at the external surface of the building envelope, and as they are related to the later case studies, the concepts are introduced.

4.1 Temperature

The microclimatic temperature will be affected by local conditions. On windy days with limited solar radiation, the local variations will be insignificant, and local temperatures will not differ from the temperatures observed under meteorological conditions. On days with high intensity solar radiation, the thermal capacity of e.g. the building envelope will cause a higher temperature in the immediate vicinity of the building. In these cases, local factors such as shielding surroundings will have an effect on the microclimatic temperature as experienced by the surface of the building envelope.

When measuring the air temperature in calm weather situations, the temperature of the air in connection with the sensor may be influenced by radiation exchange. The temperature sensor can be shielded, but the shield itself may have a temperature slighly differing from the 'true' air temperature. The air circulating through the screen spends a finite time in contact with the outer walls and may have its temperature altered thereby. This effect becomes appreciable when the wind is light and the temperature of the outer wall is markedly different from the air temperature. Thus, the temperature of the air in a screen can be expected to be higher than the true air temperature on a day of strong sunshine and calm wind, and slightly lower on a clear, calm night, with errors perhaps reaching +2.5°C and -0.5°C respectively in extreme cases. Additional errors may be introduced by cooling due to evaporation from a wet screen after rain [WMO, 1983]. In a meteorological context, measurements from the roof of a building may lead to errors owing to both the vertical temperature gradient and the influence of the building itself on the temperature. When the objective is to examine the conditions as experienced by the external surface of the building envelope, measurements in connection with the building are instrumental.

In connection with studies of window convection heat transfer, measurement of the temperature profile in the boundary layer is a potential method of describing the processes. Later in this report, a case study on window convection heat transfer is presented.

In the present project, the soil conditions have not been studied. However, the heat conduction to the ground is not significantly affected by the microclimatic factors [Rauhala, 1984].

4.2 Humidity

The air humidity in itself has not been subject to study within the framework of the present project.

The comments on humidity in relation to microclimate are very similar to the comments on temperature of the preceding section. In calm weather situations, the humidity of the local ambient air may be affected by local conditions. The air may be dried by passing heated surfaces, whereas wet areas may cause the air humidity to increase locally. In windy weather, such local variations are expected to be limited.

The ambient air humidity is an important parameter when assessing the condensation risk, e.g. external condensation on well-insulating window panes. The humidity is usually given as either relative humidity or dew point temperature.

In the present work, the relative humidity of the ambient air is measured. Conversion from relative humidity to dew point temperature is carried out, adopting the formulae suggested by Kjerulf-Jensen in [Hansen et al., 1992]. The formulae are given in Appendix III of the present report.

4.3 Long-Wave Radiation

4.3.1 Radiation heat exchange

Radiation is emitted by all substances by virtue of their temperature. Long-wave radiation is often thought of as *heat* radiation. Long-wave radiation, also known as *infrared radiation*, is originating from sources at temperatures near ordinary ambient temperatures and thus substantially all at wavelengths greater than 3 μm. Traditionally, the effects of long-wave radiation have been considered insignificant in terms of heat loss. However, the development of glazing systems with improved thermal performance has led to hitherto unknown problems with external condensation in night-time situations when long-wave radiation is significant. Moreover, the significance of the long-wave contribution to the overall heat balance gains more attention as the development leads to building envelope components with improved thermal insulation performance. In this section, the theoretical basis of long-wave radiation is introduced briefly, the relations to building physical phenomena are discussed, and a survey of the existing literature regarding approximative methods of calculation is given. Finally, measuring methods and instrumentation are described. Note that, in this section, material radiation properties are discussed, regardless that the project in principle does not deal with material aspects. This is owing to the obvious dependency of radiation exchange on material properties.

Emissivity

A solid body emits and absorbs radiation over a continuum of wavelengths. Its surface emissivity varies with wavelength as a function of its material composition and temperature. A black body is an artificial, ideal entity; a substance that absorbs all incident radiation at all wavelengths and from all directions. Since many real surfaces have radiative characteristics which are very similar to those of a black body, this concept represents a useful idealization. Normal substances will reflect or transmit part of the incident radiation. The black body concept is used to express physical laws and as a reference for characterization of real substances, referred to as *grey bodies*. The emissivity[1] is defined as the ratio of radiation emitted by a surface to the radiation emitted by a perfect black body at the same temperature and with the same surroundings. Values range from 1.0 for lampblack down to 0.02 for polished silver. A typical building material has a grey-body emissivity around 0.9.

View factors

The view factors are relative measures of the areas 'seen' by a specific radiating surface. The total view of a point on a surface is described as a hemisphere. Every object, with which the surface is exchanging radiation, has an area defined by two orthogonal angles. The area is determined by integration, and the ratio of this area to the total area of the hemisphere is the view factor. Standard view factor formulae can be found in the literature. Simple instances are the view factor from a horizontal surface to the sky: $F = 1$, corresponding to the full hemisphere; The view factor from a vertical surface to the sky: $F = 0.5$, and the view factor from a vertical surface to the (horizontal) surroundings: $F = 0.5$. In Borlinger [1996], a procedure for calculating view factors for shading objects is described. In a microclimatic context, the view factors become important, as they are a means to correct reference data in order to take local features into account.

[1] The *emissivity* is also known as the *thermal emissivity* or the *emittance*. Duffie and Beckman [1991] use the term emittance. However, as the emittance in thermodynamics signifies *the power radiated per unit area of a radiating surface*, the term emissivity has been adopted in this report.

Radiation between bodies

The radiation exchange between bodies depends on the absolute temperatures, emissivities, the areas and the view factors between the proposed surfaces. Numerous standard formulae describe the exchange depending on these factors. Duffie and Beckman [1991] state the following expression for calculation of radiation between two diffuse surfaces:

$$Q_1 = -Q_2 = \frac{\sigma\left(T_2^4 - T_1^4\right)}{\frac{1-\varepsilon_1}{\varepsilon_1 A_1} + \frac{1}{A_1 F_{12}} + \frac{1-\varepsilon_2}{\varepsilon_2 A_2}}$$

where	Q_x	is the radiation heat exchange from surface 'x'	[W]
	ε_x	is the emissivity of surface 'x'	[-]
	A_x	is the area of surface 'x'	[m²]
	σ	is the Stefan-Boltzmann constant	[5.67×10^{-8} W/m²K⁴]
	T_x	is the absolute temperature of surface 'x'	[K]
	F_{12}	is the view factor between the two surfaces	[-]

Black body in enclosure

The view factors described above are used to quantify the radiation exchange between any number of objects. In situations where the one object can be considered *large*, the problem is reduced as follows. Radiation between a small convex object (surface 1) surrounded by a large enclosure (surface 2) can be described by

$$Q_1 = \varepsilon_1 A_1 \sigma\left(T_2^4 - T_1^4\right)$$

where	Q_1	is the radiation heat transfer	[W]
	ε_1	is the emissivity of surface 1	[-]
	A_1	is the area of surface 1	[m²]
	σ	is the Stefan-Boltzmann constant	[5.67×10^{-8} W/m²K⁴]
	T_x	is the absolute temperature of surface 'x'	[K]

This result is independent of the surface properties of the large enclosure since virtually none of the radiation leaving the small object is reflected back from the large enclosure. In other words, the large enclosure absorbs all radiation from the small object and acts like a black body. The equation applies to a flat plate radiating to the sky [Duffie and Beckman, 1991]. These theoretical relationships work well in simple cases, whereas successful implementation in a microclimatic context demands a series of assumptions regarding factors such as temperature and geometry of the surroundings.

4.3.2 Atmospheric radiation phenomena

In this paragraph, the basic theory of atmospheric radiation is introduced to yield a basis for the description of the building physical issues.

Radiation quantities

Only long-wave radiation is discussed in this section, but as the discussion will benefit from an initial general perspective, the long-wave radiation is briefly related to the other meteorological radiation quantities. Meteorological radiation quantities may be classified into two groups

according to origin, i.e. solar radiation and terrestrial radiation. WMO [1983] give the following description of the quantities.

Solar radiation is the electromagnetic radiation of the sun. The solar radiation incident on the terrestrial atmosphere is called extraterrestrial solar radiation. 97% of this radiation is confined to the spectral range 0.29 μm to 3.0 μm and is called short-wave radiation. Part of this extraterrestrial solar radiation penetrates through the atmosphere to the surface of the earth, while part of it is scattered and/or absorbed by the gas molecules, aerosol particles, cloud droplets and cloud crystals in the atmosphere.

Terrestrial radiation is the long-wave radiation emitted by the earth's surface and by the gases, aerosols and clouds of the atmosphere; it is also partly absorbed within the atmosphere. For a temperature of 300 K, 99.99% of the power of the terrestrial radiation has a wavelength longer than 3 μm and about 99% longer than 5 μm. For lower temperatures, the spectrum is shifted to longer wavelengths.

Since the spectral distributions of solar and terrestrial radiation overlap very little, they can very often be treated separately in measurements and computations.

Light is the radiation visible to the human eye. The spectral range of visible radiation is defined by the spectral luminous efficiency for the standard observer. Thus, 99% of the visible radiation lies between 400 nm and 730 nm. Radiation of wavelengths shorter than 400 nm is called ultraviolet, and longer than 730 nm, infrared radiation.

Short-wave solar radiation is briefly dealt with in Section 4 of this chapter, whereas ultraviolet radiation is not considered in this report.

Composition of the atmosphere

The way the atmosphere absorbs and emits radiation is determined by its composition and by the properties of its component gases. Because the atmosphere is primarily composed of gaseous substances, it absorbs and emits long-wave radiation in spectral bands characteristic of the constituent molecules. Virtually all long-wave emission from the atmosphere is due to water vapour, carbon dioxide, and, to a lesser extent, ozone. Nitrogen and oxygen gases are transparent throughout this region.

Molecules in the atmosphere, chiefly CO_2 and H_2O, not only absorb solar radiation but also absorb radiation from earth's surface. The radiation emitted by surfaces on earth is from sources at 250 to 320 K, producing radiation of wavelengths from about 4 to 40 μm, with the peak at about 10 μm [Mills, 1992].

Atmospheric emission and absorption is mainly at wavelengths of 5 to 8 μm and above 13 μm; This radiation is not distributed like black-body radiation. The region of low atmospheric radiance between approximately 8 and 12 μm is known as the *atmospheric window*, since low emissivity gives rise to high transmissivity. Much of the radiant energy from the earth's surface passes into outer space within this spectral region. If low clouds obscure the sky, the window vanishes, so that the observed incident long-wave sky radiation approximates the black-body distribution. The base of the clouds is usually heated by the atmospheric layers underneath and by the surface of the earth , which are both usually warmer than the clouds.

Long-wave radiation emitted from the base of a cloud, or the surface of the earth, reasonably approximates black-body radiation, provided that the radiating surface has a uniform

temperature (typically in the range of 240-310 K). Such radiation is often referred to as *terrestrial radiation* to distinguish it from the *solar radiation* produced in the 6000 K temperature region at the surface of the sun.

4.3.3 Building physics and long-wave radiation

Heat loss
The general radiation balance at the building surface may be written as

$$q_{r,net} = \alpha G + \varepsilon L - \varepsilon \sigma T_s^4$$

Where	$q_{r,net}$	is the net radiance at the building surface	[W/m²]
	L	is the incident long-wave radiance	[W/m²]
	G	is the incident solar radiance	[W/m²]
	α	is the solar absorptivity	[-]
	ε	is the long-wave emissivity of the surface	[-]
	σ	is the Stefan-Boltzmann constant	[5.67×10^{-8} W/m²K⁴]
	T_s	is the surface temperature	[K]

During daytime, the solar radiation dominates, but during night-time the long-wave radiation becomes significant, particularly under clear sky conditions. Since long-wave radiation from the external surface of the building surface is not compensated by counter-radiation from sky and surroundings, the result is a long-wave heat loss from the building. The long-wave radiation heat loss from windows can be limited by means of a low-emissivity coating on the window pane.

Surface orientation
An external surface of a building envelope will exchange long-wave radiation with sky and surroundings depending on the view factors. A horizontal surface, for instance a flat roof, only exchanges long-wave radiation with the sky, whilst a vertical surface exchanges radiation with both sky and surroundings.

The long-wave sky irradiation on a horizontal plane can be determined by measurement, taken from a reference year or calculated employing empirical relationships. The conversion into an atmospheric component of the irradiation on an inclined surface is a geometrical matter. The ground component is usually determined under the assumption, that the surroundings act as a black-body radiator at ambient air temperature.

Surface inclination becomes less significant under overcast conditions, as the cloud temperature is close to the temperature of the air and the surroundings. Under clear sky conditions, however, the inclination is greatly significant as the counter-radiation from the sky is reduced.

The radiative energy balance with the atmosphere is more negative for a horizontal surface than for a vertical surface. The fact that counter-radiation is greater from the surroundings than from the sky means that a horizontal surface will have a lower temperature than a vertical surface during *night-time undercooling*, that is when then temperature of the surface is lower than the ambient air temperature owing to long-wave radiation.

Material properties
All bodies with a surface temperature above zero radiate energy with wavelengths that depend on the body surface temperature. Each facet of a surface emits rays in straight lines at right

angles to the facet. The surface of concrete is covered with numerous facets, giving off radiant energy. Polished steel or similar surfaces have no such facets. Thus, a rough surface radiates heat more efficiently than a polished surface [ASHRAE, 1995].

The normal long-wave emissivity ε_0 of a building surface is defined as the wavelength-independent emissivity of an equivalent grey surface, which has the same emissive power as the building surface.

The relation between reflectivity and emissivity is given by Kirchhoff's law, i.e. $\varepsilon = 1 - \rho$ for opaque materials and $\varepsilon = 1 - \rho - \tau$ for transparent materials. For most building materials the long-wave emissivity can be regarded equal to the long-wave absorptivity.

In the following table, some examples of these radiation material properties are given according to Zürcher et al. [1982]. The emissivity has been calculated for a surface temperature of 300 K. It can be assumed that ε_0 does not depend on the temperature. The absorptivity α_s for solar radiation of a material is defined as the absorptivity of an equivalent grey surface which absorbs the same amount of solar radiation.

Facade material	α_s	τ_s	ε_0
Concrete smooth	0.55	-	0.96
Face brick	0.54	-	0.93
Roof tile brown	0.76	-	0.94
Aluminium anodised	0.33	-	0.92
Aluminium conversion coated (Cr)	0.33	-	0.07
Aluminium with black nickel	0.87	-	0.10
Float glass (6 mm)	0.12	0.81	0.91
Solar control window, Calorex A2	0.41	0.36	0.91
Glass with In_2O_3:Sn (14Ω)	0.17	0.71	0.34
Glass with Au (100 Å)/SiO_2	0.32	0.35	0.10
Glass with TiO_2/Ag (200 Å) /TiO_2	0.11	0.21	0.03
Glass with Cu (100 Å) /SiO_2 (500 Å)	0.34	0.36	0.05

Table 4.1 Averages of solar absorptivity α_s, solar transmittance τ_s and (normal) long-wave emissivity ε_0, of selected facade materials [after Zürcher et al., 1982].

Zürcher et al. [1982] state that considerable reduction of heat losses from buildings can be achieved by means of weather resistant, long-wave mirror coating of the external surface of the envelope. At the same time, the envelope should be absorbing or transparent in the visible and short-wave regions in order to utilize passive solar heat gain. Zürcher et al. found that the energy consumption could be reduced by up to 20% for single-family houses, and by up to 12% for apartment houses in central Europe.

4.3.4 Approximative quantities

Equivalent radiation temperature
An approach that is occasionally used is to define an effective sky temperature, T_{sky}, assuming that the sky emits radiation like a black body. The effective sky temperature is always lower than the air temperature. When there is a low cloud cover we may assume $T_{sky} \approx T_a$ [Mills, 1992].

An effective sky temperature may be defined as the temperature attained by a black body in radiative equilibrium with the sky. While this may be a useful definition for some purposes, it should be emphasized that the spectral distribution of radiation received from the sky does not closely resemble the distribution for black-body radiation except under heavy overcast conditions [IEA, 1980].

The sky can be considered as a black body at some equivalent sky temperature T_{sky} so that the actual net radiation between a horizontal flat plate and the sky is given by the equation for radiation between a small convex object surrounded by a large enclosure [Duffie and Beckman, 1991]. Hence, the net radiation from a surface to the sky:

$$Q_{r,loss} = \varepsilon A \sigma \left(T_s^4 - T_{sky}^4 \right)$$

Where	$Q_{r,loss}$	is the net long-wave radiation from surface to sky	[W]
	ε	is the long-wave emissivity of the surface	[-]
	A	is the area of the surface	[m²]
	σ	is the Stefan-Boltzmann constant	[5.67×10^{-8} W/m²K⁴]
	T_s	is the absolute temperature of the surface	[K]
	T_{sky}	is the equivalent black-body sky temperature	[K]

This equivalent black-body sky temperature accounts for the facts that the atmosphere is not at a uniform temperature and that the atmosphere radiates only in certain wavelength bands. The atmosphere is essentially transparent in the wavelength region from 8 to 14 μm, but outside of this 'window' the atmosphere has absorbing bands covering much of the infrared spectrum [Duffie and Beckman, 1991].

Berdahl and Martin [1984] used extensive data from the United States to relate the effective sky temperature to the dew point temperature, dry-bulb temperature, and hour from midnight, n, by the following equation, valid for clear sky conditions:

$$T_{sky} = T_a \sqrt[4]{0.711 + 0.0056 t_{dp} + 0.000073 t_{dp}^2 + 0.013 \cos\left(2\pi \frac{n}{24} \right)}$$

Where	T_{sky}	is the black-body sky radiation temperature	[K]
	T_a	is the ambient dry-bulb temperature	[K]
	t_{dp}	is the ambient dew point temperature	[K]
	n	is the hour from midnight	[-]

The experimental data covered a dew point range from -20°C to 30°C. The range of the difference between sky and air temperatures is from 5K in a hot, moist climate to 30K in a cold, dry climate.

Lund [Hansen et al., 1992]
Lund points out that the short-wave radiation will dominate during daytime, but that during night-time, the long-wave radiation should be considered when calculating heat loss. The surface of the ground, nearby buildings or clouds at low altitudes are assumed to be at the same temperature as the air. The long-wave radiation is approximated by introducing an equivalent radiation temperature as 'seen' by the surface. The simple formulae are as follows:

Horizontal surface:

$$t_{rad} = 1.2 \cdot t_a - 14$$

Vertical surface:

$$t_{rad} = 1.1 \cdot t_a - 5$$

Where	t_{rad}	is the radiation temperature	[°C]
	t_a	is the ambient air temperature	[°C]

If the cloud cover is N *okta*[2], interpolation is made by the expression:

$$t_{rad,N} = \frac{(8-N) \cdot t_{rad} + N \cdot t_a}{8}$$

The relative share between the radiation to the sky and the radiation to the surroundings is given by the view factors. The effective radiation temperature T_{rad} (K) with which a tilted surface exchanges long-wave radiation is calculated as [Geving, 1997]:

$$T_{rad} = \frac{1+\cos(\gamma)}{2} \cdot T_{sky} + \frac{1-\cos(\gamma)}{2} \cdot T_a$$

Where	T_{rad}	is the effective radiation temperature of sky and surroundings	[K]
	T_{sky}	is the equivalent sky temperature	[K]
	T_a	is the ambient air temperature	[K]
	γ	is the surface tilt angle	[°]

For a vertical surface the view factors are 0.5/0.5 if no obstacles are taken into account. Thus, the effective radiation temperature of sky and surroundings for a vertical surface is given by

$$T_{rad} = \frac{T_{sky} + T_a}{2}$$

This simple geometric formulae does not take into account cases where the surroundings are higher than the construction, e.g. with high neighbouring buildings. Routines for the calculation of shading effects will have to be applied for this kind of problem. Borlinger [1996] suggests a method for including the effect of partial shading of long-wave radiation to the sky.

[2] Cloud cover is reported in *oktas*, as the sky is divided into 8 parts by the observer. 0 okta thus denotes clear sky conditions, and 8 okta denotes overcast conditions.

Equivalent sky emissivity
For engineering calculations, it is possible to approximate the emission from the atmosphere or sky as a fraction of black-body radiation corresponding to the temperature of the air near the ground, T_a. The sky emissivity ε_{sky} is defined such that the sky radiosity is [Mills, 1992]:

$$J_{sky} = \varepsilon_{sky} \sigma T_a^4$$

Where	J_{sky}	is the sky radiosity	[W/m²]
	ε_{sky}	is the sky emissivity	[-]
	σ	is the Stefan-Boltzmann constant	[5.67×10^{-8} W/m²K⁴]
	T_a	is the ambient air temperature	[K]

Based on data obtained at a number of locations in the United States, Berdahl and Fromberg [1982] found the following correlations for clear sky conditions:

Night-time:

$$\varepsilon_{sky} = 0.741 + 0.0062 \cdot t_{dp}$$

Daytime:

$$\varepsilon_{sky} = 0.727 + 0.0060 \cdot t_{dp}$$

Where	ε_{sky}	is the sky emissivity	[-]
	t_{dp}	is the dew point temperature	[°C]

Berdahl and Martin [1984] suggest the following, alternative formula for determination of the equivalent sky emissivity for clear sky conditions:

$$\varepsilon_{sky} = 0.564 + 0.059\sqrt{p_v}$$

Where	ε_{sky}	is the equivalent sky emissivity	[-]
	p_v	is the water vapour pressure of the ambient air	[mbar]

Cloud cover has a strong effect on atmospheric radiation, but the effect decreases in importance with cloud elevation because higher clouds are usually colder that low clouds.

4.3.5 Measuring technique and instrumentation

The incident long-wave radiation can be measured either indirectly or directly. Indirectly by measuring the total radiation (pyrradiometer) and the global radiation (diffuse and beam solar radiation, pyranometer). The long-wave radiation is found as the difference between these two radiation quantities. The incident long-wave can be measured directly by means of a pyrgeometer. A pyrgeometer is equipped with a filter which does not transmit short-wave radiation (0.3-3.0 μm). Pyrgeometers without such a filter can be used for night-time measurements.

The pyrgeometer is based on a thermal detector. The temperature of the sensor expresses the long-wave radiation balance. When the emissivity and the temperature of the sensor is known, the incident long-wave radiation can be determined, given that the convection and conduction is

eliminated or reduced and known. The convection heat loss is usually eliminated by the filter, which works as a shield. The pyrgeometer should measure (or 'see') as much of the hemisphere as possible. A desiccant is usually placed in the instrument to prevent internal condensation.

Pyrradiometers and pyrgeometers are generally installed at a site which is free from obstructions, or at least having no obstruction with angular size greater than 5° in any direction which has a low sun angle at any time during the year [WMO, 1983].

In general, the source will not be uniformly distributed over the sky. This indicates that the instrumentation should obey the Lambert's law[3] (cosine response) as close as possible because corrections can not be made [IEA, 1980].

Since all bodies emit long-wave radiation at normal temperatures, the radiation from the components constitutes one of the most significant error sources in the system.

Chapter 7 of the present report is a presentation of a case study, in which selected, approximate quantities are compared with short duration measurement series. Chapter 8 describes a study of window convection heat transfer, encompassing measurements of incident long-wave radiation.

[3] Lambert's cosine law: Law stating that the energy emitted from a perfectly diffusing surface in any direction is proportional to the cosine of the angle which that direction makes with the normal.

4.4 Solar Irradiation

The solar radiation has not been studied in the context of the present project. For completeness, and since the solar radiation clearly constitutes an important parameter in relation to the conditions at the external surface of the building envelope, the aspect is briefly commented below.

The meteorological parameters in terms of solar radiation are traditionally given for a horizontal surface as beam (direct) radiation, diffuse radiation and diffuse radiation reflected from the surroundings. Conversion of these three components into microclimatic data is carried out by correction for shading objects. Two types of shading objects are considered, namely *near* and *far*, relative to the specific surface.

Far shading objects are hills, neighbouring buildings, trees and other objects away from the considered building. Near shading objects are features of the building geometry such as canopies and other projecting parts of the surface.

The Design Reference Year gives a detailed set of solar data. Modification of such global data into microclimatic parameters is to some extent a geometrical task. Some of the fundamental radiation theory is given in the preceding section on long-wave radiation, where the solar radiation is also briefly commented in relation to atmospheric radiaton quantities. For a thorough description of solar radiation phenomena, referral is made to Duffie and Beckman [1991].

4.5 Driving Rain

In this section, the concept of airfield driving rain is described, and the calculation of the airfield driving rain as a function of wind speed and normal precipitation is presented as proposed by Lacy [1965, 1977]. In Chapter 7, measurement of driving rain is treated as a case study. A measure to characterize the driving rain exposure, the Driving Rain Index, is described in Chapter 9, where driving rain is discussed in connection with weather data for hygrothermal simulations.

Driving rain is an important moisture source in climates with frequent rain and wind. When the water in the shape of driving rain strikes a wall and the moisture is forced through the building envelope, either through the surface of the wall itself or through openings (windows, joints etc.), it is referred to as a *driving rain effect*, or *rain penetration*. The phenomenon is called rain penetration, regardless if the penetrating water is visible at the inner surface of the construction or not.

4.5.1 Airfield driving rain

Definition: In this context, Driving Rain is defined as rain drops with a horizontal velocity component due to simultaneous wind. The Driving Rain Intensity is the rate of these drops striking a vertical plane, e.g. a building surface. The CIB[4] has defined the driving rain as the *precipitation striking the surface of a vertical wall due to impact of wind* [Schwarz and Frank, 1973].

Numerous attempts have been made to establish a correlation between climate parameters and resulting driving rain. The problem is complicated due to the many variables and their interdependency. The local (micro) climate around a building is created as an interaction between meteorological influences and local characteristics such as topography, building geometry and obstacles. Calculation of the resulting driving rain impinging onto a given surface, therefore, has to be based on a set of simplifying assumptions. Researchers have suggested different empirical relationships. The details of the expressions vary, but usually they are based on correlation between drop size and thus terminal velocity, and normal rate of rainfall (on a horizontal surface). Normally only airfield driving rain is considered.

The exposure to driving rain varies due to the local features and the intrinsic nature of the microclimate around built structures. In order to yield a measure of common validity when estimating intensities of driving rain, the *airfield driving rain* has been defined. The airfield driving rain is sometimes referred to as the *free driving rain* and can be thought of as a driving rain potential. The airfield driving rain expresses the driving rain that would occur with standard exposure[5]. It must be stressed that this is a theoretical rate, assuming no deflection of the wind or the drops.

[4] CIB: Conceil International du Batiment pour la Recherche, l'etude et la Documentation.

[5] The standard exposure of wind instruments over level, open terrain is ten metres above the ground. Open terrain is defined as an area where the distance between the anemometer and any obstruction is at least ten times the height of the obstruction [WMO, 1983].

4.5.2 Calculation of airfield driving rain

Assuming that the horizontal component of the raindrop velocity equals the wind speed, a geometrical consideration yields that the ratio of the driving rain to the normal rainfall corresponds to the ratio of the wind speed to the vertical velocity of the rain drops.

$$\frac{r_v}{r_h} = \frac{u}{u_t} = \tan\xi$$

Where	r_v	is the rain intensity in the vertical plane - the driving rain intensity	[mm]
	r_h	is the rainfall intensity in the horizontal plane	[mm]
	u	is the wind speed	[m/s]
	u_t	is the terminal velocity of the raindrop	[m/s]
	ξ	is the angle of attack in the vertical plane	[°]

Sneyers et al. [1979] derive the relation in the following manner:

A raindrop with the vertical falling velocity u_t, exposed to the wind speed u, will have a resulting velocity with a magnitude, which can be approximately determined by means of Pythagoras' theorem:

$$u_R = \sqrt{u_t^2 + u^2}$$

Where	u_R	is the resulting velocity of the raindrop	[m/s]
	u	is the wind speed	[m/s]
	u_t	is the terminal velocity of the raindrop	[m/s]

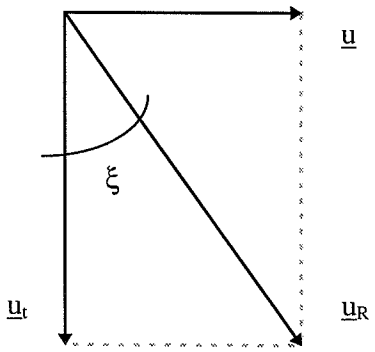

Figure 4.1 Raindrop with terminal velocity $\underline{u}_t$ exposed to wind speed $\underline{u}$. Resulting velocity $\underline{u}_R$. Angle of attack in vertical plane ξ.

In Figure 4.2, an amount of driving rain, D, is positioned inside an imaginary cylinder with cross-section Ω and longitudinal axis parallel to $\underline{u}_R$.

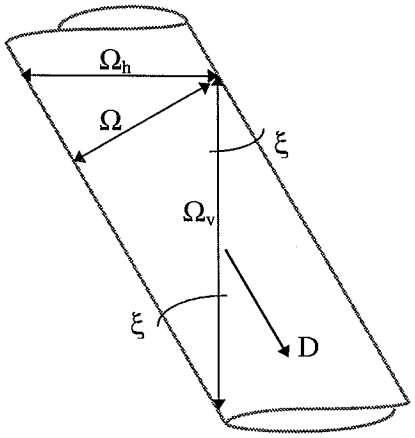

Figure 4.2 Driving rain amount D in imaginary cylinder with cross-section Ω and longitudinal axis parallel to the resulting raindrop velocity $\underline{u}_R$ [adopted from Sneyers et al., 1979].

Vertical and horizontal cross-section of the cylinder are Ω_v and Ω_h respectively. The area of an ellipse with short axis 2a and long axis 2b, is $A = \pi ab$. Hence, the following relationship:

$$\frac{\Omega_h}{\Omega_v} = \frac{u}{u_t}$$

Where	Ω_v	is the vertical cross-section of the cylinder	[m²]
	Ω_h	is the horizontal cross-section of the cylinder	[m²]
	u	is the wind speed	[m/s]
	u_t	is the terminal velocity of the raindrop	[m/s]

- as the ellipses Ω_v and Ω_h have the same short axis (i.e. the diameter of the cross-section Ω).

The flux of driving rain is the same through the cross-sections Ω, Ω_v and Ω_h. If this were not the case, water would accumulate in the considered volume.

This yields, as the amount of driving rain is given as the product of intensity and area:

$$r_v\Omega_v = r_h\Omega_h \Rightarrow r_v = r_h\frac{\Omega_h}{\Omega_v} \Rightarrow r_v = r_h\frac{u}{u_t}$$

Where	r_v	is the driving rain intensity	[mm]
	r_h	is the rain intensity in the horizontal plane	[mm]
	Ω_v	is the vertical cross-section of the cylinder	[m²]
	Ω_h	is the horizontal cross-sectional area of the cylinder	[m²]
	u	is the wind speed	[m/s]
	u_t	is the terminal velocity of the raindrop	[m/s]

In the following, this equation is referred to as the *original driving rain equation.*

The terminal velocity of a falling raindrop, u_t, depends on the drop size and is described in terms of the drop diameter. In 1950, Best's work led to the following correlation [Best, 1950; Lyberg, 1979].

$$u_t = 9.55\left(1 - \exp\left[-1.15 r_{eq}^{1.147}\right]\right)$$

Where	u_t	is the terminal velocity of the raindrop	[m/s]
	r_{eq}	is the equivalent radius of the drop	[mm]

Rain events often differ considerably and may not seem comparable, but the drop size distribution shows a pronounced pattern. On average, the distribution of drop sizes shows a marked peak corresponding to a dominant size of raindrops. The more intense the rainfall, the bigger the dominant raindrops [Lacy, 1977].

Half the volume of the rain is made up of drops with a diameter exceeding the median value d_{50}. In 1943, Laws and Parsons developed an empirical relationship between the median drop size and the rate of rainfall [Laws and Parsons, 1944; Lacy, 1977].

$$d_{50} = 1.238 r_h^{0.182}$$

Where	d_{50}	is the median drop size	[mm]
	r_h	is the rain intensity in the horizontal plane	[mm]

Combining the equations above, the terminal velocity of the raindrops can be expressed as a function of the rainfall intensity in the horizontal plane as follows [Lacy, 1977]:

$$u_t = 4.505 r_h^{0.123}$$

Where	u_t	is the terminal velocity of the raindrop	[m/s]
	r_h	is the rain intensity in the horizontal plane	[mm]

This expression for the terminal velocity is now inserted into the *original driving rain equation* yielding:

$$r_v = 0.222 u r_h^{0.88}$$

Where	r_v	is the driving rain intensity	[mm]
	r_h	is the rain intensity in the horizontal plane	[mm]
	u	is the wind speed	[m/s]

Assumptions

- *No deflection of wind or of the raindrops*
- *The wind speed is perpendicular to the (imaginary) surface at all times*
- *All raindrops have the median drop size given by the normal rainfall intensity*

The theory described above was proposed by Lacy. Other proposals have been made, but they are very similar. Again, it is important to note, that the airfield driving rain, as calculated using the expressions above, is a purely theoretical rate which should be thought of as a driving rain

potential. Variations will occur dependent on specific features of the location considered: site exposure, positioning on a building geometry et cetera.

4.5.3 Spatial distribution

The spatial distribution of driving rain over the building geometry is a complex matter. Whereas the airfield driving rain results from a combination of wind and precipitation, the driving rain striking a building surface is a result of precipitation and the air flow around the building geometry. The approaching wind will be deflected, and the flow will be forced around the building. The droplets being carried along by the wind will drop out of the flow and strike the surface of the building.

Not many measurements of driving rain have been carried out over the years. Furthermore, the results of such driving rain measurements have a validity which is restricted to very local conditions and a specific geometry. There is a pronounced need for more data for calibration of calculation routines and approaches based on application of Computational Fluid Dynamics.

It is therefore cumbersome to convey a state-of-art regarding the spatial distribution of driving rain over building geometries. In general, however, it is found that the *highest intensities occur near the edges, and in particular at the upper corners*. This is due to the wind velocity gradient at the edges, causing the droplets to drop out of the flow because of their momentum. The shape of the building is of great significance, as well as obstacles and the topology of the surroundings.

The British standard BS 8104 [BSI, 1992] gives a set of correctional factors as a rough estimate of the distribution, depending on building geometry, and characterizing the influence of surroundings and topology. The guidelines of the BS 8104 have recently been proposed as a working draft by the CEN/TC 89 in a slightly edited version [CEN/TC 89, 1998]. As part of the present project, the principles of the BS 8104 have been combined with meteorological data in a task called METREC - Meteorological Test Reference Year of Copenhagen. The METREC-work is described in Chapter 9.

Selected examples of measurements and surveys on the subject: Lacy [1965, 1977], Schwarz and Frank [1973], Beijer and Johansson [1976], Lyberg [1977, 1979], Prior [1985], Sandin [1987] and Flori [1988].

4.5.4 Measurement of driving rain

As mentioned above, there is a pronounced need for driving rain data. The measurement methods have remained virtually unchanged from the early driving rain research in the 1950s until recently. In Chapter 6, a study of driving rain measurement is presented and the measurement principles are described. An important part of the present work has dealt with the possible improvement of driving rain measurement principles.

4.5.5. CFD modelling

Increasing computer capacity has made simulation of complex fluid dynamics problems possible, thus making way for novel applications such as the modelling of driving rain. The theory of Computational Fluid Dynamics (CFD) is comprehensive and will not be described in the present report. However, since the CFD methods represent a relatively new potential for parameter studies, some general remarks are given in the following.

In connection with the present project, some exercises were carried out employing the commercially available program CFX4.1[6]. The program is based on a finite volume method, turbulence can be modelled by means of the *K-ε model* and the geometry is modelled in 2D or 3D by means of a multi-block, structured mesh.

When modelling a building, the computational domain must be large in order to eliminate, or minimize, the effects of the building geometry on the flow at the boundaries. The flow at the boundaries should not be affected by the building geometry. In the literature, the methods of modelling driving rain vary. As a boundary condition, the upstream velocity profile is usually assumed to be logarithmic.

Droplets are subsequently introduced into the fully developed flow, and particle tracking methods are used to model the trajectories of the droplets. The droplets can thus be traced from the undisturbed airfield onto the building envelope.

The ratio of the undisturbed airfield precipitation to the impinging driving rain is defined as the catch ratio. Turbulent dispersion of the droplets is usually neglected. The trajectories of the droplets depend on their size. The dropsize distribution thus becomes an important issue.

One of the major tasks in performing CFD modelling is the grid generation, which can be cumbersome and time consuming. A problem is the relation between the large domain and the need for fine mesh around the building geometry in order to resolve the flow near the building. Asymmetric cells will lead to inaccuracy.

The lacking knowledge of the driving rain dropsize distribution, the simplified boundary conditions and the gridding are the main limitations of the method. Development of the commercially available programs will lead to improvement of the user interfaces, which will undoubtedly facilitate the studies considerably. Gradually, the programs will be able to simulate still more complex problems. Grid generation is being developed to ease the modelling and to optimize the grids by defining areas of high resolution. However, the accuracy of the method will always depend on the assumptions introduced by the user, such as the boundary conditions.

Measurement data are needed for the calibration of these methods; both data describing the spatial distribution of the driving rain as a function of building shape, reference wind and precipitation and data describing the dropsize distribution of the driving rain.

The application of CFD tools is limited, due to the complexity of the simulations. Initially the methods themselves have to be refined and corroborated by measurements. Hence, the methods may yield a basis for computation of catch ratios based on parameter variations.

Selected examples of computational studies: Rodgers et al. [1974], Karagiozis and Hadjisophocleous [1995], Mook et al. [1997], Sankaran and Paterson [1997] and Choi [1993, 1994a, 1994b, 1997].

[6] CFX-F3D Version 4.1 Flow solver by AEA Technology.

4.6 Air Velocity

The reference wind observed under standard meteorological conditions differ considerably from the conditions experienced at the external surface of the building envelope. The air will flow around the building, depending on topology of the surroundings, obstacles and the geometry of the building itself. The microclimatic air flow results from the meteorological wind (speed and direction), the characteristics of the location and the position on the building geometry.

The wind does not have a great influence on the convection heat loss from normal buildings. The influence on energy consumption takes place in the shape of infiltration and ventilation losses. Rauhala [1984] states that the obstacles surrounding a building have a greater influence on the energy consumption than has the orientation of the building.

The wind has a significant effect on the microclimate, in particular in terms of condensation phenomena and driving rain. Furthermore, wind pressure is the reason for rain penetration through cracks and joints.

The wind has not specifically been subject to study as part of the present project, although it has been studied in relation to convection heat transfer and driving rain.

The meteorological wind speed can be modelled by the logarithmic wind profile [Bottema, 1992]:

$$u(z) = \frac{u_*}{\kappa} \ln\left(\frac{z}{z_0}\right)$$

Where	$u(z)$	is the wind speed at height z	[m/s]
	u_*	is the friction velocity	[m/s]
	κ	is the Von Karman constant	[0.4]
	z	is the height	[m]
	z_0	is the aerodynamic roughness length	[m]

Above, the thermal stability correction has been neglected.

Combined with the roughness length, the friction velocity characterizes the flow in terms of surface shear stress. The logarithmic law provides a basis for rough estimates of the wind speed as a function of height. A roughness length of 0.03 m corresponds to *open terrain*, i.e. level country, with low vegetation (grass). For estimative purposes, the friction velocity can be determined on the basis of a known reference wind speed and an approximate roughness length.

E X A M P L E : Reference wind speed u(10 m) = 10 m/s (in standard height, z = 10 m), roughness length z_0 = 0.03 m (grass). The friction velocity is found to be

$$u(z) = \frac{u_*}{\kappa} \ln\left(\frac{z}{z_0}\right) \Rightarrow 10 = \frac{u_*}{0.4} \ln\left(\frac{10}{0.03}\right) \Rightarrow u_* \approx 0.7 \text{ m/s}$$

An estimate of the wind speed in 15 meters height would thus be

$$u(15\text{m}) = \frac{0.7}{0.4} \ln\left(\frac{15}{0.03}\right) \approx 11 \text{ m/s}$$

Bottema [1992] presents a comprehensive study on wind climate and urban geometry, and gives values for roughness length, depending on landscape description. Bottema moreover describes the fundamental theory of wind calculation in the atmospheric boundary layer and the use of CFD for such purposes. Kobysheva [1992] (WMO) gives guidelines for estimation of wind loads.

Air flow around buildings is traditionally studied by means of scaled model tests in wind tunnel facilities. Such experiments are, however, rather expensive and the use of CFD methods, briefly discussed in the driving rain section above, constitutes a less costly alternative, which is still being developed.

The measurements of driving rain, presented in Chapter 6, and the measurements of window convection heat transfer in Chapter 8, encompass measurements of reference wind speed and direction, which may serve to illustrate specific wind variation patterns.

4.7 Convective Heat Transfer

As mentioned in the introduction to this chapter, a brief description of the fundamental theory of convective heat transfer has been included in the microclimate chapter. The previous parts of the chapter deal with climatic factors, wheras the convection heat transfer is a process involving several climatic factors. The theory has been included because it constitutes an important aspect related to the microclimatic phenomena at the external surface of the building envelope. Furthermore, the theory is related to a study of window convection heat transfer, presented in Chapter 8.

4.7.1 Fundamentals

Heat transfer caused by fluid motion is called *convective heat transfer*, or simply *convection*. A temperature difference between fluid and surface will result in a heat transfer depending on the flow. The convective heat transfer coefficient is defined as follows.

$$q_{conv} = h_c(t_s - t_a) = h_c \Delta T_a$$

Where	q_c	is the convection heat flux	[W/m²]
	h_c	is the convective heat transfer coefficient	[W/m²K]
	t_s	is the surface temperature	[°C]
	t_a	is the ambient fluid temperature	[°C]
	ΔT_a	is the temperature difference, surface-fluid	[K]

As the heat transfer is taking place in the boundary layer, h_c is also referred to as the convective film coefficient.

Depending on the character of the flow governing the convection, three types of convection can prevail, namely

- Forced convection,
- Natural convection and
- Mixed convection

Forced convection is produced by some external source, e.g. wind or ventilation. Natural convection is produced by buoyancy forces due to temperature differences. Mixed convection is a combination of forced and natural convection.

The convection heat transfer depends closely on the nature of the fluid flow. In the following it is assumed that the fluid is air, but the considerations apply for any fluid. The flow is characterized by dimensionless groups. These groups yield important measures, as the flow characteristics of situations with similar dimensionless groups are comparable, in spite of differing geometrical configurations. In particular, this is useful when conducting scaled experimental work.

Nusselt number, Nu

The Nusselt number is a dimensionless heat transfer coefficient. Calculation of the convective heat transfer consists in determination of the heat transfer coefficient for given conditions.

$$Nu = \frac{h_c L}{\lambda_{fluid}}$$

Where	Nu	is the Nusselt number	[-]
	h_c	is the convection heat transfer coefficient	[W/m²K]
	L	is the characteristic length of the surface	[m]
	λ_{fluid}	is the thermal conductivity of the fluid	[W/mK]

Prandtl number, Pr

The Prandtl number characterizes the transport media by both forced and natural convection, and is given as the ratio of the molecular diffusivity to the thermal diffusivity of the fluid.

$$Pr = \frac{c_p \mu}{\lambda_{fluid}} = \frac{\nu}{\alpha}$$

Where	Pr	is the Prandtl number	[-]
	c_p	is the specific heat at constant pressure (fluid)	[J/kgK]
	μ	is the viscosity (dynamic, fluid)	[kg/ms]
	λ_{fluid}	is the thermal conductivity of the fluid	[W/mK]
	ν	is the kinematic viscosity (fluid)	[m²/s]
	α	is the thermal diffusivity (fluid)	[m²/s]

Often, the Prandtl number is determined at a reference temperature, T_m, of the transporting media. This reference temperature is referred to as the *mean film temperature* [Mills, 1992].

$$T_m = \frac{T_s + T_a}{2}$$

Where	T_m	is the mean film temperature	[K]
	T_s	is the surface temperature	[K]
	T_a	is the ambient fluid temperature	[K]

Reynolds number, Re

In case of forced convection, the Reynolds number tells whether the flow is laminar or turbulent. The Reynolds number is the ratio of the inertia to the viscous forces.

$$Re_L = \frac{u_\infty L}{\nu}$$

Where	Re_L	is the Reynolds number (length or height, L)	[-]
	u_∞	is the free stream velocity	[m/s]
	L	is the characteristic length of the surface	[m]
	ν	is the kinematic viscosity (fluid)	[m²/s]

Grashof number, Gr

When the convection is natural with Pr ~ 1 (gas), the Grashof number tells whether the flow is laminar or turbulent. The Grashof number is the ratio of the buoyancy forces to the viscous forces.

$$Gr_L = \frac{\beta \Delta T g L^3}{\nu^2} = \frac{\Delta T g L^3}{T_m \nu^2}$$

Where	Gr_L	is the Grashof number (length or height, L)	[-]
	β	is the coefficient of thermal expansion	[K^{-1}]
	ΔT	is the temperature difference, T_s - T_a	[K]
	g	is the gravitational acceleration	[9.81 m/s²]
	L	is the characteristic length/height of the surface	[m]
	ν	is the kinematic viscosity (fluid)	[m²/s]
	T_m	is the mean film temperature	[K]

For a gas, $\beta \approx 1/T_m$ yields an adequate approximation.

Rayleigh number, Ra

In case of natural convection with Pr >> 1, the Rayleigh number tells whether the flow is laminar or turbulent.

$$Ra = Gr_L \cdot Pr$$

Where	Gr_L	is the Grashof number	[-]
	Pr	is the Prandtl number	[-]

4.7.2 Convection type

The ratio between these dimensionless groups is used to assess the convection type. The three types are given by the following criteria.

a)	Forced convection	Gr/Re^2	<<	1	→	Nu = func(Re, Pr)
b)	Natural convection	Gr/Re^2	>>	1	→	Nu = func(Gr, Pr)
c)	Mixed convection	Gr/Re^2	≈	1	→	Nu = func(Re, Gr, Pr)

The relation Gr/Re^2 characterizes the ratio of buoyancy forces to inertia, and provides an estimate of the relative importance of the mechanisms [Mills, 1992; Quintela and Viegas, 1995].

Forced convection

The forced convection is characterized by the Reynolds number. Transition from laminar to turbulent flow occurs at $Re_{tr} = 5 \times 10^5$, where *tr* designates *transition*.

I. Laminar flow: $Re < Re_{tr}$

$$Nu_{average} = 0.664 Re_L^{0.5} Pr^{0.33}$$

II. Turbulent flow, $Re > Re_{tr}$

$$Nu_{average} = 0.664\,Re_{L}^{0.5}\,Pr^{0.33} + 0.036\,Re_{L}^{0.8}\,Pr^{0.43}\left(1-\left(\frac{Re_{tr}}{Re_{L}}\right)^{0.8}\right)$$

The formula shows that transition from laminar to turbulent flow occurs at $Re = Re_{tr}$.

The average convection heat transfer coefficient for the surface is subsequently given by the following equation.

$$h_{c,average} = \lambda\frac{Nu_{average}}{L}$$

Where	$h_{c,average}$	is the average convection heat transfer coefficient	[W/m²K]
	λ	is the thermal conductivity of the fluid	[W/mK]
	$Nu_{average}$	is the average Nusselt number	[-]
	L	is the characteristic length (dimension) of the surface	[-]

Natural convection

Analogously, the natural convection is characterized by the Rayleigh number. Transition occurs at $Ra_x = 10^9$. Ra_x is the Rayleigh number at position x.

I. Laminar flow: $Ra_x < 10^9$.

$$Nu_{average} = 0.68 + 0.670\left(Ra_L\psi\right)^{0.25}$$

II. Turbulent flow: $Ra_x > 10^9$

$$Nu_{average} = 0.68 + 0.670\left(Ra_L\psi\right)^{0.25}\left(1+1.6\times10^{-8}Ra_L\psi\right)^{1/12}$$

Where

$$\psi = \left(1+\left(\frac{0.492}{Pr}\right)^{9/16}\right)^{-16/9}$$

Again, the average heat transfer coefficient is given by the following equation.

$$h_{c,average} = \lambda\frac{Nu_{average}}{L}$$

Mixed convection

In a building physical context, mixed convection will be the typical situation. Above, the theoretical formulae for forced and natural convection have been given according to Mills [1992]. Numerous formulae have been suggested for the various applications of building physics. The formulae all employ different ratios of the Nusselt number for forced and natural

convection. This issue will be subject to discussion later in the report. Mills [1992], states the following theoretical formula for a *vertical surface*.

$$\overline{Nu} = \sqrt[3]{Nu_f^3 + Nu_n^3}$$

Where Nu_f is the average Nusselt number for forced convection [-]
Nu_n is the average Nusselt number for natural convection [-]

- both determined according to the preceding paragraphs.

As before, the average convection heat transfer coefficient is given by the following equation.

$$h_{c,average} = \lambda \frac{Nu_{average}}{L}$$

Mills [1992] states the following expression for a horizontal surface, e.g. a flat roof, with transition from laminar to turbulent flow at $Re_{tr} = 10^5$.

$$Nu_{average} = \left(Nu_f^{7/2} + Nu_n^{7/2}\right)^{2/7}$$

Where the contribution from forced convection is given by

$$Nu_f = 0.664 Re_{tr}^{1/2} Pr^{1/3} + 0.036 Re_L^{0.8} Pr^{0.43} \left(1 - \left(\frac{Re_{tr}}{Re_L}\right)^{0.8}\right)$$

The contribution from natural convection is given by

$$Nu_n = 0.14(Gr_L Pr)^{1/3} = 0.14 Ra_L^{1/3}$$

As before, the average convection heat transfer coefficient is given by the following equation.

$$h_{c,average} = \lambda \frac{Nu_{average}}{L}$$

Chapter 8 of this report presents a study of window convection heat transfer. In Appendix II, design-notes on a convection measurement apparatus are given.

4.8 Surface Coefficients

In the preceding sections, the complex heat transfer mechanisms at the surface of the building envelope have been described. The heat flux from a surface takes place in the shape of both long-wave radiation and convection.

The radiation exchange with the surroundings depends (non-linearily) on the temperature and emissivity of the surroundings and the surface as well as on geometrical aspects as described by view factors. The convection heat loss depends on air velocity and temperature conditions.

Detailed description of these complex conditions is not practicable in connection with ordinary hygrothermal calculations. The need for practicable approximations for calculation purposes has lead to the introduction of *surface coefficients*, as a pragmatic method of expressing the heat flux from surface as a function of the temperature difference between the surface and the ambient air:

$$q = \frac{\Delta T_a}{R_{s,e}}$$

Where	q	is the heat flux from the surface	[W/m²]
	ΔT_a	is the temperature difference, surface-air	[K]
	$R_{s,e}$	is the external surface resistance	[mK/W]

The surface coefficients are given in design guidelines. In the Danish standard *DS 418* [1986], the values are given as follows:

External surface: $R_{s,e} = 0.04$ mK / W
Internal surface: $R_{s,i} = 0.13$ mK / W

Current approximative calculation routines are meant to include both the radiation and the convective heat transfer coefficients in the surface resistances. In this context, it should be noted that the two quantities physically relate to two different temperatures. The common practice is based on non-physical, empirical relationships. This is due to the need for *easy-to-use* formulae and the fact that, usually, the objective is to evaluate the resulting heat transfer as opposed to specific surface conditions.

The approximation has been introduced in recognition of the complexity of the heat transfer processes at the surface of the building envelope. The quantities constitute a pragmatic model, not considering that the radiation heat loss depends on the temperature of the surroundings and the view factors of the surface. The non-linear dependence of the radiation exchange and the complex dependence on the surroundings are thus not included in normal hygrothermal calculations. The convective part of the surface coefficient is based on assumptions regarding the wind speed, considering neither the shape and orientation of the building nor the position on the building geometry. Chapter 8 presents a full-scale study of window convection heat transfer.

Chapter 5

FULL-SCALE MEASUREMENT SET-UP

5.1 Location

A full-scale measurement set-up has been established at a west facing (288°), 3-storey, masonry gable at the department. The specific site has been chosen for pragmatic reasons, as service and inspection of the equipment is made easy and data acquisition is carried out from an office nearby. It has not been possible to include more than one orientation in the studies and, since driving rain is studied in particular, and since west is the predominant wind direction, a relatively exposed west facing gable has been chosen. The 3-storey masonry building is a typical Danish building type, thus constituting an acceptable example.

In front of the gable, a small road is passing in a lower level. Across the road, a row of small trees shield to some extent. In the photographs below, the surroundings are seen from the south-west corner, respectively the north-west corner, of the building.

Photo 5.1 Building 118. View from south. The 5 metre reference mast is visible above the west facing gable.

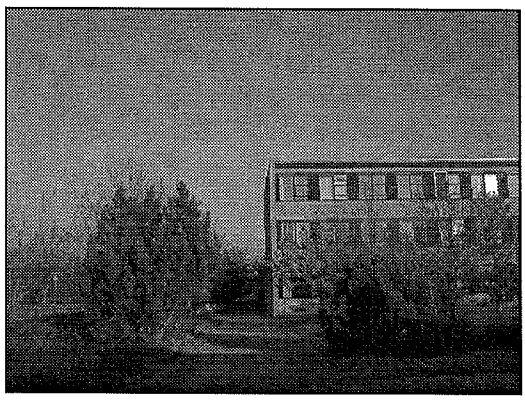

Photo 5.2 Building 118. View from north west. Driving rain is measured in four positions and reference measurements of air humidity, air temperature, wind speed and wind direction are taken from the reference mast. Long-wave radiation is measured from the roof.

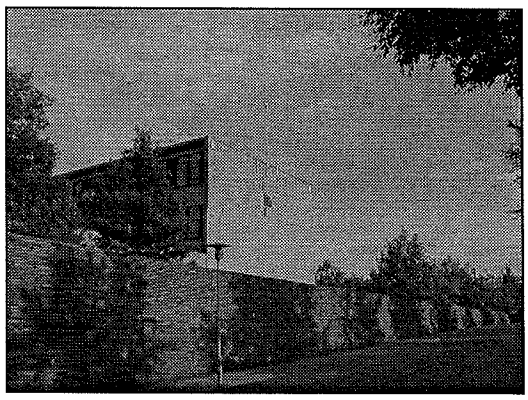

The gable is relatively unobstructed, but the complex geometry of the near surroundings, including vegetation, may cause turbulent conditions at the gable.

5.2 Reference Measurements

A 5 metre reference mast is mounted at the gable. Reference measurements of precipitation, wind speed, wind direction, air humidity and air temperature are all taken from the top of the mast. Measurements of long-wave irradiation are taken from the guard rail.

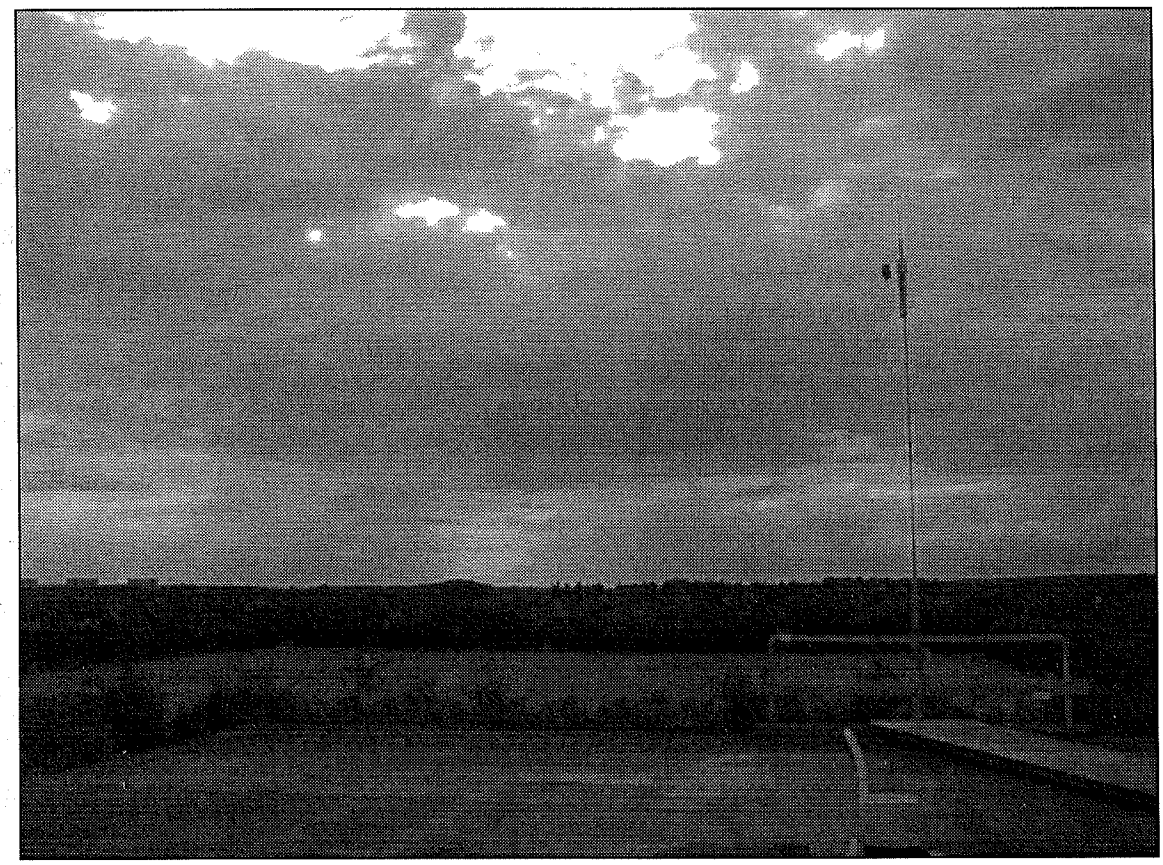

Photo 5.3 Reference mast. View towards west from the roof of Building 118.

Note that there are no high-rise buildings upwind from the gable. Apart from trees across the road, there are few obstacles in the area.

Photo 5.4 Reference mast.
Top: Gill WindMaster, ultrasonic 3-axis anemometer.
Left: Vaisala humidity and temperature probe in Gill radiation shield. An additional Cu/Cu-Ni thermo-couple is mounted in the shield.
Right: Young pluviometer.

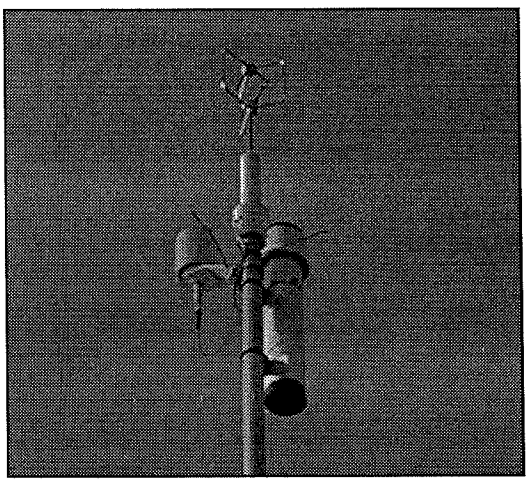

5.2.1 Precipitation

Reference precipitation is measured by means of a *Young*[1], *Model 50202 Precipitation Gauge.* Collected water is directed into a reservoir (*measurement chamber*), where a capacitive probe senses the liquid level. This way of measuring continuously permits differentiation to determine the rain intensity at any desired point in time. The pluviometer has a catchment-area of 100 cm² and the reservoir holds up to 50 mm of precipitation (~ 0.5 litres). The manufacturer states the following specifications:

Precipitation	Threshold	1 mm	
	Accuracy	± 1 mm	
	Chamber drain time	approx. 30 s	
	Offset	±0.01 m/s	
Environmental	Operating temperature	-20 ... +50°C	

5.2.3 Air humidity and temperature

The relative humidity of the ambient air and the ambient dry-bulb temperature are both measured by means of a *Vaisala*[2] *HMP45A Humidity and Temperature Probe.* The probe is mounted in a Gill radiation/precipitation shield. The manufacturer states the following specifications:

Relative humidity	Range	0.8 ... 100 % RH	
	Accuracy, 20°C	0 ... 90 % RH 90 ... 100 % RH	±2 % RH ±3 % RH
	Temperature dependence	±0.05 % RH / °C	
	Response time (90%) at 20°C	15 s	
Temperature	Range	-40 ... 60°C	
	Accuracy, 20°C	±0.2°C	
Environmental	Operating temperature	-40 ... +60°C	

In addition, the ambient air temperature (dry-bulb) is measured by means of a *Cu/Cu-Ni thermocouple* (copper-constantan), *Type TT*, positioned in the Gill radiation/precipitation shield. The accuracy of thermocouple is estimated to be ±0.2°C.

[1] R. M. Young Company, Michigan, USA.
[2] Vaisala Oy, Helsinki, Finland.

5.2.3 Wind speed and direction

An ultrasonic anemometer has been chosen for the wind measurements. The instrument has no moving parts and responds quickly with great accuracy. The specific instrument is a *Gill*[3] *SOLENT WindMaster, 3-Axis Ultrasonic Meteorological Anemometer.* The output is in the shape of horizontal wind speed, vertical wind speed component, and wind direction. The manufacturer states the following specifications:

Wind speed	Range	0 ... 60 m/s	
	Accuracy	0 ... 20 m/s	1.5% rms
		20 ... 30 m/s	1.5% rms to 3% rms
		35 ... 60 m/s	3% rms
	Resolution	0.01 m/s	
	Offset	±0.01 m/s	
Wind direction	Range	0 ... 360°	
	Accuracy	< 25 m/s	±2°
		> 25 m/s	±4°
	Resolution	1°	
Environmental	Operating temperature	-40 ... +60°C	
	Humidity	5 ... 100% RH	
	Precipitation	300 mm/h	operation maintained up to 300 mm/h

This type of anemometer has been recommended by Building Research Establishment, Watford, UK.

5.3 Long-Wave Irradiation

The long-wave radiation is measured with a *Kipp & Zonen*[4] *CG 1 pyrgeometer.* The instrument is designed for routine measurements with *limited accuracy.* The pyrgeometer is sensitive to radiation from 5 to roughly 25 μm. The pyrgeometer consists of a silicon window with an interference filter deposited on it, a thermal detector, a temperature sensor and a heating resistor. The silicon window acts as a filter, letting only long-wave radiation pass. The thermal detector is a 60-thermocouple thermopile, essentially black over the whole spectrum. The Pt-100 temperature sensor is built in at the edge of the thermal detector.

[3] Gill Instruments Ltd., Hampshire, UK.
[4] Kipp & Zonen, Delft, The Netherlands.

The thermal detector outputs a signal (voltage, V) proportional to the net long-wave radiation balance at the detector. In order to establish the absolute value of the radiant flux, the calibration factor and the sensor temperature have to be taken into account. The incident long-wave radiation, L, is calculated as follows:

$$L_{net} = L - L_{loss} \Rightarrow \frac{V}{K} = L - \varepsilon\sigma T_s^4 \Rightarrow L = \frac{V}{K} + \varepsilon\sigma T_s^4$$

Where	L	is the incident long-wave radiance	[W/m²]
	V	is the voltage output of the pyrgeometer	[μV]
	K	is the calibration factor	[μV/Wm^{-2}]
	ε	is the long-wave emissivity of the thermal detector	[~1]
	σ	is the Stefan-Boltzmann constant	[5.67 x 10^{-8} W/m²K^4]
	T_s	is the sensor temperature	[K]

The particular pyrgeometer has a calibration factor, K, of 14.04 μV/Wm^{-2}.

The CG 1 does not have the ideal 180° field of view. The field of view is 150°. The radiation exchange within this view, however, is quite representative for the radiation exchange within 180°. A constant correction factor is assumed, and taken into the calibration factor. This assumption however limits the absolute accuracy of the instrument [Kipp and Zonen, 1992].

The overall accuracy of the output signal V/K is estimated to be ±10% plus window heating offset. The error source called *window heating offset*, is caused by the heating of the silicon window by the sun. The offset is specified to be 25 W/m² at 1000 W/m² normal solar radiation.

When water is deposited on the window (e.g. dew), the sensor signal will read zero. To prevent deposition of dew, the instrument is equipped with an incorporated heating resistor, which keeps the pyrgeometer above the dew point of the ambient air.

Long-wave irradiation	Irradiance range	-250 ... 250 W/m²	
	Spectral range	5 ... 25 μm	
	Estimated accuracy	10 %	plus window heating offset
	Window heating offset	max. 25 W/m²	1000 W/m² incident solar radiation
	Temperature dependence	± 0.05 % RH / °C	
	Response time	63 % 99%	5 s 25 s
Environmental	Operating temperature	-30 ... +40°C	

The pyrgeometer has been mounted horizontally on the guard rail at the roof for reference measurements and transferred into vertical positions for short-duration measurement series.

Photo 5.5 Reference mast. View towards west. Left: pyrgeometer mounted vertically.

The photograph above shows the pyrgeometer tilted into a vertical position for measurement of incident long-wave radiation from the surroundings of the gable. The position has been changed in connection with measurement series of short duration.

The following photograph shows the pyrgeometer, mounted in connection with the window convection study:

Photo 5.6 Seen from above: pyrgeometer mounted vertically in connection with window convection study.

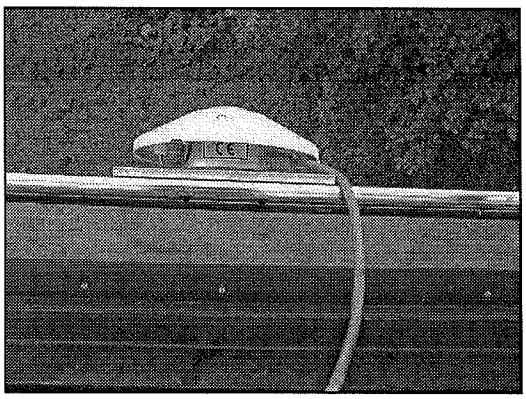

5.4 Driving Rain

Driving rain collectors are mounted in four positions on the west facing gable of Building 118. Three collectors are positioned along the top edge, and two are placed one third down on the vertical centre line of the gable. Two types of driving rain collectors (DRCs) are employed.

A *traditional driving rain collector* consisting of a Teflon coated collector tray (catchment-area: 0.80m × 0.80m = 0.64 m²), drained to a *Young Model 50202 Precipitation Gauge* similar to the one used for measurement of reference precipitation.

The second collector type has been designed as part of the present project and consists of a collector tray (catchment-area: 0.46m × 0.46m ≈ 0.21m²) and a reservoir, both suspended from

a load cell. The load cell is a *HBM*[5], *Type Z6FC3* load cell with a capacity of 10 kg. In order to reduce reflection, by dispersion of the impinging droplets, a net with a mesh size of 1 mm is mounted inside the collector tray, approximately 1 cm in front of the collector plate. A detailed description of both DRC types and the general set-up is given in Chapter 6 on driving rain measurement.

Photo 5.7 Novel load cell DRC. Catchment-area: 0.21 m². The collector tray (including reservoir) is suspended from a load cell and kept in place with steel wires. The self-siphoning reservoir has a capacity of approximately 300 ml. A net is mounted inside the collector to minimize reflection.

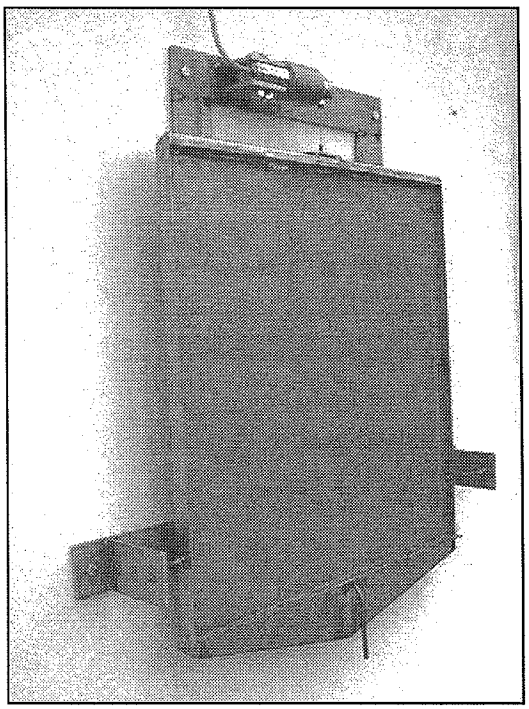

5.5 Data Acquisition

Acquisition of data is PC based. Two types of *Solartron*[6] *dataloggers* are employed. Solartron was chosen because of previous experience with the equipment at the department. Only few adjustments of existing software were required in preparation for the present set-up. The system is flexible, as the loggers work as IMPs (Isolated Measurement Pods). One *IMP Type 35951A (20 channels)* is used for analogous voltage measurements and thermocouples, and one *IMP Type 35951B (10 channels)* is used for the strain gauge measurements, i.e. the load cell driving rain collectors.

The scan frequency is 0.1 s^{-1}. Logging is carried out as 10-second instantaneous values of wind, precipitation and driving rain. Moreover, all parameters are logged as 1-, 10- and 60-minute values (wind, precipitation, driving rain, air humidity and temperature, long-wave irradiation). These logged values are averages computed from the 10-second instantaneous values. A total data amount of approximately 2 MB is logged every 24 hours.

[5] Hottinger Baldwin Messtechnik GMBH, Darmstadt, Germany.
[6] Solartron Instruments, Hampshire, UK.

Chapter 6

DRIVING RAIN MEASUREMENT

6.1 Measurement Principles

In this case study, various aspects of driving rain measurement are treated. The objective is to assess the driving rain amounts striking a typical Danish building, to assess the spatial distribution of the driving rain over a building geometry and to improve the existing method of measuring driving rain.

Essentially, a driving rain gauge has two functions:

- Catching of impinging driving rain
- Gauging of the collected amount

Traditionally, the catching is achieved by one of two methods. One is to establish a hole in the surface under consideration. The other is to mount a collector tray onto the surface. From the collector the water is drained to a reservoir. The reservoir can be self-siphoning for automatic functioning, or be emptied manually, depending on the accessibility of the set-up and the wish for automation.

Registration of the collected amount can be carried out in a number of ways:

Manual volume registration
The most classic way is to simply drain the collector to a container and record the collected volume manually. This method is time consuming and does not allow for high frequency measurements.

Tipping bucket
The method can be automated by means of the *tipping bucket principle*, by which a pulse is recorded every time a certain volume is collected, typically 0.2 ml.

Balance
The collected amount can be recorded by weighing the reservoir. This method is permitting differentiation to obtain the intensity in any desired time interval.

Capacity
The collected amount can be recorded in terms of the liquid level of the reservoir. Also this method is permitting differentiation to give driving rain rates at any point in time.

The tipping bucket principle and the capacity principle are applied in common, commercially available pluviometers.

Error sources
In the following the error sources encountered in connection with driving rain collectors (DRCs) are briefly introduced. The following factors will influence measurements driving rain measurements:

- Reflection
- Evaporation
- Disturbance of local air flow
- Draining delay
- Wind pulsation
- Siphoning
- Precision of auxiliary equipment

Reflection
Raindrops striking a surface (for instance a collector) will be partly reflected. The main objective of driving rain measurements is to quantify the total incident driving rain. Studies of reflection are relevant, but should be carried out separately. Thus, reflection should be minimized.

Evaporation
Droplets will tend to stay on the collector owing to adhesion. Evaporation of droplets staying on the collector may lead to underestimation of the driving rain.

Disturbance of local flow
The presence of a DRC will influence the local air flow, and consequently the driving rain.

Draining delay
The funnelling of the collected driving rain to the reservoir will be delayed because of distance and adhesion.

Wind pulsation
Fluctuating wind and changes of pressure can disturb the set-up.

Siphoning
Erroneous results are recorded when the reservoir is being emptied.

Precision of auxiliary equipment
Regardless of how the collected amount is registered, the measurement will have a certain threshold value and a certain accuracy.

Traditional DRC
Initially, one traditional capacity DRC was produced to gain experience and begin with state-of-the-art equipment. The adopted design is similar to a design used by the BRE[1] in Watford UK. The principle is based on a large collector tray, drained to a commercially available capacity pluviometer (Young precipitation gauge, Model 50202). The original catchment-area of the pluviometer is covered by a lid. The collector tray measures $0.80 \times 0.80 = 0.64$ m². The tray is Teflon coated to minimize friction. The DRC is positioned one third down at the centre line of the gable, position *Mid-Centre*. The DRC is shown in the photograph below.

[1] Building Research Establishment.

Photo 6.1 Traditional DRC, mounted at west gable. The collector tray measures 0.80×0.80= 0.64 m^2 and has a depth of 15 mm. The tray is Teflon coated to minimize friction. The collector is drained to a Young Precipitation Gauge, Model 50202 by means of a Teflon tube (internal diam. 10 mm)

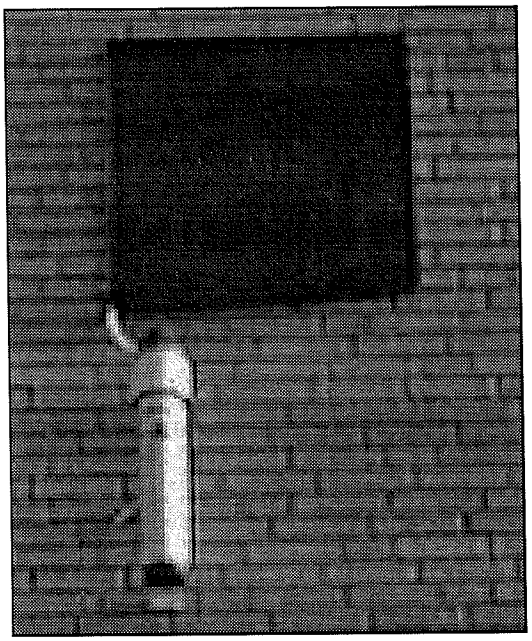

The pluviometer measures the water level in the reservoir. By differentiation, this allows for determination of the driving rain intensity at any desired point in time.

The Teflon coating is minimizing the number of droplets staying on the collector. However, it was found that, during rain, the tray is covered with drops regardless of the Teflon. When the tray is completely covered, impinging droplets make the droplets already on the collector run to the drain. This way, the expected result could be a threshold value corresponding to 'saturation' of the collector. Evaporation from the collector will be an important error source.

Novel DRC

In order to carry out measurements of the spatial distribution on the gable, additional DRCs were produced. Having produced a traditional DRC, the objective was to further develop the technique and aim for an improved gauge at minor cost. Since the system is to be mount on a masonry gable, the collector is of the tray type. The result is a novel DRC which aims at reducing some of the error sources described above.

The catchment-area is 0.46m × 0.46m ≈ 0.21m^2. The weight of the collector and reservoir is measured by means of a load cell. The whole system is suspended from a load cell permitting detection of droplets on the collector. The load cell has a capacity of 10 kg and the weight of dry collector and reservoir is approximately 3 kg. The volume of the reservoir is approximately 300 ml. The load cell is an *HMP Type Z6FC3, C3* signifying that the load cell is certified with an accuracy of 3/1000 of the capacity. In this case, the accuracy of the load cell is certified as 3.3 g.

In order to reduce reflection, a net is mounted inside the collector tray, approximately 1 cm in front of the collector plate. On impact, impinging droplets will be dispersed by the net. Some droplets will stay on the net, some will continue through to the collector plate after dispersion and a limited part will be reflected. On the following pages, the load cell DRC is shown in a series of photographs.

Photo 6.2 Novel load cell DRC. Frontal view. The collector tray measures 0.46×0.46 ≈ 0.21 m², with a depth of 15 mm. The tray is suspended from a 10 kg load cell. The reservoir is self-siphoning with a capacity of approximately 300 ml.

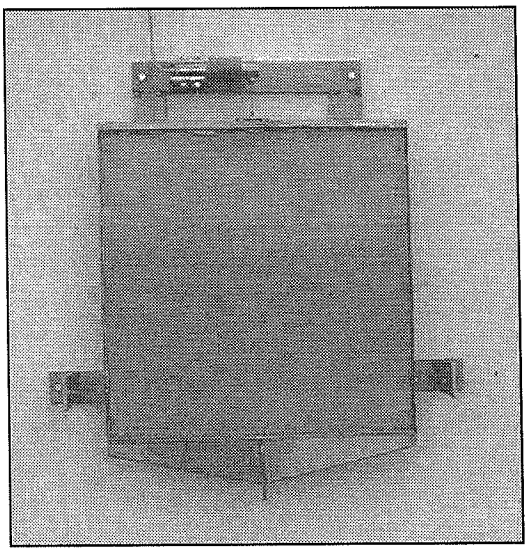

The self-siphoning reservoir is relatively small (~ 300 ml) in order to reduce the total load. The net has a mesh size of 1 mm. The weight of the collector plate and empty reservoir is approximately 3 kg. The capacity of the load cell is 10 kg.

Photo 6.3 Novel load cell DRC. Side view.

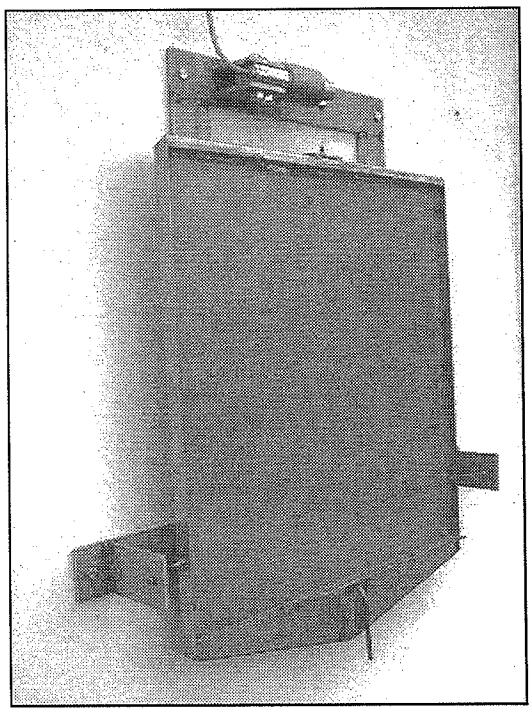

Photo 6.4 Novel load cell DRC. Top view. Load cell detail. The collector is kept in place with steel wires.

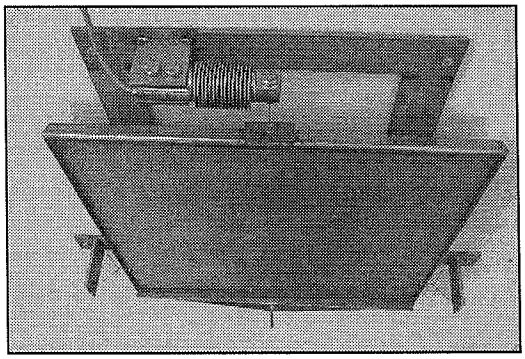

Photo 6.5 Novel load cell DRC. Frontal view. A net is placed inside the collector tray in order to minimize reflection of impinging droplets. The shape of the reservoir ensures lateral stability by gravitation.

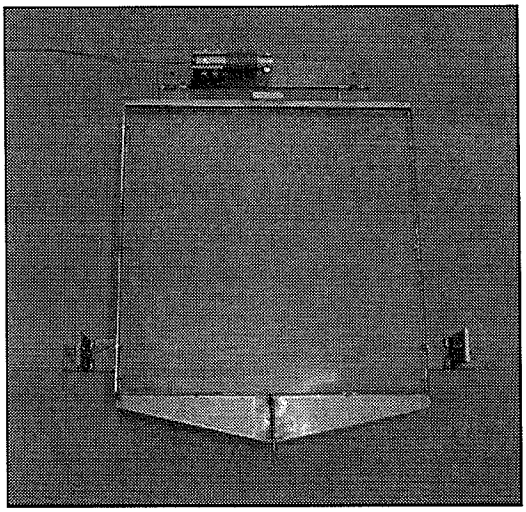

Photo 6.6 Novel load cell DRC. Side view. Drain detail. Siphon and reservoir. The volume of the reservoir is approximately 300 ml. The internal diameter of the siphon is approx. 4 mm.

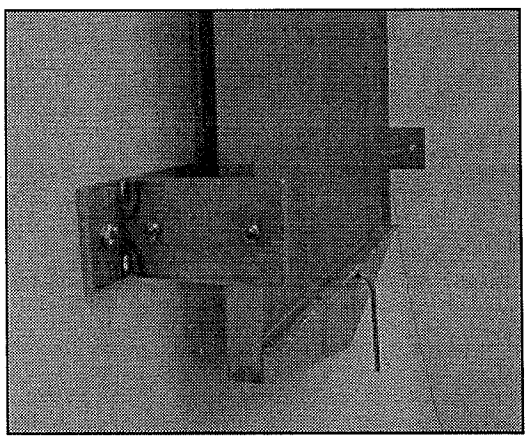

6.2 Measurement Series: Selected Rainfall Events, April 27th to July 12th 1998

Data selection
The present, preliminary measurement series was initiated shortly after the production of four load cell DRCs. A number of rainfalls took place in the course of the preliminary measurement period from April 27th to July 12th 1998. In order to only operate with significant rain events, periods with clearly detectable precipitation has been selected for the present study. A total of 16 events of differing nature have been recorded between May 3rd and July 11th. The time and duration of the events are specified in the table below.

Date	Event start	Event end
98.05.03	18.30	21.40
98.05.06	09.50	14.30
	18.10	22.50
98.05.21	12.10	17.00
98.05.24	16.30	19.30
98.05.27	12.00	18.00
98.06.09	18.50	-
98.06.10	-	24.00
98.06.15	16.10	-
98.06.16	-	-
98.06.17	-	03.10
	09.10	12.40
98.06.26	02.30	17.30
	20.10	24.00
98.06.30	16.30	18.30
98.07.01	04.00	09.30
98.07.05	05.20	09.00
	16.20	23.50
98.07.11	07.50	10.40

Table 6.1 Measurement series. Selected rain events, May 3rd to July 11th 1998.

In the course of the series, a total precipitation amount of 71 mm has been recorded.

Objective
A number of aspects are studied. The objective of this measurement series is to investigate:

- Alternative DRC designs
- Spatial driving rain distribution
- Driving rain and reference wind correlation
- Driving rain and reference precipitation correlation

The different issues are addressed on the basis of typical examples in the following.

Driving rain gauges
As mentioned above, two types of driving rain collectors (DRCs) are considered, allowing for comparison of two different principles. The two types are the following:

- Traditional capacity type
- Novel load cell type

The novel principle is compared with the traditional principle in one position, as the two collector types are mounted side-by-side. Additional three novel load cell DRCs are mounted in other positions to observe the driving rain distribution on the gable.

Notation, four positions on west gable
To ease interpretation, the considered DRC position on the gable is symbolised by the dark square in the following symbol:

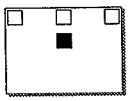

Four positions on the gable are considered. In the position Mid-Centre, indicated with the symbol above, a traditional capacity type DRC and a novel load cell DRC are mounted side-by-side for comparative studies. Additional three load cell DRCs are positioned along the upper edge of the facade to yield information regarding the spatial distribution of the driving rain. The positions are referred to as *North-Top* (symbol upper left), *Mid-Top* (symbol upper centre), *South-Top* (symbol upper right) and *Mid-Centre*.

The photograph below shows the west gable and the five driving rain collectors.

Photo 6.7 West gable. Frontal view.

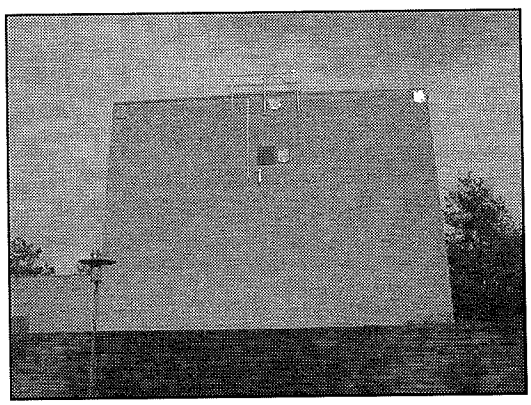

Reference measurements are taken from the reference mast at the gable, 5 metres above the roof. The mast is visible in the following photograph.

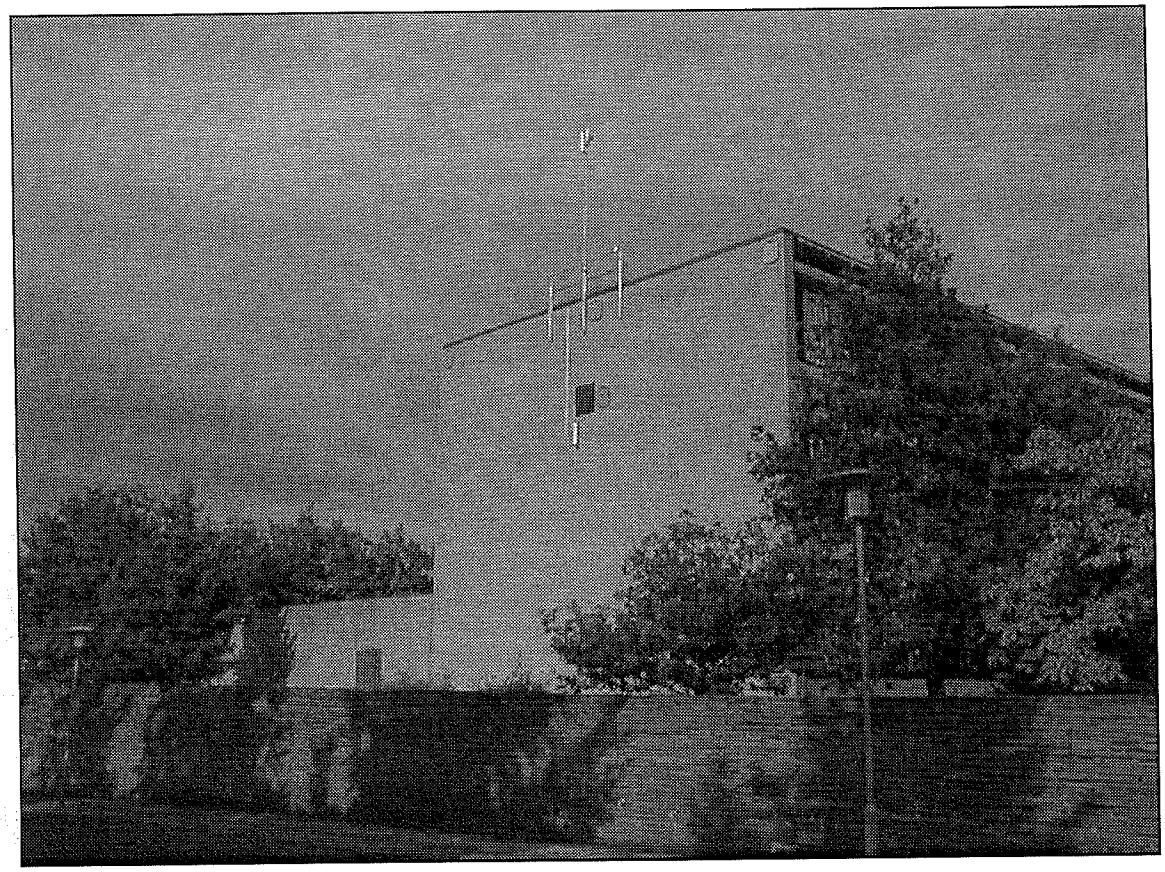

Photo 6.8 West gable (288°). Above the roof, the 5 metre reference mast is visible.

Surroundings
The gable is relatively exposed. Apart from vegetation, no significant obstacle appear in front of the building. There are no high rise buildings in the area. In front of the gable, a road passes in a lower level (see photograph above). The immediate surroundings may cause turbulent conditions at the gable. Note that a wall is attached to the gable on the north side. Thus, the geometry is not completely symmetrical. The view from the roof can be seen in connection with the general description of the measurement set-up.

6.3 Studies

6.3.1 Reference precipitation and driving rain

The distribution of the recorded precipitation on wind direction and wind speed is illustrated in the following figures. The analysis is based on 10-minute averages. Average values of wind speed and direction serve to characterize the weather situations, whereas real situations will be influenced by high frequency variations.

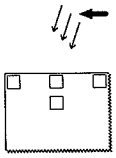

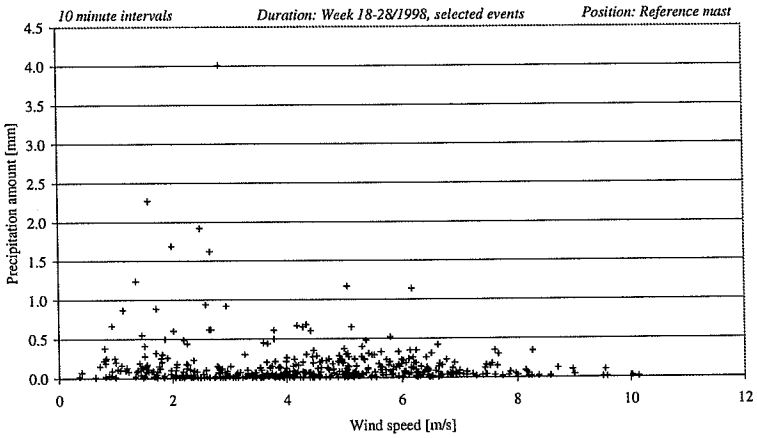

Figure 6.1 Reference precipitation and wind speed. Position: Reference mast. 10 minute values. Total precipitation, entire series: 71 mm.

The rain events occur at a wide range of wind speeds (~ 0.5 - 10 m/s). The major part of the events takes place at wind speeds between 1 and 7 m/s. The highest intensities are recorded at wind speeds around 2 m/s.

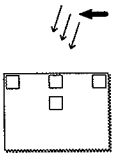

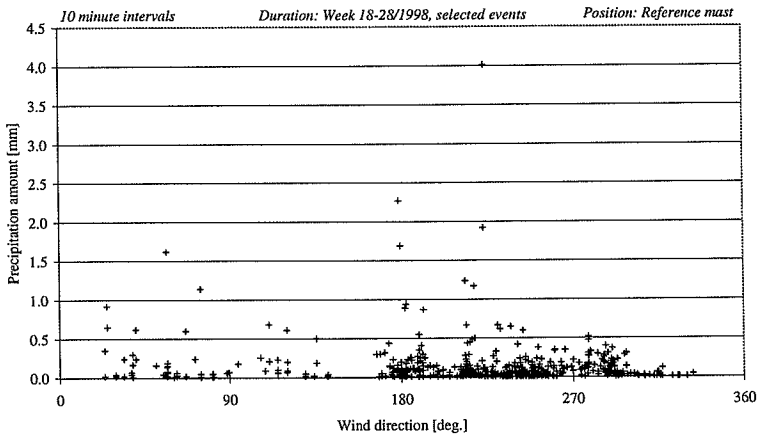

Figure 6.2 Reference precipitation and wind direction. Position: Reference mast. 10-minute values. Total precipitation, entire series: 71 mm.

The major part of the rain events occur at wind directions between 180° and 330°. The highest intensities are recorded at wind directions between 180° and 230° (south and south-west).

6.3.2 Wind speed and driving rain

In the following, the correlation between wind speed and driving rain is illustrated for the considered four positions on the gable. For each position, the total recorded driving rain amount is given.

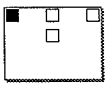

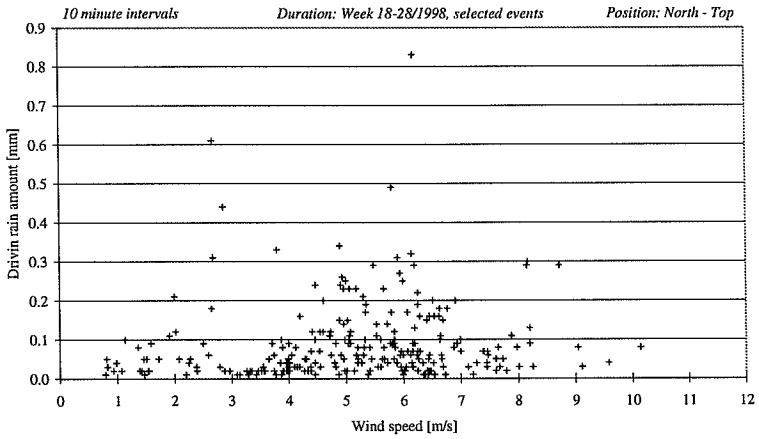

Figure 6.3 Driving rain and wind speed. North-Top. 10-minute values. Total driving rain amount, entire series: 23 mm.

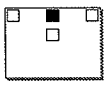

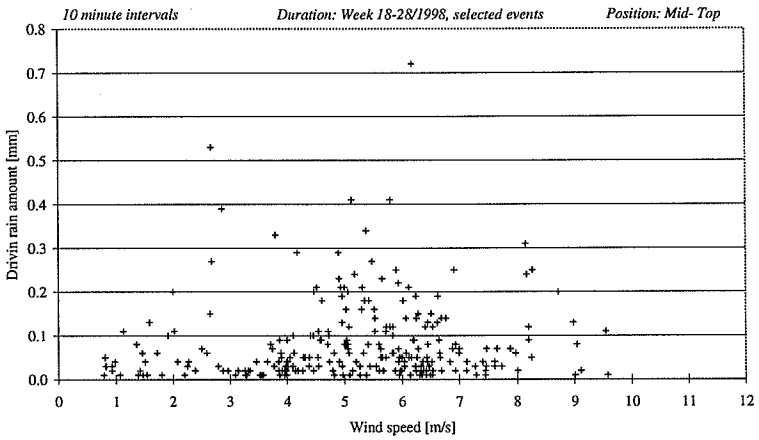

Figure 6.4 Driving rain and wind speed. Mid-Top. 10-minute values. Total driving rain amount, entire series: 22 mm.

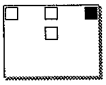

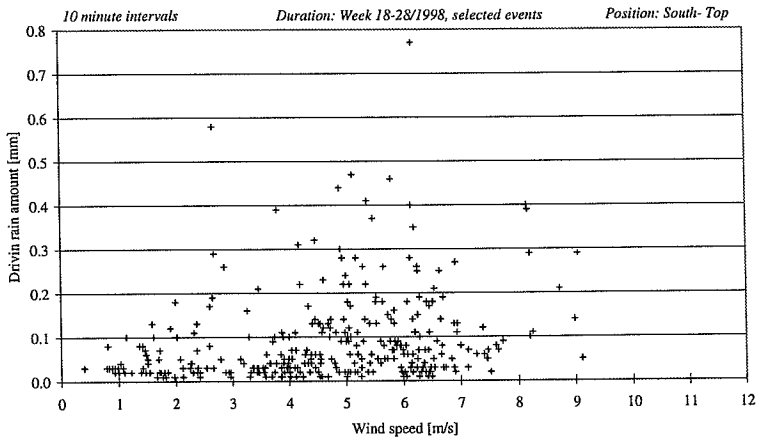

Figure 6.5 Driving rain and wind speed. South-Top. 10-minute values. Total driving rain amount, entire series: 29 mm.

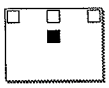

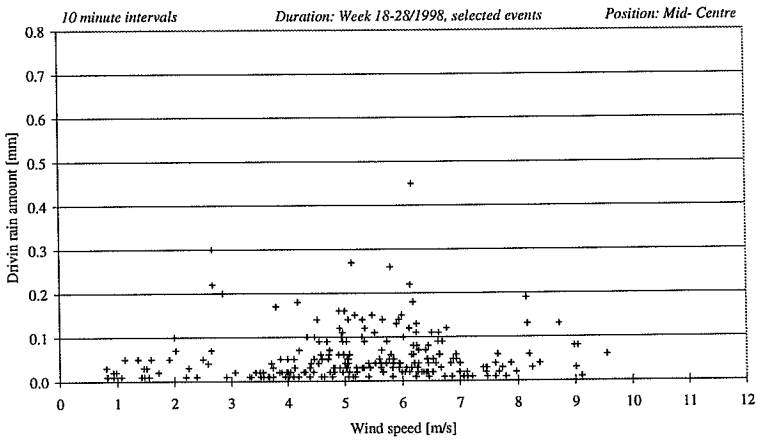

Figure 6.6 Driving rain and wind speed. Mid-Centre. 10-minute values. Total driving rain amount, entire series: 13 mm.

A lower level is noticeable at the centre part of the gable, when compared with the positions at the top of the gable (previous figures).

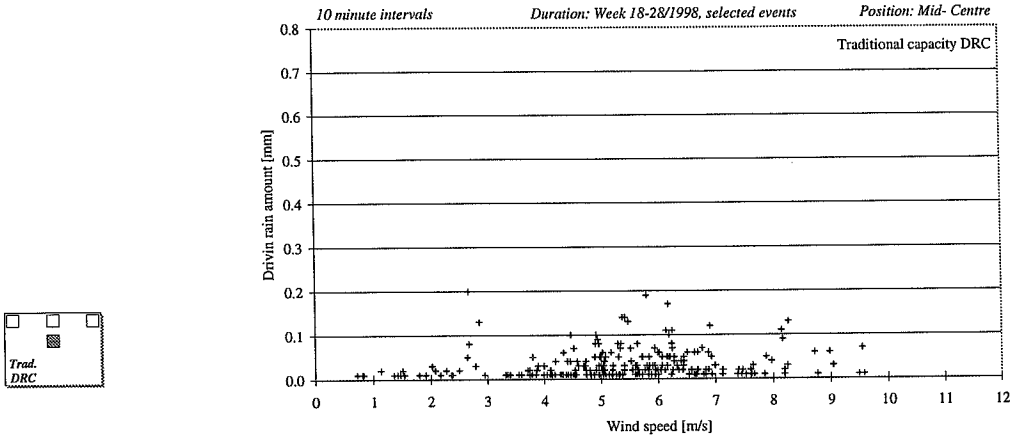

Figure 6.7 Driving rain and wind speed. Mid-Centre. 10-minute values. *Traditional capacity DRC*. Total driving rain amount, entire series: 8 mm.

The two figures above show that the novel load cell DRC collects significantly more driving rain than the traditional DRC (13 mm and 8 mm respectively).

6.3.3 Wind direction and driving rain

In the following, the driving rain amounts and corresponding wind direction are presented graphically for each collector.

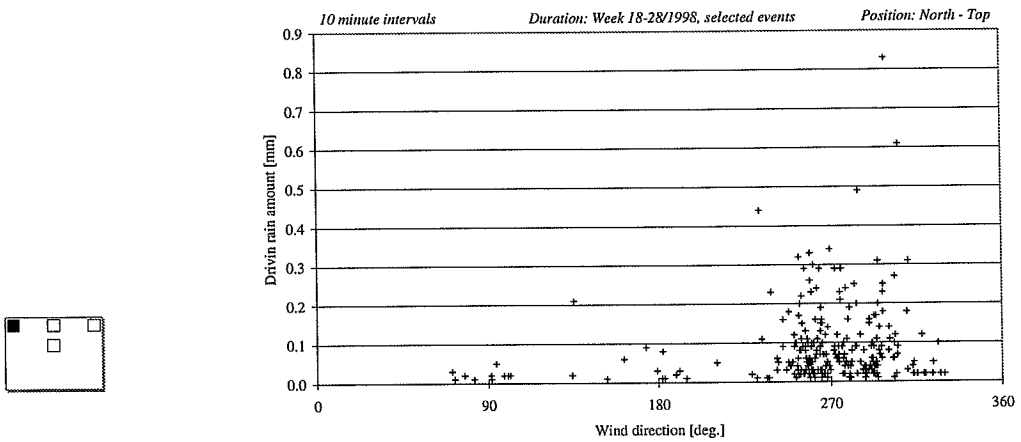

Figure 6.8 Driving rain and wind direction. North-Top. 10-minute values. Total driving rain amount, entire series: 23 mm.

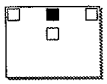

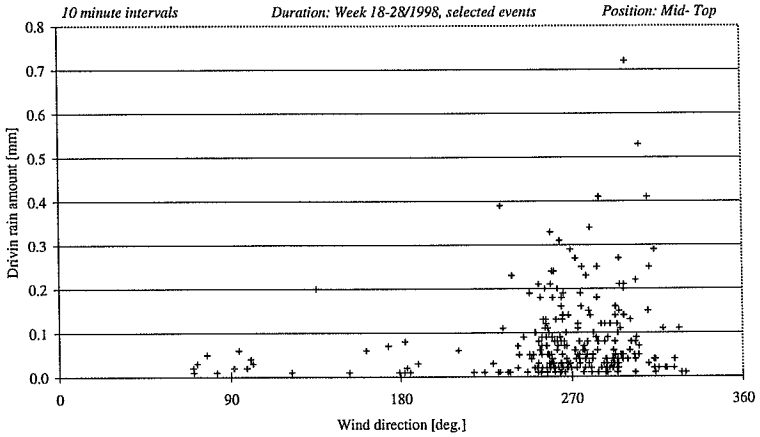

Figure 6.9 Driving rain and wind direction. Mid-Top. 10-minute values. Total driving rain amount, entire series: 22 mm.

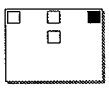

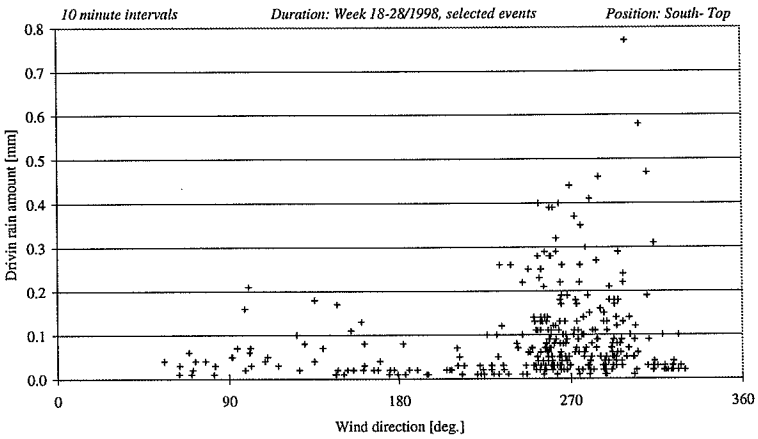

Figure 6.10 Driving rain and wind direction. South-Top. 10-minute values. Total driving rain amount, entire series: 29 mm.

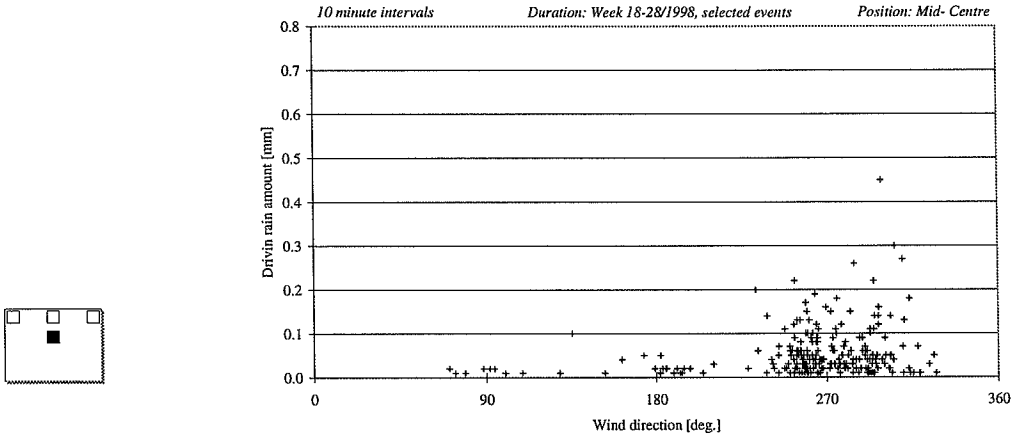

Figure 6.11 Driving rain and wind direction. Mid-Centre. 10-minute values. Total driving rain amount, entire series: 13 mm.

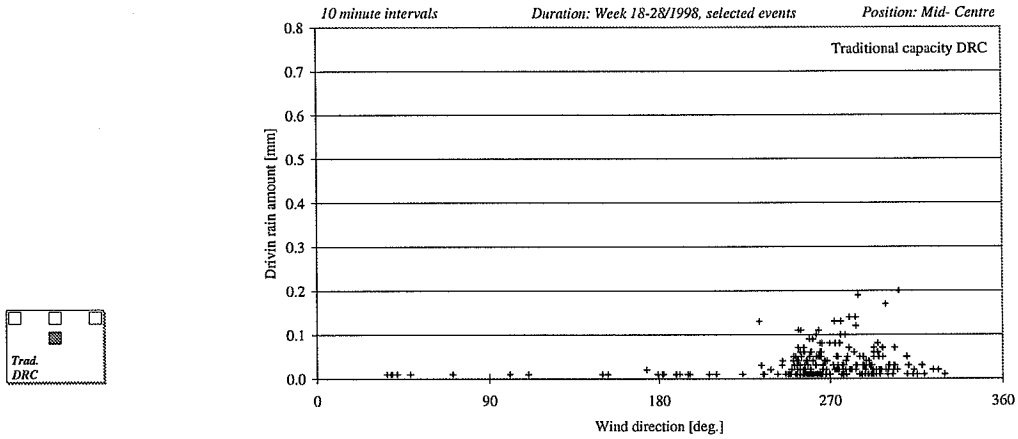

Figure 6.12 Driving rain and wind direction. Mid-Centre. 10-minute values. *Traditional capacity DRC*. Total driving rain amount, entire series: 8 mm.

The distributions on wind directions are similar for the different collectors. The driving rain is mainly recorded at wind directions towards the gable. Again, it should be noted that the 10-minute averages serve to characterize the weather situations, whereas the actual impingement may be due to instantaneous combinations of precipitation and wind. In the following, examples of the time history of such instantaneous values are presented.

6.3.4 May 3rd 1998 16hrs to 24hrs, short duration - high intensity

This example serves to demonstrate the difference between the output of the two types of DRCs positioned *side-by-side*. Also, the effect of 10-minute averaging is evaluated. The rainfall took place between 18hrs and 22hrs on May 3rd, 1998. Extreme gusts towards the gable, combined with precipitation, resulted in a well-defined driving rain event.

The first figure shows the output of the load cell DRC. The output represents the weight of collector plate, reservoir and collected amount of driving rain. The absolute level of the weight is insignificant, as only differences are considered. The catchment-area of the collector measures 0.46 m × 0.46 m ≈ 0.212 m². A collected amount of 100 g thus corresponds to a driving rain amount of 0.1 kg / 0.212 m² ≈ 0.47 kg/m² or, adopting a volume terminology: *100 g ~ 0.47 mm.*

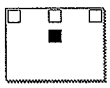

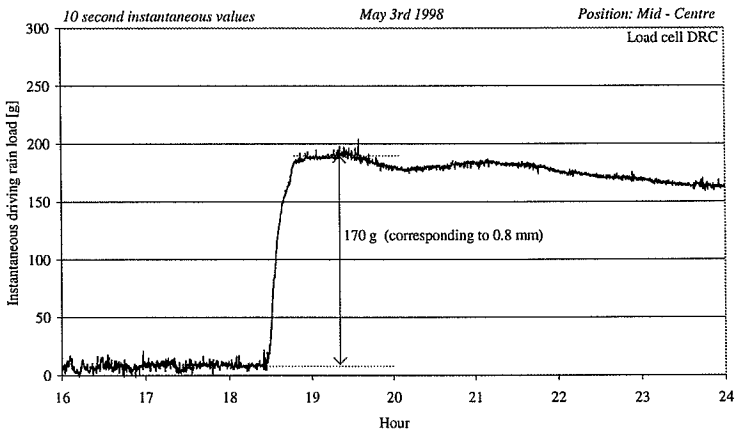

Figure 6.13 May 3rd. Cumulative driving rain load. Mid-Centre. 10-second instantaneous values. Driving rain amount: 0.8 mm.

The short time scale fluctuations are due to wind pulsation. The figure shows that such a distinct driving rain is clearly detectable. A total of approximately 170 g is recorded[2], corresponding to 0.8 mm driving rain (1.7 × 0.47 mm ≈ 0.8 mm). The wind fluctuations only cause minor deviations on a larger scale. The driving rain is followed by a small decrease attributed to evaporation and a small increase which may be the result of simultaneous evaporation and low intensity driving rain. The evaporation issue is addressed later in this chapter.

The following figure shows the same event as recorded by the traditional capacity DRC.

[2] Estimated graphically from the diagram.

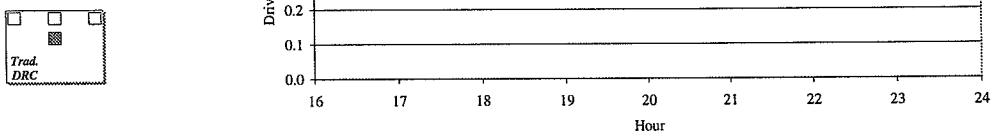

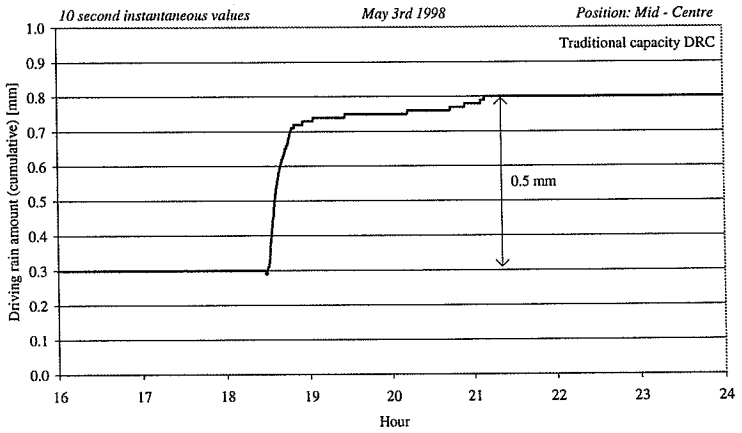

Figure 6.14 May 3rd. Cumulative driving rain. Mid-Centre. 10-second instantaneous values. *Traditional capacity DRC.* Driving rain amount: 0.5 mm (between 18.30 and 19.30: ~ 0.45 mm).

The traditional DRC detects the collected volume directly by means of draining to a capacity pluviometer. The event is stretched in time, although with reduced intensity after the initial high intensity spell. A total amount of 0.5 mm is recorded, which is substantially lower than the amount recorded by the load cell DRC (0.8 mm). No evaporation is detected; as the output expresses the water level in the closed pluviometer reservoir, the detectable evaporation loss will be intrinsically limited.

Below, the weather situation is described in terms of the precipitation and wind history of the considered period. Two consecutive spells appear, the first spell of short duration (~ 15 minutes) and the second spell approximately six times longer (~ 90 minutes). A total precipitation amount of 8.2 mm is recorded.

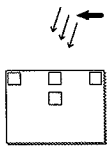

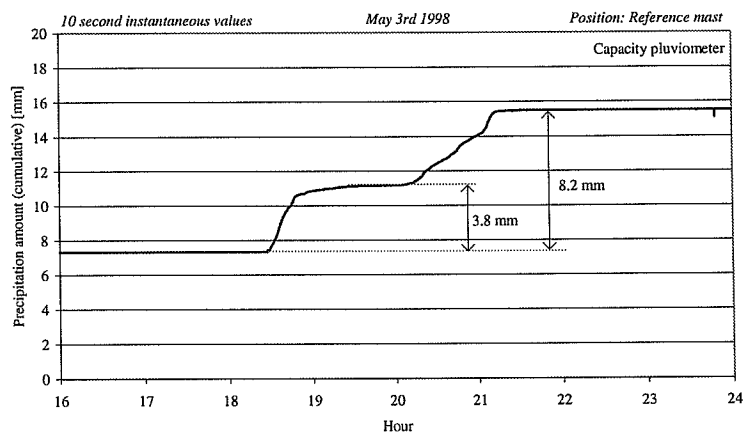

Figure 6.15 May 3rd. Cumulative precipitation. Reference mast. 10-second instantaneous values. Total precipitation amount: 8.2 mm (between 18.30 and 19.30: 3.8 mm).

In the figure below, extreme wind gusts up to more than 40 m/s are observed at the time of the first spell. During the rest of the period under consideration, the wind speed is relatively stable, around 3-5 m/s.

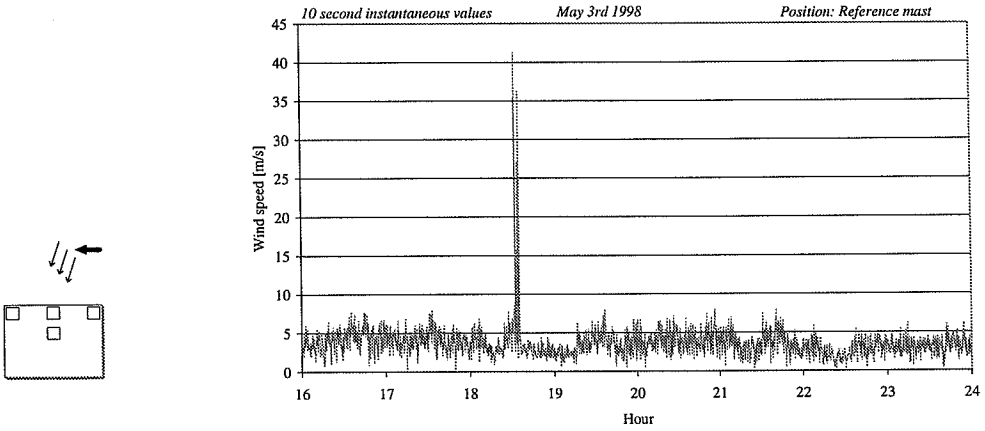

Figure 6.16 May 3rd. Wind speed. Reference mast. 10-second instantaneous values. Extreme gust effects.

Figure 17 shows that the wind direction is varying from 1) before the first spell: ~ 0° (north) to 2) during the first spell: ~ 300° (~ north-west) and, finally 3) during the second spell: ~ 30° (~ north-east). Thus, the extreme gusts described above are combined with frontal wind leading to high exposure. Note that the lines across the diagram indicate changes past 0°.

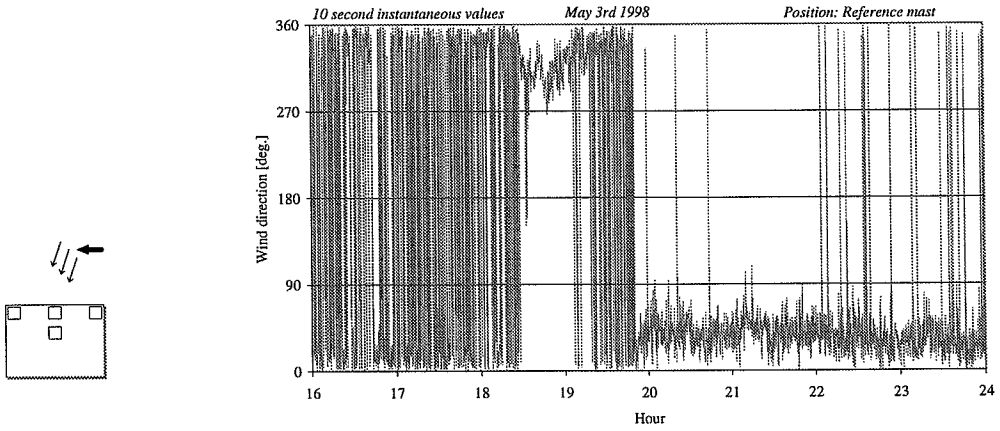

Figure 6.17 May 3rd. Wind direction. Reference mast. 10-second instantaneous values. Lines across the diagram indicate changes past north (0° and 360°).

The change of wind direction can explain the low driving rain intensity during the second spell, as the gable is close to being leeward.

Above, the cumulative driving rain amount was presented as instantaneous 10-second values. In order to filter out the wind fluctuations, and at the same time reduce the amount of data, averaging is a necessity. The preliminary results of this project are based on 10-minute averages. The issue will be subject to discussion later in this chapter. This example serves to demonstrate the effect of 10-minute averaging on the recorded amount of driving rain, in case of a well defined, short duration event.

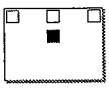

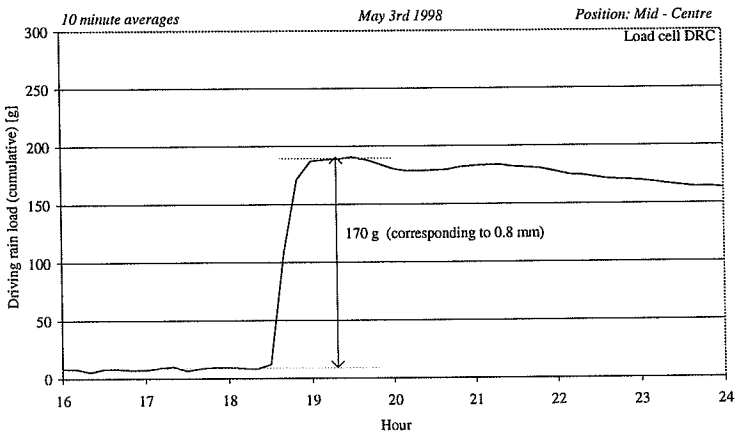

Figure 6.18 May 3rd. Cumulative driving rain load. Mid-Centre. *10-minute averages.* Driving rain amount: 0.8 mm.

The figure above shows the same event, only this time as a plot of 10-minute averages. In this case, the average values are found to adequately represent the instantaneous values. The recorded amount of driving rain is in agreement with the amount recorded by means of the 10-second instantaneous values (0.8 mm in both cases).

6.3.5 June 16th 1998 10hrs to 18hrs, continuous rain

The previous example showed a rain event consisting of to consecutive spells of limited duration. In the following example, 8 hours of continuous precipitation is considered. The cumulative precipitation is shown in Figure 6.19.

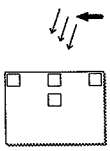

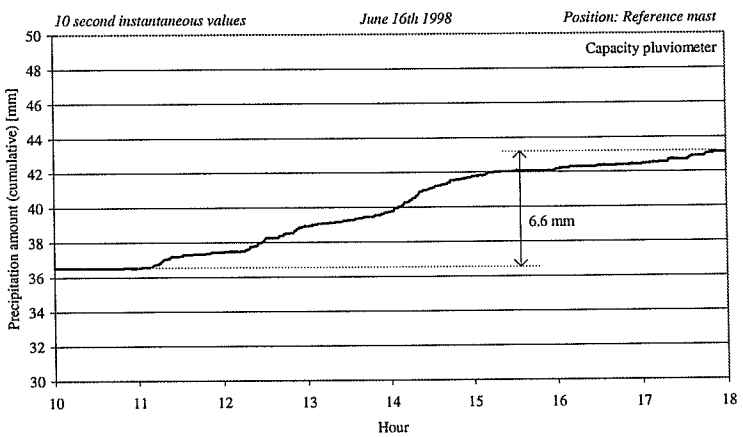

Figure 6.19 June 16th. Cumulative precipitation. Reference mast. 10-second instantaneous values. Total precipitation amount: 6.6 mm.

In the figure below, the wind speed and wind direction are seen to be relatively stable throughout the period under consideration. The wind is frontal, at wind speeds mainly between 4 and 10 m/s.

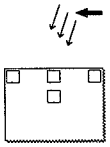

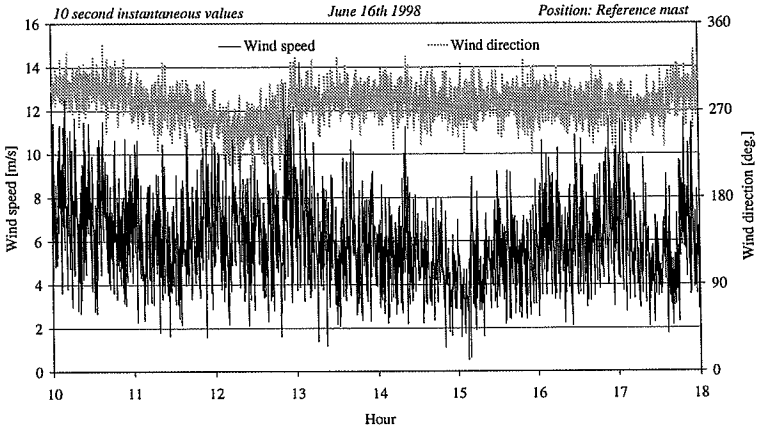

Figure 6.20 June 16th. Wind speed and wind direction. Reference mast. 10-second instantaneous values.

The DRCs are equipped with *self-siphoning* reservoirs. When the maximum capacity is reached, the reservoir is emptied by a *siphon effect*. In the diagrams, the siphoning shows as a sudden drop on the cumulative curve.

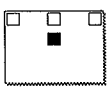

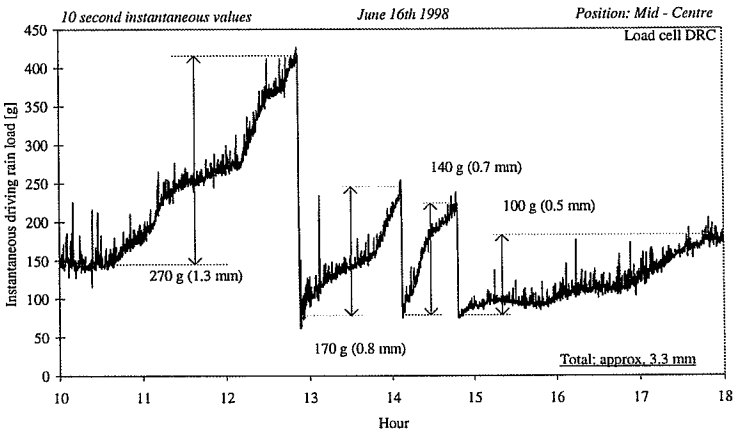

Figure 6.21 June 16th. Cumulative driving rain load. Mid-Centre. 10-second instantaneous values. Driving rain amount: 3.3 mm.

The load cell DRC is emptied three times in the figure above. The differences in maximum level are attributed to wind effects and adhesion to the siphon. A total driving rain amount of 3.3 mm is recorded.

Below, the same data are presented as 10-minute values, in order to evaluate the significance of 10-minute averaging in case of continuous rain and repeated siphoning.

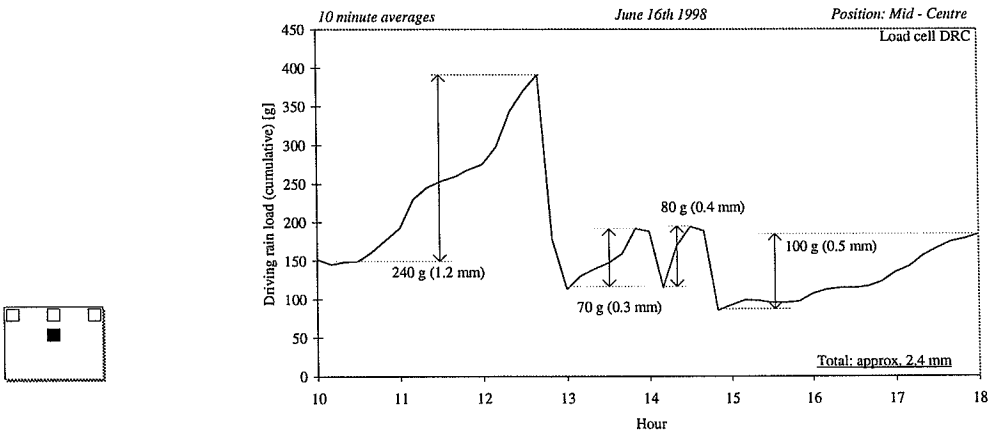

Figure 6.22 June 16th. Cumulative driving rain load. Mid-Centre. *10-minute averages.* Driving rain amount: 2.4 mm.

The shape of the curve is similar to the *10-second graph*, but the extremes are not expressed accurately. A peak will lead to underestimation. In the specific case, the difference is 3.3 - 2.4 = 0.9 mm. I.e., only 73% of the *10-sec* amount is detected as *10 min* values.

Below, the corresponding graph of the traditional capacity DRC is shown.

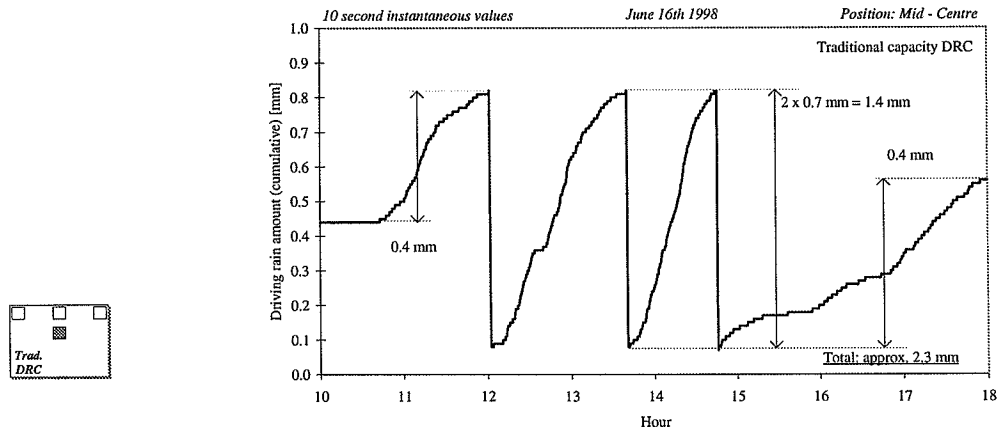

Figure 6.23 June 16th. Cumulative driving rain. Mid-Centre. 10-second instantaneous values. *Traditional capacity DRC.* Driving rain amount: 2.3 mm.

Here, the maximum level is more well-defined, as it expresses the capacity of the pluviometer reservoir. Wind effects do not interfere with the siphoning. A total driving rain amount of 2.3 mm is recorded. This should be compared with the 3.3 mm recorded by means of the load cell DRC in the same position.

To demonstrate the effect of averaging, 10-minute average values are shown in the following figure.

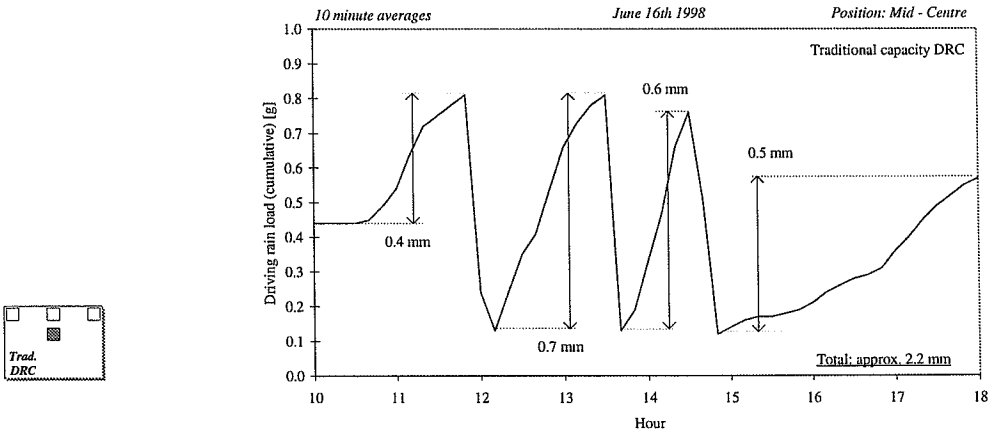

Figure 6.24 June 16th. Cumulative driving rain. Mid-Centre. *10-minute averages. Traditional capacity DRC.* Driving rain amount: 2.2 mm.

In this case, the 10-minute averages correspond relatively well to the 10-second values.

When processing the data, positive differences between 10-minute averages are interpreted as driving rain amounts. As shown above, this will lead to underestimation depending on the character of the rain event (number and frequency of siphoning). Also the position of the peaks in relation to the 10-minute intervals will influence the result. For comparison, the results of the five DRCs are given below.

June 16th, 1998 **10hrs to 18hrs, continuous rain**	**Graphical driving rain [mm]** ***10 sec instant. values***	**Algorithm driving rain [mm]** ***10 min average values***	**Ratio**
Load cell DRC, North-Top	6.0	4.4	0.73
Load cell DRC, Mid-Top	6.1	4.0	0.66
Load cell DRC, South-Top	6.2	5.3	0.85
Load cell DRC, Mid-Centre	3.3	2.4	0.73
Capacity DRC, do.	2.3	2.2	0.96

Table 6.2 June 16th. Comparison of driving rain amounts determined by graphical estimation based on 10-second instantaneous values and the algorithm employing 10-minute averages.

The specific period with continuous precipitation, and consequently frequent siphoning, clearly represents a *worst case*.

On a longer time scale, the magnitude of errors will be distributed on the different positions, depending on the gradient of the curve and the time of the siphoning relative to the averaging period. Longer periods of averaging would not allow for detection of siphoning. The underestimation could be reduced by means of shorter averaging periods and/or reservoirs with larger capacity. A better solution would be development of improved data processing, allowing for location of maximum values and siphoning. It has not been possible to further develop the data processing within the framework of the present project. Consequently, the 10-minute average procedure has been adopted as an approximative method.

6.3.6 June 15th 1998 06hrs to 16hrs, wind disturbance

The wind fluctuations were expected to disturb the signal from the load cells. In most cases, these fluctuations turn out to be insignificant on a larger scale; typically the wind fluctuations form a band with a width of approximately 20g, corresponding to a driving rain amount of 0.1mm. However, during the measurement series, situations with significant fluctuations in zero-precipitation situations have been observed. In the figure below, an example of such a situation is presented. The figure shows both reference precipitation and the load cell DRC output in position South-Top.

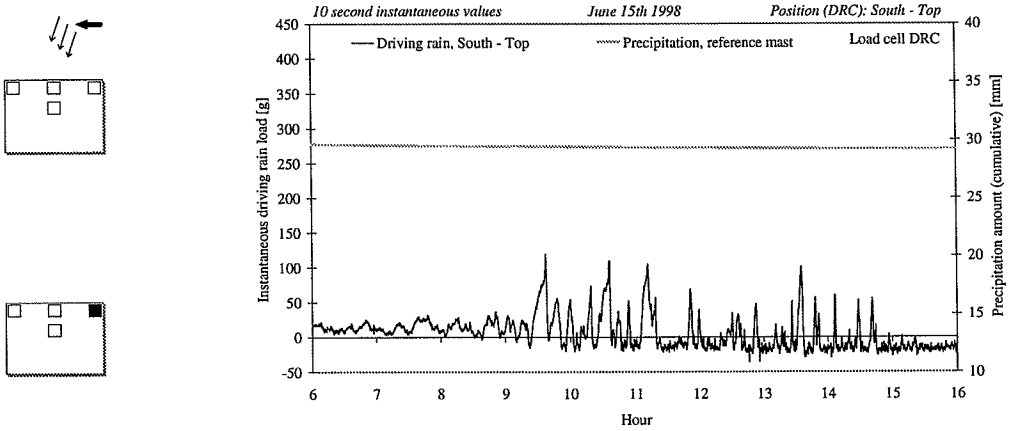

Figure 6.25 June 15th. Cumulative driving rain load at position South-Top and cumulative precipitation at reference mast. 10-second instantaneous values.

The load cell signal is fluctuating significantly. No precipitation is recorded. If a 10-minute average approach is applied, such fluctuations will be interpreted as driving rain. Note that a negative load level is not significant, as this is a matter of setting the zero load level. However, since driving rain is computed as increments in averages, the absolute level is not significant. The wind variation of the period is shown in the following two figures.

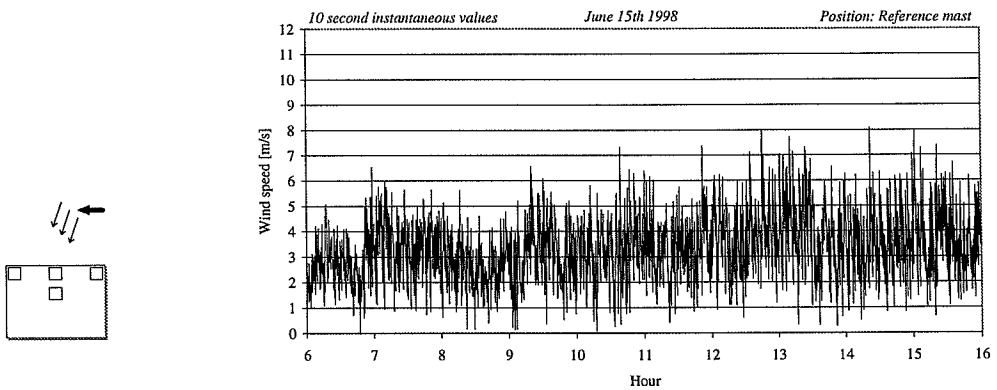

Figure 6.26 June 15th. Wind speed. Reference mast. 10-second instantaneous values.

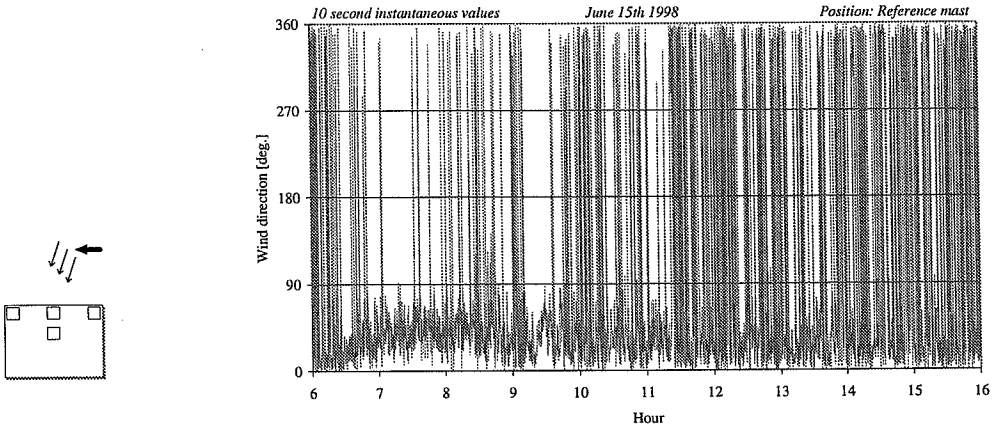

Figure 6.27 June 15th. Wind direction. Reference mast. 10-second instantaneous values. Lines across the diagram indicate changes past north (0° and 360°).

The gable is leeward and the wind speed is varying. The phenomenon may thus be due to turbulence at the collector position.

During the measurement series, these situations occur primarily at the South-top position. This may indicate that the position is more exposed than the other positions and/or that the particular DRC has a mechanical malfunction. The fluctuations, however, do not resemble the ordinary wind effects, as some build over more than one 10-second observation. After concluding the measurement series, it was discovered that the cable leading to the specific DRC was loose and was hanging along the gable from the DRC. In general, malfunctioning of a particular DRC can be examined by switching positions, but it has not been practicable within the time frame of the present project. The phenomenon may be explained by a malfunction in the set-up, as the cable may have been disturbing the load cell measurement under turbulent conditions.

Ordinary wind fluctuations can be eliminated by averaging over sufficiently long periods but, as mentioned earlier, long averaging periods is not an option if local driving rain maximum values are to be detected.

As the data processing has not yet been fully developed, the data has been selected to only deal with periods of significant precipitation. Errors due to wind fluctuation will thus be reduced relatively. This data selection can be further justified by the fact, that primarily significant precipitation events are of interest in a driving rain context.

6.3.7 May 21st 1998 10hrs to 16hrs, evaporation

Evaporation from the driving rain collector is an error source which should be subject to future studies. In the presentation of the example *May 3rd*, the evaporation loss was briefly mentioned. In the following, an example is given with focus on the evaporation. Basis for the study is a series of three spells, combined with frontal wind at the gable.

The three spells are shown in the following figure:

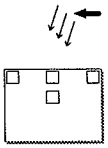

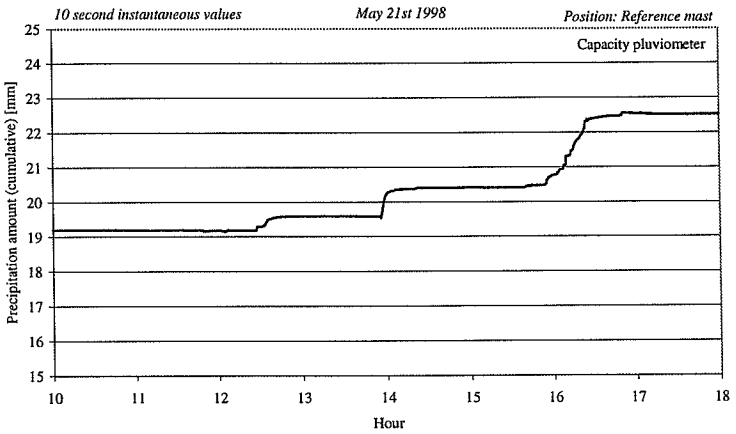

Figure 6.28 May 21st. Cumulative precipitation. Reference mast. 10-second instantaneous values.

Driving rain at position North-Top:

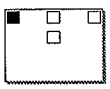

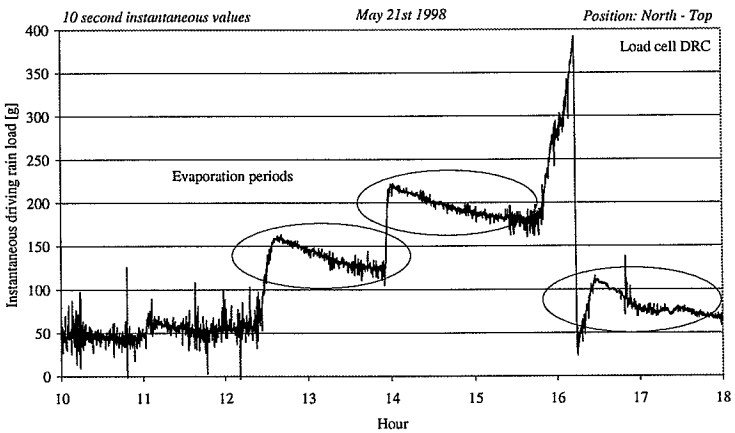

Figure 6.29 May 21st. Cumulative driving rain load. North-Top. 10-second instantaneous values. *Evaporation periods.*

In the figure above, the evaporation periods are marked with ellipses. The nature of the evaporation periods appear independent of load level, indicating that evaporation is mainly taking place from the collector net. The net is dried out by the wind, even if the humidity of the ambient air is high. Evaporation from the reservoir will progress at a lower rate, and will be less influenced by the wind.

As seen in the following figure, the gable is mainly windward and the wind speed is changing throughout the considered period.

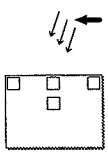

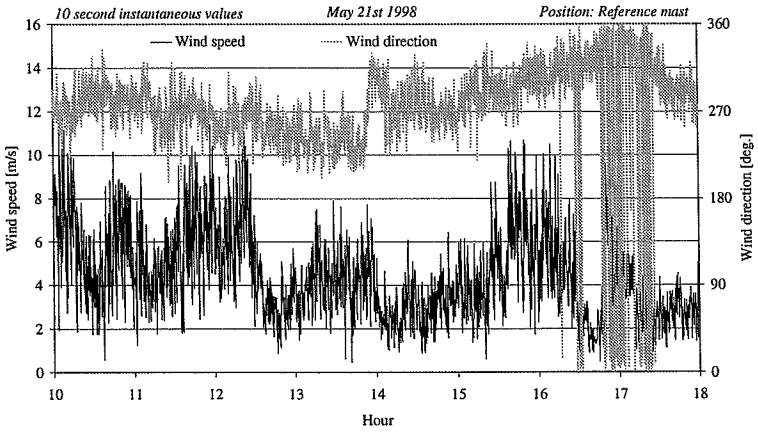

Figure 6.30 May 21st. Wind speed and wind direction. Reference mast. 10-second instantaneous values. Lines across the diagram indicate direction changes past north.

In order to evaluate the significance of the position on the gable, the following figure shows the results in position Mid-Centre for the same event.

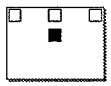

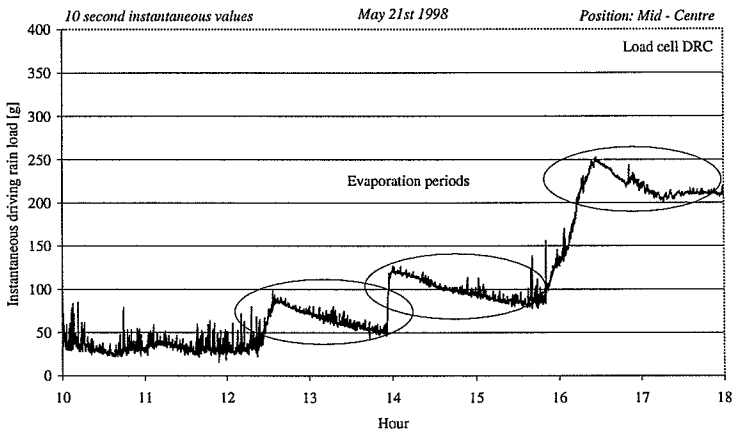

Figure 6.31 May 21st. Cumulative driving rain load. Mid-Centre. 10-second instantaneous values. *Evaporation periods.*

The DRC in position Mid-Centre exhibits a behaviour similar to the DRC in the North-Top position. In all of the considered evaporation periods, the evaporated amount is approximately 40 g in a period of 1½ hours. Thus, the evaporation rate is approximately 30 g/h, or 0.14 mm/h, independent of position on the gable.

For comparison, May 3rd, displayed an evaporation of 30 g in 4½ hours. This low rate may be the result of simultaneous low intensity driving rain and evaporation. The gable was leeward during the evaporation period on May 3rd, which may also reduce the evaporation. Also on May 3rd, positions Mid-Centre and North-Top were found to exhibit similar behaviour.

Due to continuous precipitation, no evaporation is visible on the figures of June 16th. However, the results above indicate that evaporation may occur during rain.

Evaporation during rain will lead to underestimation of driving rain. The phenomena have to be studied further to allow for possible corrective measures.

6.3.8 January to June 1998, precipitation and driving rain

The measurements have been going on longer than the driving rain series under consideration in this chapter. In the following table, key figures indicate the local differences in precipitation and the relatively small amounts of driving rain collected by the traditional DRC. Note that low temperature periods may cause uncertainty, as the equipment is not designed for measurement of snow. Low temperature periods are of minor interest in a driving rain context.

January - June 1998		**Jan**	**Feb**	**Mar**	**Apr**	**May**	**Jun**
Precipitation [mm]	*Denmark, average*	68	50	60	79	28	78
	Denmark, normal	57	38	46	41	48	55
	Værløse, meteorological station	55	57	63	85	15	65
	Project reference, 5 meter mast	29	26	37	62	20	49
Driving rain [mm]	*Traditional DRC*	2	8	3	1	1	5

Table 6.3 January to June 1998. Key figures, precipitation and traditional DRC.

The meteorological data have been acquired from the Danish Meteorological Institute (DMI). The meteorological station at Værløse has been chosen because of its situation not far from the university.

The project reference precipitation and the driving rain data are based on 10-minute average values. A threshold difference of 0.01mm/10min has been adopted as a criterion. The meteorological precipitation data are based on 3-hour values. DMI reports precipitation with a threshold value of 0.1mm/3h.

May is seen to be an unusually dry month, whereas June was more rainy than normally. Note that, except for the month of May, the reference precipitation amounts are significantly smaller than the amounts recorded by the meteorological institute. The microclimate measurements have been shut down due to work on the set-up and problems with the PC-capacity, but only in limited periods which cannot explain the observed difference. The difference may be due to an error in the set-up, but can also be explained by physical differences between the two stations.

The differences between the Værløse data and the reference data may be due to *regional variations* in climate, the data material is too limited to yield a basis for statistical analysis.

Another difference is the *microclimatic conditions*; the reference mast differs from standard meteorological conditions, 1.5 m above the ground. The DMI states that a reduction of 15% can be expected in an altitude of 10m, compared with the standard 1.5m position. The reference mast is in a height of approximately 14 metres leading to a reduction in the order of 20%. These guidelines apply for a logarithmic wind profile over a terrain with a relatively well-defined

roughness. It is consequently difficult to translate the correctional factors into a statement about a complex geometry such as the surroundings of the measurement station.

Some inaccuracy is introduced during *low temperature periods*. Snow is melted at the DMI station. The pluviometer at the reference mast is heated to prevent freezing, but snow is not melted.

In future studies, the reference precipitation measurements should be extended with an additional pluviometer, preferably mounted in a position comparable to standard meteorological conditions.

By means of the 3-axis ultrasonic anemometer, the vertical wind speed component is recorded simultaneously with the horizontal reference wind speed. The wind elevation angle is defined as the angle between the wind velocity and the horizontal, as given by

$$\xi = \text{Arc}\tan\left(\frac{w}{u}\right)$$

Where	ξ	is the wind elevation angle	[°]
	w	is the vertical wind speed component	[m/s]
	u	is the horizontal wind speed component	[m/s]

The elevation angle yields a measure of the influence of the building geometry on the reference wind. In order to evaluate the positioning of the pluviometer, the wind elevation angle is described as a function of wind direction and wind speed in the following two figures. Only the selected rain events of the measurement series are presented.

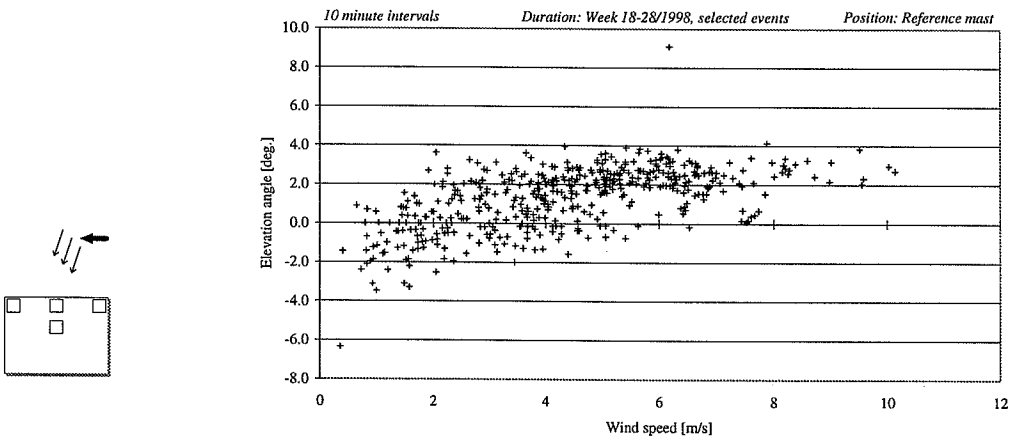

Figure 6.32 Wind elevation angle and wind speed. Position: Reference mast. 10-minute values.

With few exceptions, only small elevation angles are observed (< 4°). A linear relationship appears, but the data are too scattered to show any clear correlation.

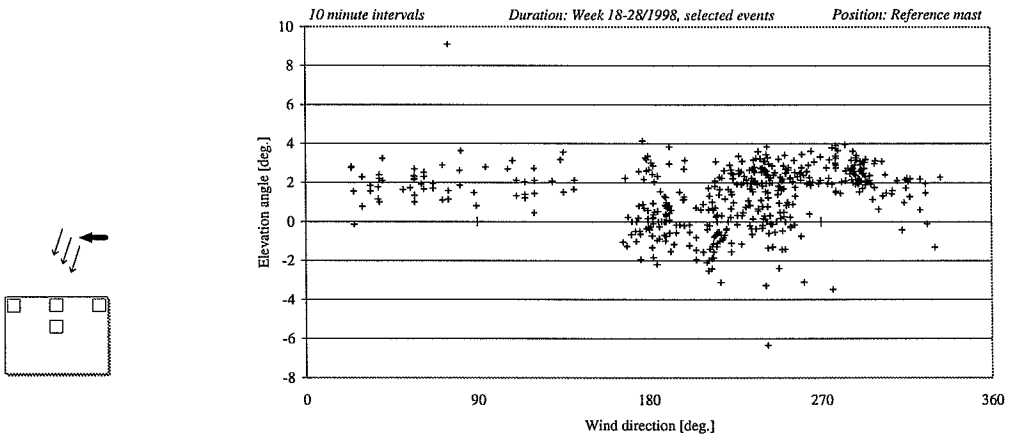

Figure 6.33 Wind elevation angle and wind direction. Position: Reference mast. 10-minute values.

There is no apparent correlation between wind direction and elevation angle. Negative values of the elevation angle are chiefly observed at wind directions between 180° and 270°.

The small elevation angles indicate that the wind at the reference mast is relatively undisturbed by the building. However, it cannot be excluded that the vertical wind speed component will affect the air flow around the pluviometer, particularly at high wind speeds - i.e. in connection with high intensity driving rain. It should be noted that the conditions in the immediate vicinity of the pluviometer may moreover be influenced both by the mast, which itself represents an obstacle, and by the adjacent humidity/temperature sensor equipped with radiation shield (see photograph below).

Photo 6.9 Reference mast.
Top: ultrasonic 3-axis anemometer.
Left: humidity and temperature probe in radiation shield.
Right: pluviometer.

6.3.9 Totals, selected series

To yield estimates of the ratio of driving rain to precipitation as well as of the spatial distribution of the driving rain on the gable, key figures are given in the table below. The results are obtained on the basis of differences between 10-minute average values.

Results	**Total observed amount [mm]**	**Ratio to precipitation**
Precipitation - Reference mast	71	1
Driving rain		
Capacity DRC, Mid - Centre	8	0.1
Load cell DRC, do.	13	0.2
Load cell DRC, North - Top	23	0.3
Load cell DRC, Mid - Top	22	0.3
Load cell DRC, South - Top	29	0.4

Table 6.4 Measurement series. Selected rain events, May 3rd to July 11th 1998. Totals and ratio of driving rain to reference precipitation.

Schematic of the estimated catch ratios:

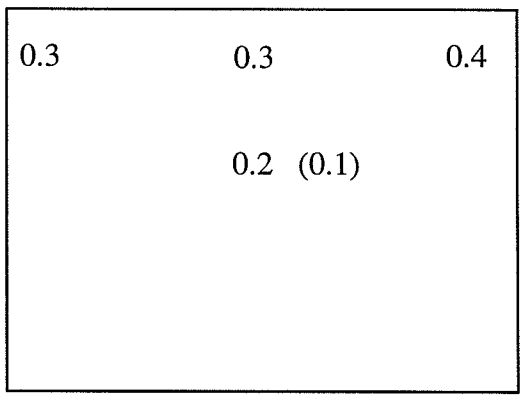

Figure 6.34 Catch ratios. Ratio of collected driving rain to normal precipitation. Load cell DRCs in four positions on the gable.

The catch ratios above correspond well with the Wall Factors of the British standard BS 8104 [BSI, 1992], currently being introduced as a CEN standard in a slightly edited form [CEN/TC89, 1998]. Qualitatively the descriptions match for the specific building shape, and on the basis of the present data material. The standard operates with a set of site-specific, correctional factors to account for local conditions such as topology, terrain roughness and obstacles (the description is elaborated in Chapter 9). A quantitative comparison should be based on hourly values of wind and precipitation, combined with the correctional factors, according to the method of the standard. Such a comparison should be carried out, when the data processing of the load cell DRCs have been fully developed and preferably on the basis of measurement series of longer duration. However, as the standards are based on findings by means of traditional driving rain collectors, and as the preliminary results indicate a substantial discrepancy between the catch of the traditional and the load cell DRCs, it would be expected that the present guidelines underestimate the driving rain amounts.

6.3.10 Comparative full-scale test of alternative DRC designs

As a result of collaboration with Fabien van Mook, Eindhoven University of Technology and Anneli Högberg, Chalmers University of Technology, comparative testing of three types of DRCs has been ongoing since the beginning of July 1998. Three different DRC designs have been mounted side-by-side on the facade of a high rise building at the university.

The three DRC types are:

I	Load cell DRC	(Kragh)
II	DRC with wiper	(van Mook)
III	Tipping bucket DRC	(Högberg)

The set-up is shown in the following photograph:

Photo 6.10 Comparative test of three DRC designs. Facade of a high-rise building at Eindhoven University of Technology.

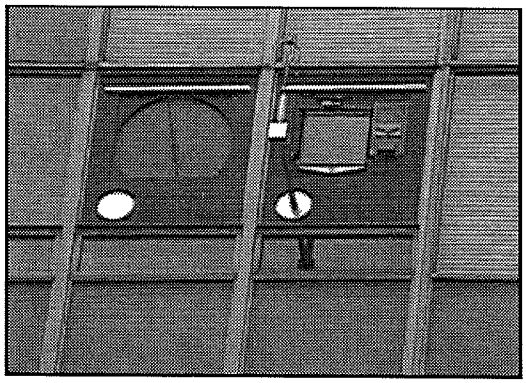

Left: DRC with wiper; middle: load cell DRC; right: tipping bucket DRC. In front of the DRCs, the surface wind speed and direction is measured by means of a Gill WindMaster, ultrasonic 3-axis anemometer [Photograph: ir. Fabien J.R van Mook, Eindhoven University of Technology].

Preliminary results indicate that the DRC with wiper collects twice the amount of driving rain collected with a similar DRC without wiper [Mook, 1998]. This result corroborates the findings of the present work, namely that, when employing a traditional DRC, evaporation of droplets staying on the collector reduces the collected amount significantly.

6.4 Case Study Summary

In the present study, two types of driving rain collectors are compared:

- Traditional capacity DRC
  - Catchment-area: 0.64 m²
  - Teflon coated collector
  - Young capacity pluviometer
- Load cell DRC
  - Catchment-area: 0.21 m²
  - Net mounted inside collector tray
  - Load cell measurement of collector and reservoir

The two types are mounted side-by-side on the gable.

The novel load cell DRC has been developed in order to improve performance by reducing errors due to reflection, delayed draining and evaporation from the collector. The principle is based on use of a load cell which results in a low-cost, flexible solution.

To investigate the spatial distribution of the driving rain, additional three load cell DRCs have been mounted along the top edge of the gable.

The case study is based on preliminary results, recorded in the period of April 27th to July 12th 1998. Only significant rain events have been selected for the study.

Estimation of the driving rain amounts and the distribution on wind direction and wind speed is based on 10-minute average values. A positive difference in 10-minute average value is interpreted as an increment in the cumulative driving rain amount.

Reference precipitation is recorded at a wide range of wind speeds (~ 0.5 - 10 m/s). The major part of the rain events occur at wind directions between approximately 180° and 330°, i.e. the considered gable is mainly windward.

In all of the four positions, driving rain is recorded at a wide range of wind speeds. The highest driving rain intensities, and the largest number of cases, occur when the gable is windward. Small amounts of driving rain is recorded when the gable is leeward. This is ascribed to turbulent conditions at the gable and may also be due to brief wind fluctuations combined with precipitation.

The novel load cell DRC detects substantially more driving rain than the traditional capacity DRC. During the measurement series, at total driving rain amount of 8 mm was collected by means of the traditional DRC, whereas an amount of 13 mm was collected by means of the load cell DRC. In general, the traditional DRC collects approximately 60% of the amount collected by the load cell DRC. This result is corroborated by preliminary findings of Mook [1998] in Eindhoven, who has developed a DRC with a wiper mechanism.

Droplets staying on the collector plate are not detected by the traditional DRC, thus evaporation and lacking draining will result in significant underestimation.

A driving rain event of high intensity and short duration is clearly detectable by the novel DRC. Fluctuations owing to wind pulsation turn out to be insignificant on a larger scale. Detection of low intensity driving rain may be counteracted by simultaneous evaporation (e.g. May 3rd).

The output of the novel DRC is in the form of the total weight of collector, reservoir and collected driving rain. In order to filter out the wind fluctuations, and reduce the amount of data, averaging is necessary. The preliminary results are based on 10-minute average values, as an increment in weight is interpreted as onslaught driving rain. Consequently, the effect of 10-minute averaging has been investigated.

The reservoir is self-siphoning. When the reservoir is emptied, the weight drops suddenly. Thus, the accuracy of the averaging is sensitive to the number and frequency of siphonings. The error introduced will result in underestimation, as the extreme values are not detected accurately. June 16th is presented as a *worst case*. In this specific case, 8 hours of continuous rain resulted successive siphoning. Depending on the history of the specific load cell DRC, the

ratio between driving rain amounts estimated graphically (10-second instantaneous values) and driving rain amounts determined by the 10-minute averaging approach range between 0.66 and 0.85. This error can be reduced by means of a reservoir with larger capacity, or by means of shorter averaging periods.

Wind fluctuations are found to cause insignificant fluctuations during rain, whereas disturbances have been considerable in no-precipitation situations. As a consequence, only clearly detectable rain event have been selected for the present case study. An example (June 15th) is presented in order to demonstrate a situation giving rise to errors if the 10-minute averaging approach is adopted uncritically. In the specific situation, the gable is leeward and the wind speed is changing rapidly. The large fluctuations are attributed to a malfunction of the set-up: a cable was found to hang from the DRC along the gable and may have influenced the load cell measurements when exposed to turbulence.

It is found that, even in periods of high relative air humidity in connection with rain events, water is evaporating from the collector. A driving rain event is superseded by an evaporation period corresponding to drying of the collector net. Independent of the position on the gable, an evaporation rate of approximately 0.14 mm/h is found in no-precipitation situations where the gable is windward. Evaporation from the reservoir is progressing at a lower rate. In cases with continuous precipitation, evaporation is not detectable. However, the results above indicate that evaporation occurs during rain. Evaporation during rain will lead to underestimation of driving rain. The phenomena should be subject to future studies to yield guidelines for correction of data. Superimposition of a correctional evaporation rate is an option.

It has not been possible to complete the development of data processing for the novel load cell DRC. A fundamental approach has been adopted to generate an approximate characterization of the measurement series. Selected studies are presented graphically to demonstrate selected aspects. Further development of the data processing will be a straight forward programming and mathematics task.

To give a rough measure of the exposure of the gable and the spatial distribution of the driving rain, the ratio of driving rain to reference precipitation has been determined. A total reference precipitation of 71 mm has been recorded during the measurement series. Schematic representation of the estimated catch ratios:

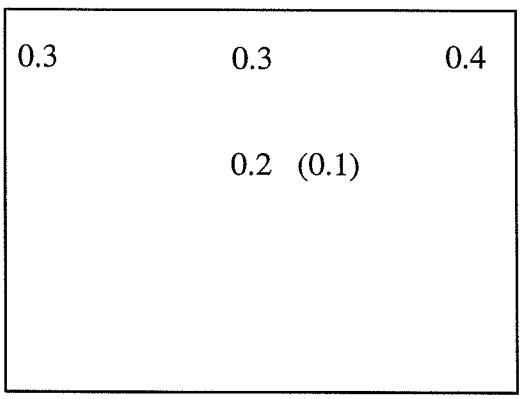

Figure 6.35 Catch ratios. Ratio of collected driving rain to normal precipitation. Load cell DRCs in four positions on the gable.

These ratios are based on 10-minute averaging, which may result in underestimation, cf. previous remarks. The ratios provide a preliminary basis for quantification of driving rain

loads. Qualitatively, the spatial distribution corresponds well to the guidelines of the British standard BS 8104 [BSI, 1992]. The preliminary nature of the series does not allow for generalization in terms of more exact correlation between wind and driving rain. In particular, it is noticeable that the novel load cell DRC detects substantially more driving rain than the traditional DRC. Improvement of the data processing routines, and further knowledge of the extent of evaporation, will lead to increasing catch ratios for the load cell DRCs.

Preliminary results indicate that the traditional DRC type leads to underestimation owing to lacking draining and subsequent evaporation from the collector. The present guidelines are based on results obtained by means of traditional DRCs - If future studies corroborate that the evaporation loss leads to underestimation, it may have implications for future guidelines. However, measurement series of longer duration have to be carried out.

In order to assess the difference between the measurement principles, a comparative test of the load cell DRC, a DRC with a wiper and a tipping bucket DRC is currently being carried out side-by-side at the facade of a high-rise building at the Eindhoven University of Technology.

Chapter 7

LONG-WAVE IRRADIATION

7.1 Theory

Numerous empirical relationships describing the atmospheric component of the incident long-wave radiation have been proposed and corroborated. The long-wave sky radiation is expressed as a function of the ambient air temperature and possibly the air humidity and cloud cover.

The Danish Design Reference Year, DRY, contains typical values for the sky radiation. When DRY is not applicable, and when measured long-wave data are not available, approximative calculation of the incident long-wave radiation is an option.

Whereas horizontal surfaces only exchange radiation with the sky vault, inclined surfaces will moreover exchange radiation with the surroundings.

Studies have shown that the surroundings can be assumed to act as a black-body radiator at air temperature as an acceptable approximation. However, apart from the relation to the air temperature, the actual temperature of the surroundings depends on cloud cover and the specific heat of the materials involved. On a clear night, materials with low specific heat will have a lower temperature than the air, owing to the radiation to the sky vault, whilst materials with a high specific heat will tend to have a higher temperature because of the energy stored during the preceding day.

The ratio of the radiation to the surroundings to the sky radiation depends on the purely geometrical view factors as well as on the anisotropic distribution of the radiation. The latter aspect may result in significant errors under clear sky conditions when employing simplified empirical formulae.

Example
In the following, an example is presented to convey an impression of the magnitudes. A flat roof is exchanging radiation with the sky on a clear night with an ambient dry-bulb temperature, t_a, of 10°C. For this example, the surface is assumed to have the same temperature as the ambient air. Hence, $T_s = T_a = 283$ K. The roof has emissivity, $\varepsilon_s = 0.9$. The long-wave sky irradiation would typically have a magnitude of L = 270 W/m² [Cole, 1979]. Thus, the radiosity of the surface is given by

$$J_s = \varepsilon_s \sigma T_s^4 = 0.9 \times 5.67 \times 10^{-8}\ \mathrm{W/m^2K^4} \times (283\ \mathrm{K})^4 \approx 330\ \mathrm{W/m^2}$$

Where	J_s	is the radiosity of the horizontal surface	[W/m²]
	ε_s	is the long-wave emissivity of the surface	[-]
	σ	is the Stefan-Boltzmann constant	[5.67×10^{-8}W/m²K⁴]
	T_s	is the absolute temperature of the surface	[K]

Consequently, at the surface, the result is a net radiation loss, J_{loss}, of

$$J_{loss} = 330 - 270 = 60\ \mathrm{W/m^2}$$

In this situation, the equivalent black-body sky temperature, T_{sky}, is defined by

$$J_{loss} = \varepsilon_s \sigma \left(T_s^4 - T_{sky}^4 \right)$$

Hence

$$T_{sky} = \sqrt[4]{T_s^4 - \frac{J_{loss}}{\varepsilon_s \sigma}} = \sqrt[4]{(283\text{K})^4 - \frac{60\text{W/m}^2}{0.9 \times 5.67 \times 10^{-8}\text{W/m}^2\text{K}^4}} \approx 269\text{K}$$

The actual radiation is equivalent to the exchange between the surface and a black-body radiator at temperature $t_{sky} = -4°C$.

Note that the surface under consideration is assumed small compared with the surroundings and the sky. The problem is categorized as a *small convex object surrounded by a large enclosure*, and the emissivity of surroundings and sky are consequently set equal to 1.

In connection with the present project, long-wave sky radiation incident upon a horizontal surface has been measured at a flat roof. Partly in order to acquire a 'full' set of local parameters for hygrothermal calculations, partly to compare the results with existing empirical formulae. Strictly speaking, computation of long-wave sky radiation is not a microclimatic problem, however, the comparison of long-wave radiation incident upon horizontal and vertical surfaces is relevant to microclimatic calculations. Consequently, apart from the horizontal measurements, two short duration measurement series have been carried out on vertical surfaces facing 18° (~ north - north east) and 288° (~ west - north west) respectively. Ideally, simultaneous measurements on a horizontal surface should have been carried out, but only one instrument was available to the project.

Long-wave radiation incident upon horizontal and vertical surfaces *[Cole, 1979, 1976]*
Cole carried out a study on long-wave radiation incident upon external surfaces of buildings, during which both horizontal and inclined surfaces were investigated. Cole concluded that the assumption of the surroundings acting as a black-body radiator yields acceptable approximations. He proposed a set of equations for the calculation of incident long-wave radiation on the basis of ambient dry-bulb temperature and cloud cover. The formulae for horizontal and vertical surfaces are given below, whereas referral is made to Cole [1979, 1976] for elaborate details.

The incident long-wave radiation is given by the sum of the atmospheric and ground components, $L_{A(\gamma)}$ and $L_{G(\gamma)}$.

$$L_{(\gamma)} = L_{A(\gamma)} + L_{G(\gamma)}$$

Where	$L_{(\gamma)}$	is the long-wave radiance incident upon an inclined building surface	[W/m²]
	$L_{A(\gamma)}$	is the atmospheric component of do.	[W/m²]
	$L_{G(\gamma)}$	is the ground component of do.	[W/m²]
	γ	is the surface tilt angle	[°]

Horizontal surface, $\gamma = 0°$

A horizontal surface only 'sees' the sky. Thus, only the contribution from the sky vault is considered.

$$L_h = L_{h,clear} + (65 + 1.39t_a)c$$

Where	L_h	is the atmospheric radiance incident upon a horizontal surface	[W/m²]
	$L_{h,clear}$	is the clear sky do.	[W/m²]
	t_a	is the ambient air temperature	[°C]
	c	is the fractional cloud cover	[-]

The atmospheric radiation upon a horizontal surface during clear sky conditions; $L_{h,clear}$, is expressed as a function of the ambient air temperature, t_a:

$$L_{h,clear} = 222 + 4.94t_a$$

Vertical surface, $\gamma = 90°$

Ground component

$$R_{G(\gamma)} = \sigma T_a^4 \sin^2\left(\frac{\gamma}{2}\right) = \sigma T_a^4 \sin^2\left(\frac{90°}{2}\right) = 0.5\sigma T_a^4$$

Where	T_a	is the ambient air temperature	[K]
	σ	is the Stefan-Boltzmann constant	[5.67×10^{-8}W/m²K⁴]

Atmospheric component

$$L_{A(90°)} = 0.5L_h + 0.3457\psi_1\sigma T_a^4$$

As stated above, the atmospheric radiance incident upon a horizontal surface, L_h, is given by

$$L_h = L_{h,clear} + (65 + 1.39t_a)c = 222 + 4.94t_a + (65 + 1.39t_a)c$$

Where	L_h	is the atmospheric radiance incident upon a horizontal surface	[W/m²]
	$L_{h,clear}$	is the clear sky do.	[W/m²]
	t_a	is the ambient air temperature	[°C]
	c	is the fractional cloud cover	[-]

The auxiliary quantities ψ_1 and ψ_2 are given by

$$\psi_1 = 0.09(1 - \psi_2 c)$$

$$\psi_2 = 0.7067 + 0.00822t_a$$

Note that, in the above example, the terminology has been slightly edited, compared with Cole [1979]. The complex nature of the relationship above is owing to Cole's generally applicable set of formulae and constants for inclined building surfaces.

The following three approximative methods from the references have been described in connection with the chapter on long-wave radiation. The formulae are briefly summarized below.

a) Lund [Hansen et al., 1992]

The most simple formulae are given by Lund in Hansen et al. [1992]. The formulae express the radiation temperature as a function of ambient air temperature with possible correction for cloud cover.

Horizontal surface:

$$t_{rad} = 1.2 \cdot t_a - 14$$

Vertical surface:

$$t_{rad} = 1.1 \cdot t_a - 5$$

Where	t_{rad}	is the equivalent black-body radiation temperature	[°C]
	t_a	is the ambient air temperature	[°C]

If the cloud cover is N okta, interpolation is made by the expression

$$t_{rad,N} = \frac{(8-N) \cdot t_{rad} + N \cdot t_a}{8}$$

b) Berdahl and Martin [1984]

The following empirical relationship is suggested by Berdahl and Martin on the basis of data from USA. The correlation is valid for clear sky conditions.

Horizontal surface:

$$T_{sky} = T_a \sqrt[4]{0.711 + 0.0056 t_{dp} + 0.000073 t_{dp}^2 + 0.013 \cos\left(2\pi \frac{n}{24}\right)}$$

Where	T_{sky}	is the black-body sky radiation temperature	[K]
	T_a	is the ambient air temperature	[K]
	t_{dp}	is the ambient dew point temperature	[K]
	n	is the hour from midnight	[-]

The quantity under the root sign is also known as the equivalent sky emissivity.

Vertical surface:

It is common practice to assume the surroundings to have the same temperature as the ambient air. The view factors of an unobstructed, vertical surface are 0.5/0.5 for sky/ground. Assuming

the surrounding ground to be at ambient air temperature, the black-body radiation temperature is given as follows:

$$T_{rad} = \frac{T_{sky} + T_a}{2}$$

Where	T_{rad}	is the black-body radiation temperature	[K]
	T_{sky}	is the black-body sky radiation temperature	[K]
	T_a	is the ambient air temperature	[K]

For comparison, this assumption has been adopted in the computing of equivalent radiation temperature for a vertical surface.

c) Cole [1979]

Horizontal surface:

$$L_h = L_{h,clear} + (65 + 1.39t_a)c = 222 + 4.94t_a + (65 + 1.39t_a)c$$

Where	L_h	is the atmospheric radiance incident upon a horizontal surface	[W/m²]
	$L_{h,clear}$	is the clear sky do.	[W/m²]
	t_a	is the ambient air temperature	[°C]
	c	is the fractional cloud cover	[-]

Vertical surface:

The incident radiation is given as the sum of the ground component and the atmospheric component. Combining the previously described expressions yields

$$L_v = 0.5\sigma T_a^4 + 0.5L_h + \left[0.031 - c \times (0.022 + 0.00026t_a)\right] \times \sigma T_a^4 \Rightarrow$$

$$L_v \approx 0.5L_h + \left[0.53 - c \times (0.022 + 0.00026t_a)\right] \times \sigma T_a^4$$

Where	L_v	is the atmospheric radiance incident upon a vertical surface	[W/m²]
	L_h	is the atmospheric radiance incident upon a horizontal surface	[W/m²]
	T_a	is the ambient air temperature	[K]
	c	is the fractional cloud cover	[-]
	σ	is the Stefan-Boltzmann constant	[5.67×10^{-8} W/m²K⁴]

Radiation temperature:

The equivalent black-body radiation temperature, T_{rad}, is obtained as follows:

$$L = \sigma T_{rad}^4 \Rightarrow T_{rad} = \sqrt[4]{\frac{L}{\sigma}}$$

Where L	is the incident long-wave radiance		[W/m²]
σ	is the Stefan-Boltzmann constant		[5.67×10^{-8} W/m²K⁴]
T_{rad}	is the black-body radiation temperature of the surface		[K]

7.2 Measurements

Three periods are studied, namely

Horizontal surface				
	I	Winter	2 weeks	January 5th to 18th
Vertical surface				
	II	North	2 weeks	June 1st to 14th
	III	West	2 weeks	July 6th to 19th

The measured incident long-wave radiation is converted into an equivalent radiation temperature (black-body) and compared to the methods as suggested by the three different references described above.

Meteorological data
Meteorological data have been acquired from the Danish Meteorological Institute (DMI). Observations of cloud cover are available from the meteorological station at Værløse, not far from the university. The cloud data are recorded every 3 hours. For this study, every 3rd, hourly average value has been used as basis for the presentation.

7.3 Results

The ambient air temperature and the relative humidity of the ambient air are recorded at the microclimate full-scale set-up. The relative humidity has subsequently been converted into dew point temperature, employing the formulae stated in an appendix to the present report. Data have been recorded in three positions from the end of December 1997 (sequence: horizontally at the roof, vertically at the north facing facade, vertically at the west gable). In the following, the results of these three periods are presented.

The figure below shows the results of the horizontal surface during two weeks in January 1998.

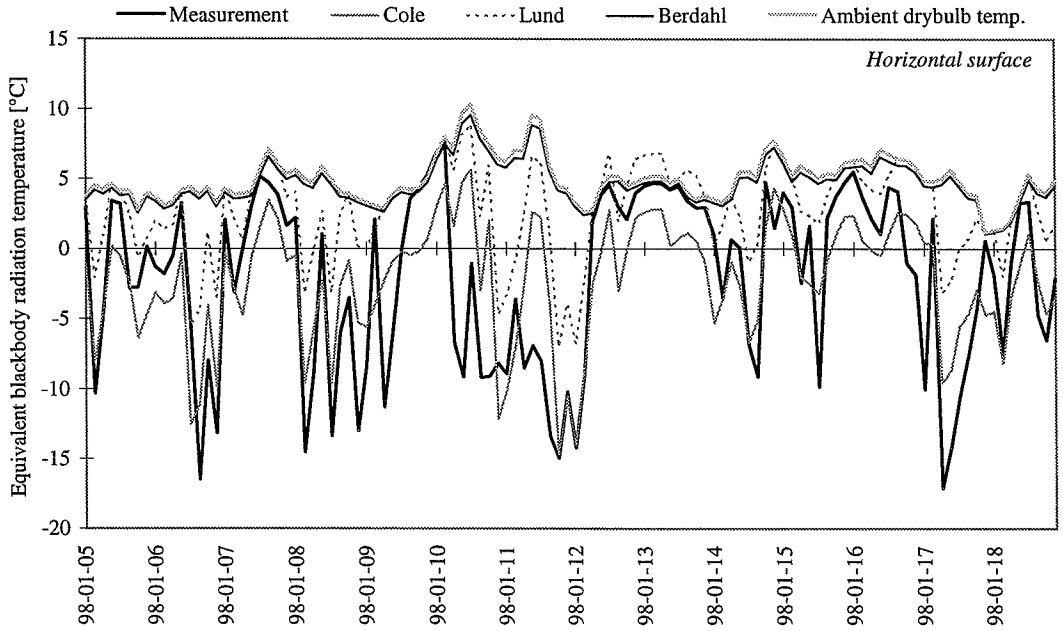

Figure 7.1 Equivalent black-body radiation temperature and ambient air temperature. Horizontal surface. January 5th to 8th. 1-hour averages every 3rd hour.

In the figure above, the measured incident long-wave radiation has been converted into an equivalent black-body radiation temperature. This *measurement* value is compared with both the results obtained by means of empirical formulae and the ambient air temperature.

The best approximation is obtained by the *Cole formulae*. Generally, however, large discrepancies appear. In the following figure, the equivalent black-body radiation temperature and the ambient air temperature are seen in context with the observed cloud cover.

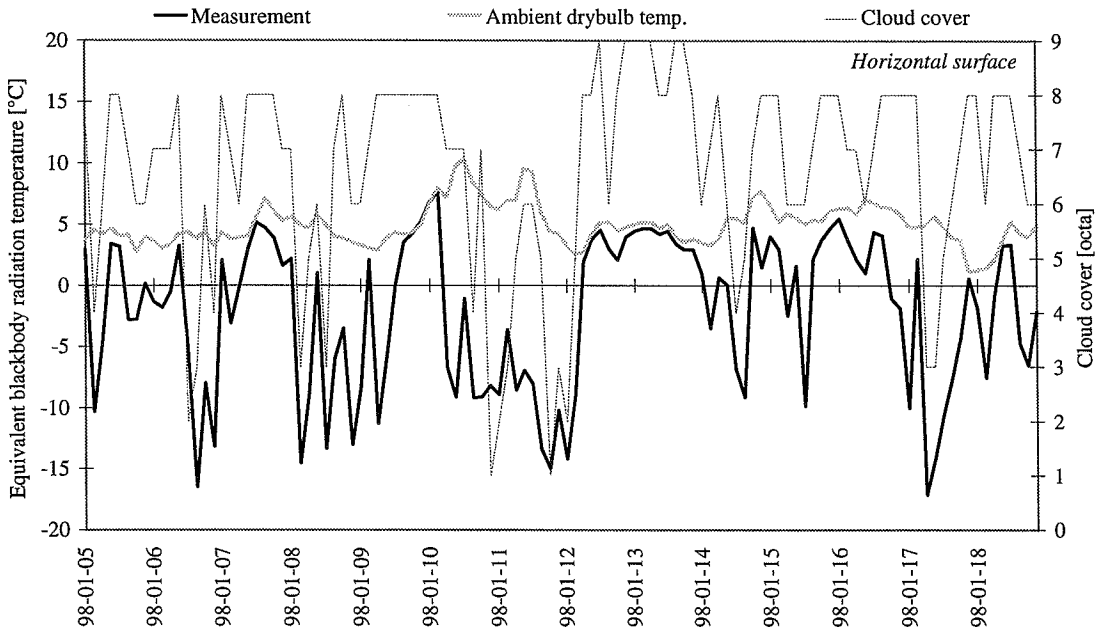

Figure 7.2 Equivalent black-body radiation temperature, ambient air temperature and cloud cover (0: clear sky, 8: overcast, 9: no observation available due to fog or other circumstances). Horizontal surface. January 5th to 8th. 1-hour averages every 3rd hour.

The period is dominated by overcast conditions. The radiation temperature is seen to approach the ambient air temperature when the sky is overcast.

The figure below shows the results of a vertical, north facing surface during two weeks in June 1998. Note that on June 3rd, the pyrgeometer was briefly disconnected because of work on the set-up. As the influence of the sky radiation is reduced, the empirical expressions yield more similar results in this situation. The *Cole formulae* yield the best approximation. The equivalent black-body radiation temperature is generally close to the ambient air temperature.

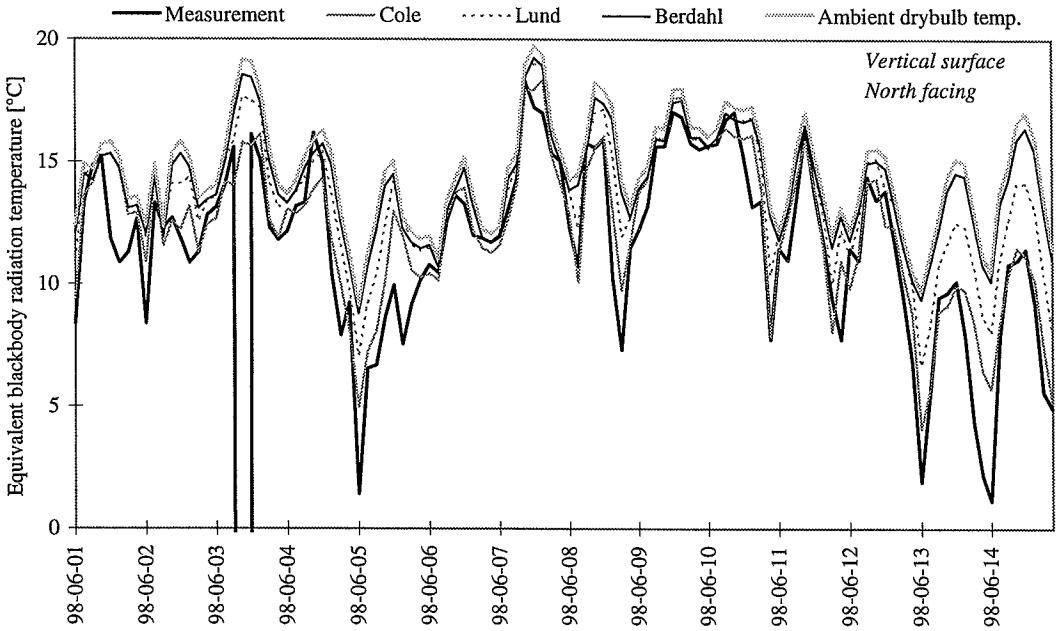

Figure 7.3 Equivalent black-body radiation temperature and ambient air temperature. Vertical, north facing surface. June 1st to 6th. 1-hour averages every 3rd hour. The pyrgeometer was briefly disconnected on June 3rd.

Towards the end of the series, the curves are spread and the Cole curve is closest to the measured values. In the following figure, the equivalent black-body radiation temperature and the ambient air temperature are seen together with the observed cloud cover. The spread of the curves at the end of the series is due to reduced cloud cover.

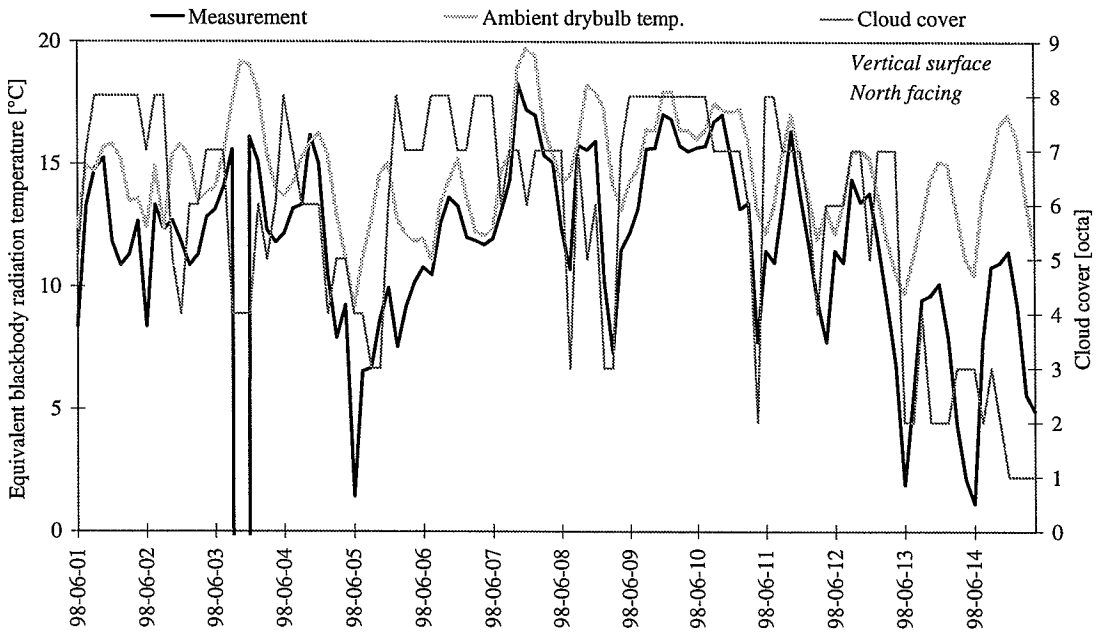

Figure 7.4 Equivalent black-body radiation temperature, ambient air temperature and cloud cover. Vertical, north facing surface. June 1st to 6th. 1-hour averages every 3rd hour. The pyrgeometer was briefly disconnected on June 3rd.

A similar series of a vertical, west facing surface is shown in the following figure. Again, the Cole expression yields the best approximation.

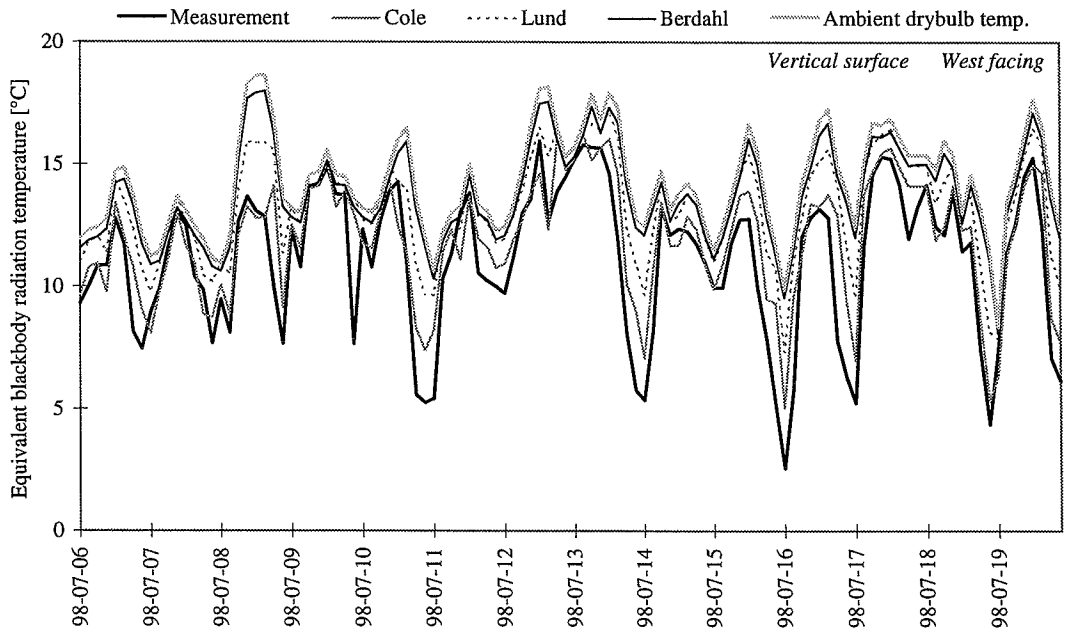

Figure 7.5 Equivalent black-body radiation temperature and ambient air temperature. Vertical, west facing surface. July 6th to 19th. 1-hour averages every 3rd hour.

The following figure shows the equivalent black-body radiation temperature and the ambient air temperature in context with the observed cloud cover. The largest discrepancies appear in situations with limited cloud cover and consequently minor influence of the clear sky radiation.

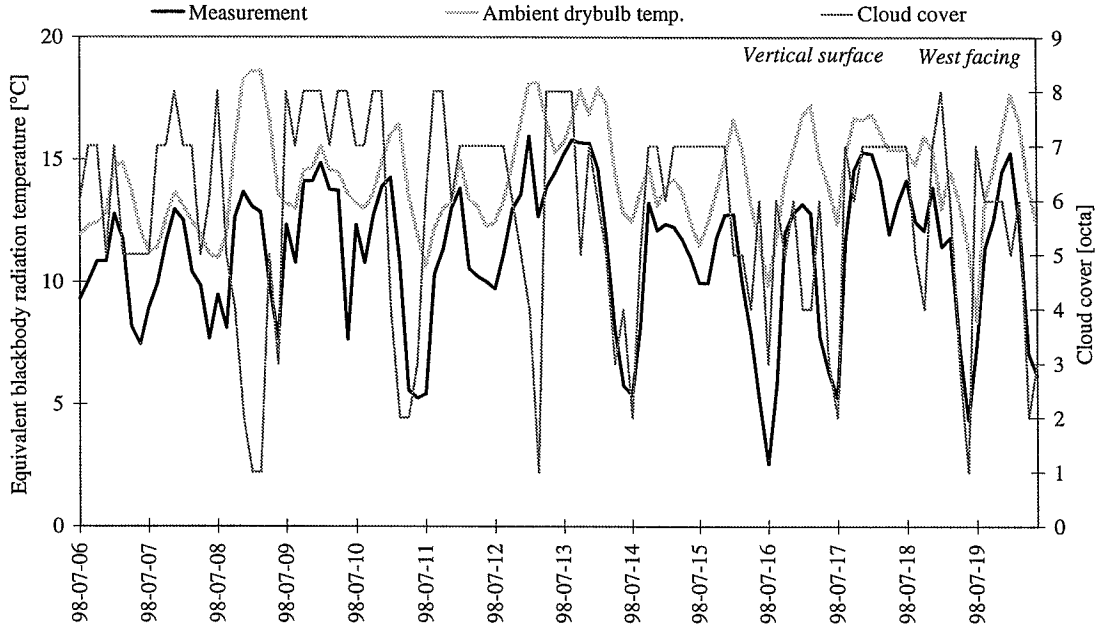

Figure 7.6 Equivalent black-body radiation temperature, ambient air temperature and cloud cover. Vertical, west facing surface. June 6th to 19th. 1-hour averages every 3rd hour.

7.4 Findings

The estimation of long-wave irradiation on the basis of standard meteorological parameters such as ambient air temperature and dew point temperature is not a microclimatic issue. However, in lack of measured data, the correction of reference data into local parameters can be a necessary measure. Thus, it is relevant to investigate the validity of the assumptions as to the behaviour of the surroundings in terms of long-wave radiation exchange with, for instance, vertical surfaces of buildings.

The Danish Reference Year (DRY) contains long-wave sky radiation data, but these are not accurate.

Empirical expressions have been established for the determining of sky radiation on the basis of standard meteorological data. These are not very accurate. Particularly during clear sky conditions they may result in large errors.

When estimating the long-wave radiation exchange between a building envelope and its surroundings, it is common practice to assume the surroundings to be black-body radiators at ambient air temperature. In situations/positions with no shading objects or obstacles, the view factors are 0.5/0.5 for sky and surroundings.

In situations with significant radiation to the sky vault (e.g. clear night conditions), and surroundings with limited thermal capacity, these assumptions are expected to result in errors, as the surroundings are undercooled by radiation. Analogously, surroundings with large thermal capacity will remain at temperatures above the ambient air after periods with solar irradiation.

Measurements of long-wave irradiation have been carried out from horizontal and vertical surfaces, in order to compare with common empirical expressions.

Simultaneous pyrgeometer measurement from vertical and horizontal surfaces would have been valuable, but the project was at the disposal of only one instrument. Such measurements should be subject of future studies.

The atmospheric component of the long-wave irradiation clearly constitutes the most uncertain part of the estimation. This is reflected in large discrepancies between the measured and the theoretically determined values.

The determination is more accurate for the vertical surfaces, as the most uncertain part - the atmospheric component - becomes less significant.

The assumption of the surroundings acting as a black-body radiator at ambient air temperature appears to yield an adequate approximation under the considered conditions - particularly when the uncertainty of the atmospheric component is taken into account.

The best fit to the measured data was achieved by Cole's formulae for long-wave radiation incident upon inclined building surfaces [Cole, 1979].

An empirical expression developed by Berdahl and Martin [1984] turned out to overestimate the equivalent sky radiation temperature. The expression was developed for clear sky conditions, and should thus be expected to underestimate the sky temperature. The expression is based on data from USA which may explain some of the difference.

Overcast conditions, which was the prevailing situation during the series, are easier to estimate, as the temperature of the clouds approaches ambient air temperature.

Chapter 8

WINDOW CONVECTION HEAT TRANSFER

8.1 Theory

The convective heat transfer coefficient is of particular interest in relation to studies of condensation phenomena. When calculating heat loss, very rough guidelines relate the film coefficient to reference wind velocities.

The objective of this case study is to assess the magnitude of the convective heat transfer coefficient of a 'normal' double pane glazing and relate the findings to the guideline values. As the main interest is the risk of occurrence of condensation on the exterior surface of modern well-insulating glazing systems, only night-time observations are considered. Consequently, the solar radiation is not part of the surface energy balance.

Surface energy balance
The night-time energy balance at the exterior surface of the building envelope can be expressed as

$$q_g + \varepsilon L = \varepsilon\sigma T_s^4 + h_c(T_s - T_a)$$

Where	q_g	is the glazing heat flux from the interior	[W/m²]
	L	is the incident long-wave radiance	[W/m²]
	ε	is the emissivity of the external surface	[-]
	σ	is the Stefan-Boltzmann constant	[5.67×10^{-8} W/m²K⁴]
	h_c	is the convection heat transfer coefficient	[W/m²K]
	T_s	is the temperature of the external surface	[K]
	T_a	is the temperature of the ambient air	[K]

Note that the heat capacity of the building envelope and effects of moisture transfer have been neglected.

Figure 8.1, below, shows a schematic representation of the energy balance at the external surface of the glazing. The heat flux from the inner side of the glazing comprises heat transfer in the cavity of the window pane. The thermal resistance of the glazing, without surface coefficients, is calculated theoretically by use of the programme WINDOW 4.1. Given the thermal resistance of the centre part of the glazing, R_c, and the two surface temperatures, the glazing heat flux is calculated as follows:

$$q_g = \frac{\Delta T_g}{R_c} = \frac{T_{s,i} - T_s}{R_c}$$

Where	q_g	is the glazing heat flux from the interior	[W/m²]
	T_s	is the external surface temperature of the glazing	[K]
	$T_{s,i}$	is the internal surface temperature of the glazing	[K]
	ΔT_g	is the temperature difference across the glazing	[K]
	R_c	is the thermal resistance of the glazing (centre part)	[m²K/W]

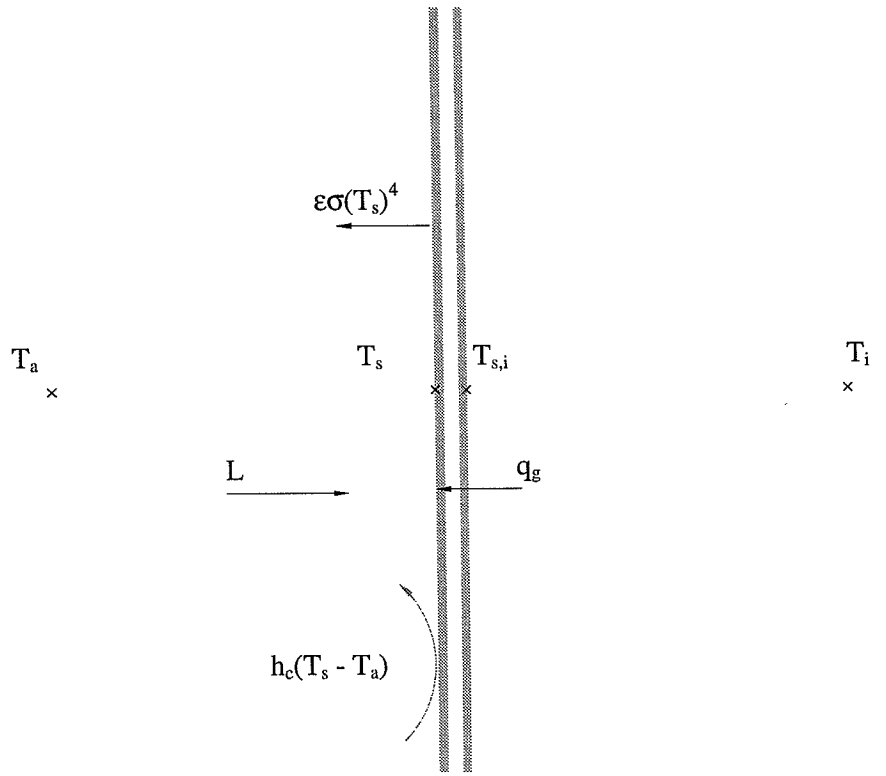

Figure 8.1 *Night-time* energy balance at the external surface of the double pane glazing. Heat capacity of the glazing and effects of moisture transfer are neglected.

Convective heat transfer coefficient

The thermal resistance of the window is calculated employing well-founded formulae, adapted to the appropriate temperature interval. The emissivity of the surface is considered a known material property. Consequently, the only unknowns of the equation are L, T_s, $T_{s,i}$ and T_a.

The convection heat transfer coefficient is given by

$$h_c = \frac{1}{T_s - T_a}\left(\frac{T_{s,i} - T_s}{R_c} + \varepsilon L - \varepsilon\sigma T_s^4\right)$$

Where	L	is the incident long-wave radiance	[W/m²]
	ε	is the emissivity of the external surface	[-]
	σ	is the Stefan-Boltzmann constant	[5.67×10^{-8} W/m²K^4]
	h_c	is the convection heat transfer coefficient	[W/m²K]
	R_c	is the thermal resistance of the glazing (centre part)	[m²K/W]
	T_s	is the external surface temperature of the glazing	[K]
	$T_{s,i}$	is the internal surface temperature of the glazing	[K]
	T_a	is the temperature of the ambient air	[K]

8.2 Recent Studies of Convection and Condensation

8.2.1 Heat transfer at the external surface of windows *[Furler, Switzerland, 1988]*

Furler carried out a study of window heat transfer processes. The experiments encompassed determination of the forced convective heat transfer coefficient at the external surface of glass panes mounted in a test cabin (H×W×D: 3×4.8×3 m^3). Surface temperatures of the glass panes were measured employing both thermocouples and radiometers. Reference measurements encompassed ambient air temperature, wind speed and direction as well as solar and long-wave irradiation. In addition, scaled wind tunnel tests were carried out. In this context, only qualitative findings are referred, as the quantitative findings are closely related to the specific lay-out of the experiment.

The emissivity of the glass pane was found to be virtually independent of temperature within the frame of the study. The convection heat transfer coefficient was found to strongly depend on wind direction, position on the building envelope and the shape of the building. Conclusions for the test period:

- Long-wave exchange is the dominant mode of heat loss.
- Forced convection heat losses are significant, except for still air conditions.
- Natural convection heat losses are less important, except when both radiation and forced convection losses are small.
- Radiometer readings of the glass temperatures are more reliable than thermocouple readings. The latter are too high when heated by solar radiation during the daytime.
- h_c strongly depends on the wind direction.
- h_c is less influenced by the window environment.
- h_c varies with position on the building envelope.
- Minimum h_c in cases with frontal laminar wind, or when the window is leeward.
- Maximum h_c in cases with turbulent frontal wind.

The conclusions of the study are valid for geometries corresponding to the test cabin. Furler states that there is still a need for more general relations, applicable to a wider range of geometrical configurations.

8.2.2 Heat transfer at the internal surface of windows *[Wallentén, Sweden, 1998]*

Wallentén conducted detailed studies of energy transfer processes at the internal surface of a window exposed to natural climate. Both analytical studies and full-scale measurements were carried out. Solar irradiation and temperatures were measured, and long-wave radiative heat exchange was calculated on the basis of surface temperatures, emissivities and geometry. The convective heat transfer from the window was determined as the difference between transmission through the window and long-wave radiation loss. The method is not as accurate as more direct measurement of long-wave radiation, but allows keeping the experiment under realistic conditions. Such indirect determination of the long-wave exchange is possible for indoor experiments with relatively well-defined temperatures and emissivities of the surrounding surfaces. Outdoor experiments, however, do not permit this type of indirect measurement. The surface temperatures of the window panes were measured employing thin thermocouples (0.08 mm), glued to the surface and covered by a thin slice of glass (0.1 mm). The latter in order to achieve both a better contact and the emissivity of the glass. With the thin thermocouples, absorption of solar radiation was found to be no problem. Air temperatures in sun-lit places were measured with thin, unshielded thermocouples, with an estimated accuracy of 0.5 K at 400 W/m^2 solar irradiation. It was found that it is possible to continuously measure the convective heat transfer coefficient, yet with limited accuracy (at best ±15%). In order to

attain an error less than 30%, the convection heat transfer from the window should be at least 4 W/m². It was found that the measurements of the convective heat transfer coefficient at the window pane are reasonable if the temperature difference is $\Delta T < -4$ K or $\Delta T > +1$ K. Wallentén did not suggest generalized relationships between temperature differences and convective heat transfer coefficient. For the specific case - the internal surface of a window, with a radiator mounted below the window - Wallentén states the following estimate:

$$h_c = f \times 1.34\left(\frac{\Delta T_a}{H}\right)^{1/4} \quad \text{for} \quad \Delta T H^3 < 9.5 \text{ m}^3\text{K}$$

$$h_c = f \times \left(1.33(\Delta T_a)^{1/3} - \frac{0.474}{H}\right) \quad \text{for} \quad \Delta T H^3 > 9.5 \text{ m}^3\text{K}$$

Where	h_c	is the convection heat transfer coefficient	[W/m²K]
	ΔT	is the temperature difference, surface-air	[K]
	H	is the window height	[m]

The constant f depends on the radiator heating. Radiator power on: f = 2.5, do. off: f = 0.7. Wallentén compares to previous studies reported in the literature, giving values of h_c between 0 and 4.5 W/m²K for temperature differences ΔT between 0 and 8 K.

A method for measuring the temperature profile in the boundary layer close to the surface was studied. The Mayer ladder technique is based on such measurements with thermocouples in series. The study indicates that the measurement error can be reduced to less than 10 % on the convective heat transfer coefficient.

8.2.3 Condensation on the external surface of windows *[Jonsson, Sweden, 1995]*
Jonsson recorded external surface temperature and ambient air temperature in connection with windows. The external surface temperature was subsequently computed by use of i) $h_c = A + Bu$, and ii) $h_c = Au^B$, where u is the reference wind speed. Constants A and B were determined so that the average value of the difference $\Delta(\Delta T_{measured} - \Delta T_{computed})$ was zero (ΔT: temperature difference between surface and ambient air). The best result was obtained with A = 5.0 and B = 2.7 in the linear expression (standard deviation 0.317):

$$h_c = 5.0 + 2.7u$$

The linear expression is chosen because it yields values corresponding to the natural convection at low wind speeds.

Condensation was detected by means of a moisture sensor. Two wires were fixed to the external surface of the window pane. The wires were mounted parallel to each other with a distance of 4 cm, and the formation of condensation was sensed as a voltage change owing to the change of resistance caused by the water film. The results were compared with dew point and surface temperature, and were found to give a correct measure of the occurrence of condensation. However, the method is sensitive to disturbances, e.g. depositions on the surface under consideration. Conclusions of the study:

- External condensation occurs generally during the night, and usually disappears before dawn.
- External condensation occurs primarily during autumn, with the majority of cases in the months from August to November.

- The temperature difference between the ambient air and the temperature of the surroundings (including sky) can be up to 10-15K for a vertical surface, and up to 20-30K for a horizontal surface being more exposed to the sky.
- Most cases are occurring between 00 and 07hrs.
- After 07hrs, the condensation reduces rapidly.
- All condensation disappears in the course of the morning.
- In the evening, condensation may start to appear from around 20-21hrs.
- Condensation is usually appearing when the temperature difference (surface - ambient air) is between 4 and 7K.
- Condensation occurs at high relative humidity. No condensation is registered at air humidity below 95 % RH.
- Condensation occurs mainly at ambient air temperatures of 0°C (spring) and 10°C (autumn).
- Condensation primarily occurs at low wind speeds. Radiation transfers energy from the surface, whilst convection transfers energy to the surface (in the relevant cases). Increasing wind speed thus leads to increasing transfer of energy to the surface, consequently reducing the condensation risk. The wind tends to reduce the temperature difference (surface - ambient air).
- As condensation mainly occurs at low wind speeds, the wind direction is not significant.
- In this measurement series, it was found that condensation typically takes place in climatic situations with: clear nights and high relative humidity (>95%), and often with low wind speeds. The ambient air temperature varied around 0°C in the spring cases and around 10°C in the autumn cases.

8.3. Measurements

8.3.1 Set-up

Measurements were carried out on a vertical window, facing 18° (~ north - north-west) in the period from May 12th to June 16th 1998. Only night-time weather situations are considered, since these represent the highest condensation risk.

Physical

The studied window measures 1 m x 2 m (W x H). The glazing is a double pane, with ordinary 4 mm float glass (uncoated soda lime glass) and air in the cavity. The thermal resistance of the centre part of the glazing is calculated to be $R_c = 0.18$ m²K/W and the emissivity is $\varepsilon = 0.84$[1] [WINDOW, 1994]. The ground below window is a court covered by vegetation, the building in front of the window is not obstructing the view. Later in this section, the set-up is illustrated by photographs 8.1 to 8.4.

[1] The value of the emissivity varies slightly in the references: Zürcher et al. [1982] state a normal emissivity, ε_n, of 0.91. The normal emissivity is corrected to account for the spectral reflectance properties. prEN 673:1996 states $\varepsilon/\varepsilon_n = 0.94$ [1996], giving $\varepsilon = 0.86$. Both references state that the emissivity is not strongly dependent on the temperature.

Instrumentation
Surface temperatures on the external and internal surface of the double pane, are measured by means of an extremely thin copper-constantan (Cu/Cu-Ni) thermocouple, taped to the inside, and a thermopile between the two surfaces.

The incident long-wave radiation is measured with a pyrgeometer mounted vertically adjacent to the window.

Reference measurements encompass ambient air temperature, relative air humidity, wind speed and wind direction. All reference measurements are taken from a 5 m mast above the roof, at the gable of the building. It has not been possible to record surface air velocities within the framework of the present project.

The thermal emissivity of the glazing has not been measured. The sensitivity to this uncertainty will be subject to evaluation and should be seen in context with the precision of the pyrgeometer. Clearly, the value of the emissivity depends on the condition of the surface. The adopted value applies for clean surfaces, whereas the actual surface will be coated by depositions. Moreover, the thermopile is fixed to the surface with a thin tape with slightly differing radiation properties compared to the glazing itself.

Long-wave radiation is measured by means of a Kipp & Zonen CG1 pyrgeometer with an estimated accuracy of ±10% of the net long-wave radiation *plus window heating offset*. As only nocturnal measurements are regarded, the window heating offset owing to solar irradiation is not relevant. The accuracy is estimated to be ±6 W/m².

The thin wire thermocouple and thermopile were calibrated against a precision temperature meter[2], and were found to have an accuracy better than 0.1 K (at approximately 20°C). The calibration was performed in air, in connection with the set-up. The type TT thermocouple used for ambient air temperature measurements were found to have an accuracy better than 0.2 K.

Below, the set-up is illustrated by photographs 8.1 to 8.4.

Photo 8.1 North facing window, seen from the exterior. External surface temperature is measured by means of a thermopile from the internal surface. Below, the thermo-couple measuring the internal surface temperature is visible.

[2] S 1220 Series High Precision Digital Temperature Meter. Systemteknik AB. Sweden.

Photo 8.2 North facing window, seen from the interior. Thermocouple and thermopile are visible on the centre part of the tall window pane.

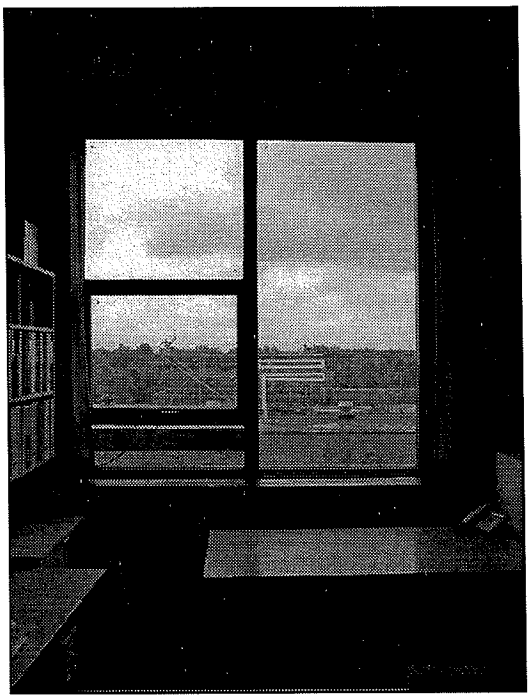

In front of the window, the adjacent Building 119 with the Solar Measurement Station is visible. There are no obstacles in the level of the window. The pyrgeometer is mounted on a stainless steel plate outside, below the smaller, operable window.

Photo 8.3 Pyrgeometer mounted vertically, below the small, operable window. Note that the instrument has been placed out from the surface, free of the otherwise shading window frame.

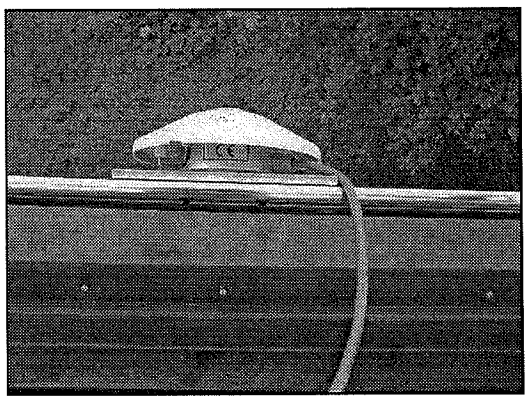

The ground in front of the facade is covered by vegetation. In the level of the window and pyrgeometer, there are no shading obstacles to the sides.

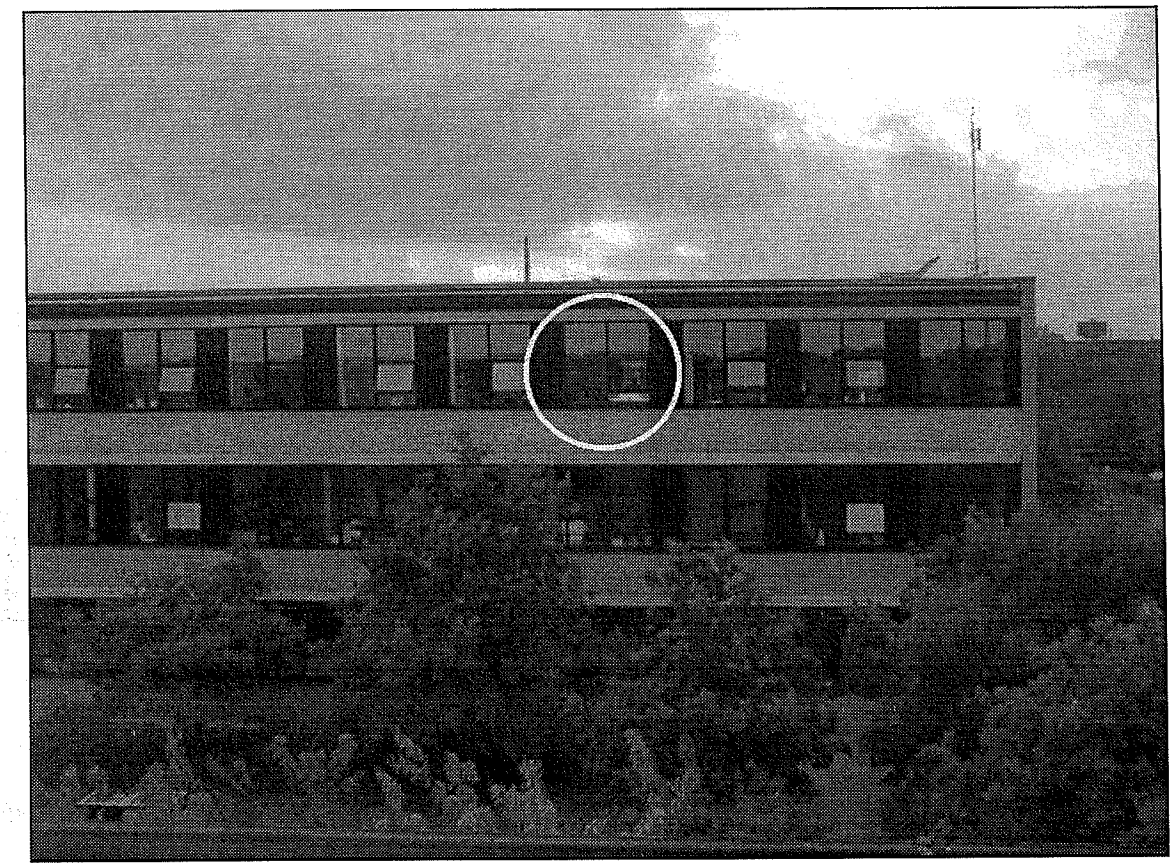

Photo 8.4 North facing window, seen from the roof of the adjacent Building 119. The pyrgeometer shows dimly below the small, operable window. Above the roof, at the west gable, the 5 metre high reference mast is visible.

8.3.2 Possible error sources

The experiment is elementary, aiming at determining the magnitude of the convection heat loss as occurring from a real window glazing surface. The heat flux is limited this time of year, and this may result in difficulties when interpreting the results. In order to yield a basis for the discussion, the possible error sources are listed below.

- Limited temperature differences
- Thermal resistance of the double pane glazing
- Emissivity of the glazing
- Temperature measurement
- Long-wave radiation measurement

Limited temperature differences

The experiment has been carried out over a period during May and June, which means that the inside/outside temperature differences are small. The small temperature differences will tend to increase the significance of the measuring accuracy; The accuracy may even, at times, be of similar magnitude as the convection heat flux itself. It was decided to carry on in spite of these problems, as the experiment would, under all circumstances, yield information for a further discussion of aspects regarding the measuring technique. For instance, the convection heat loss could be increased by supplying electrical effect to the test area of the window. In this series it

was, however, decided to study a real surface in an attempt to record realistic convection values. Design notes regarding a novel apparatus for measurement of convection heat transfer are reported in an appendix to this report.

Thermal resistance of double pane
The thermal resistance of the double pane glazing, R_c, has been calculated theoretically employing well-founded methods. Measurement of R_c would lead to a change of the set-up which was not justified by attainable improvement of accuracy. It should be noted, that small temperature differences will reduce the heat flux through the glazing and thus diminish the influence of the thermal resistance.

Emissivity of the glazing
The value of the long-wave emissivity of the glazing has been taken from the literature. Measurement of the emissivity is complicated by the fact, that the temperature sensors have been fixed to the pane with adhesive tape. The uncertainty has been estimated to be ±0.02. The significance of this uncertainty is discussed in connection with the system error estimation.

Temperature measurement
Thin wires are used for the thermocouple and thermopile measurements of surface temperatures on the glazing. The thermal capacity of the wires should thus not influence the surface temperature significantly. The contact between sensor and surface can result in recorded temperatures differing from the true surface temperature. The accuracy is estimated to be ±0.1 K.

The reference air temperature is recorded at the reference mast, 5 metres above the roof. The temperature is recorded using a type TT (Cu/Cu-Ni) thermocouple. No thermopile was installed between glazing and ambient air. The accuracy is estimated to be ±0.2 K,

Long-wave radiation measurement
The measurements are carried out in a period with small temperature differences, both across the glazing and from the surface to the ambient air. Consequently, the heat flux through the double pane will be limited. Moreover, there will be a tendency towards night-time undercooling caused by long-wave radiation to the sky. These factors lead to an increase in significance of the accuracy of the radiation measurements.

Inversion of convective heat transfer
During nights with clear sky conditions, the convection heat transfer will change direction, as the ambient air will be warmer than the surface of the glazing. Natural convection will be directed downwards instead of upwards, but will remain limited due to the small temperature differences only giving rise to small buoyancy forces.

In terms of determining the magnitude of the film coefficient, a switch in direction of the flux should thus not interfere or change the principle.

8.4 Results

Measurements have been carried out over the period from May 12th to June 16th 1998. In this section, the results from four nights are presented. The selected nights yield a basis for a discussion of relative significance of the parameters as well as an evaluation of the adopted measurement technique.

In the following, the results of the particular four nights are presented and commented. In connection with the graphical presentation of each set of data, the main findings are emphasized, while a general comparison and discussion concludes the section.

Unless otherwise stated, 10 minute average values are used. The wind is presented as 10 second instantaneous values to express to fluctuations.

8.4.1 Four cases

In the table below, key figures of four selected cases are presented. Note that the convection quantities represent the *results obtained with the adopted method and the specific model.*

Nocturnal series, Average values	**May 13th**	**May 21st**	**June 5th**	**June 6th**	**Units**
Convective film coefficient, h_c	-1.4	2.1	3.3	4.9	[W/m²K]
Reference air temperature, t_a	8.0	6.6	11.6	11.8	[°C]
External surface temperature, t_s	10.1	8.9	14.3	14.5	[°C]
Internal surface temperature, $t_{s,i}$	17.2	16.3	19.3	18.9	[°C]
Ambient dew point temperature, t_{dp}	1.4	3.7	6.0	10.8	[°C]
Temperature diff., $\Delta T_g = t_{s,i} - t_s$	7.0	7.5	5.0	4.4	[K]
Temperature diff., $\Delta T_a = t_s - t_a$	2.2	2.2	2.7	2.7	[K]
Wind speed	1	3	2	4	[m/s]
Wind direction	137	320	66	101	[°]
Incident long-wave radiance, L	316	315	364	374	[W/m²]
Glazing heat flux, q_g	39	41	28	24	[W/m²]
Long-wave radiosity ($\varepsilon\delta T_s^4$)	307	301	325	326	[W/m²]
Absorbed irradiation (εL)	265	265	306	314	[W/m²]
Convection heat loss	-3	5	9	13	[W/m²]

Table 8.1 Selected nights. Key average values. Glazing: $\varepsilon = 0.84$; $R_c = 0.18$ m²K/W; Window orientation = 18°; Duration from 20hrs to 04hrs (true solar time).

The table shows erroneous results in terms of a negative value for the convective heat flux of May 13th. The negative value for the convective heat flux is in disagreement with the physical conditions, namely the positive temperature difference between surface and ambient air. The erroneous results are found to be owing to the combination of limited temperature differences and limitations of radiation measurement accuracy. The other three cases (May 21st, June 5th and June 6th) display more realistic results and demonstrate the effects of different climatic scenarios. In the following, the results are commented and discussed in detail.

8.4.2 *CASE 1.* May 13th

A night with calm weather. Almost exclusively negative values are found for the convective film coefficient. The result is erroneous, as the temperature of the ambient air is lower than the external surface temperature.

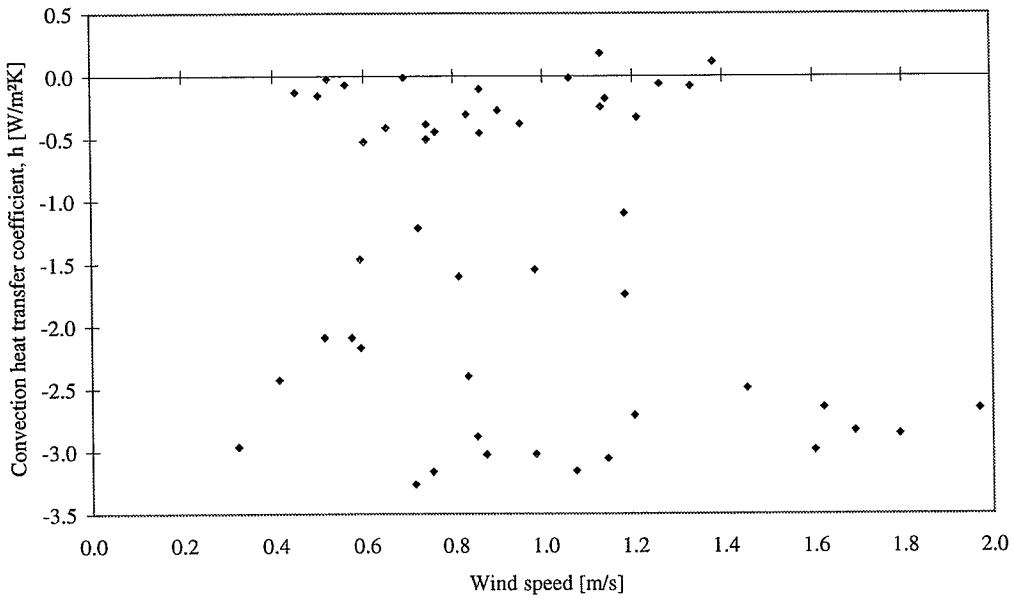

Figure 8.2 May 13th. Convective film coefficient as a function of reference wind speed.

In order to assess possible causes of the error, the variation of the other parameters is presented in the following.

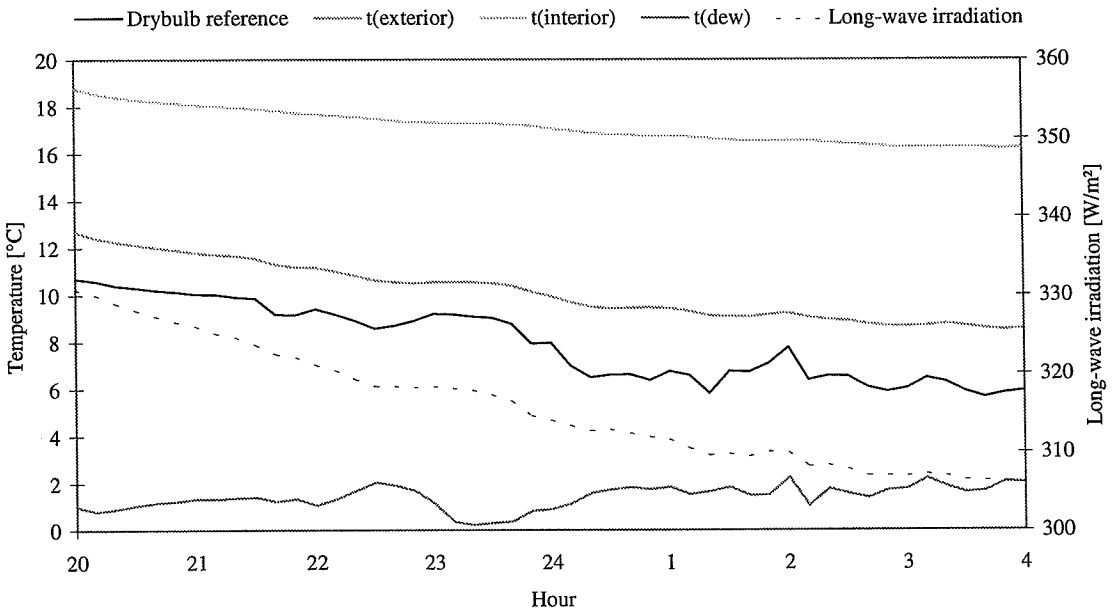

Figure 8.3 May 13th. Night-time variations of temperatures and long-wave irradiation. Dew point temperature has been calculated from measured values of ambient air temperature and relative humidity.

The temperatures are decreasing slightly during the night. Whereas the ambient air temperature becomes stable from around 24hrs, the surface temperatures of the glazing and the ambient dew point temperature are still decreasing. The incident long-wave radiation is seen to decrease steadily from approximately 330 to 305 W/m².

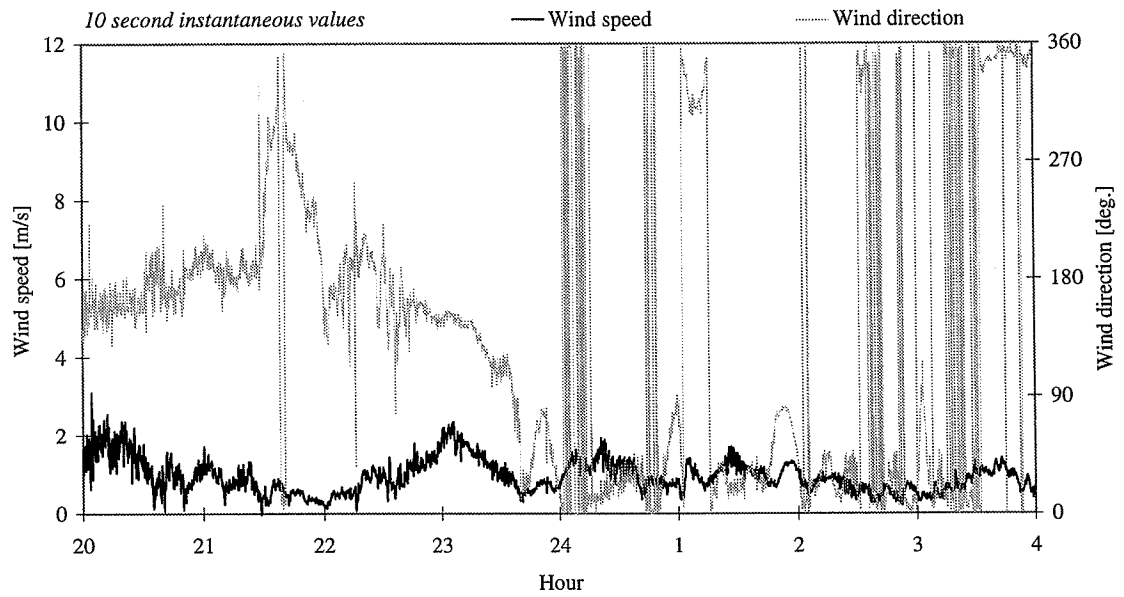

Figure 8.4 May 13th. Night-time variations of reference wind speed and direction.

The weather is calm, with an average wind speed of 1 m/s. The wind direction changes from mainly south to fluctuations between north and east around 24hrs.

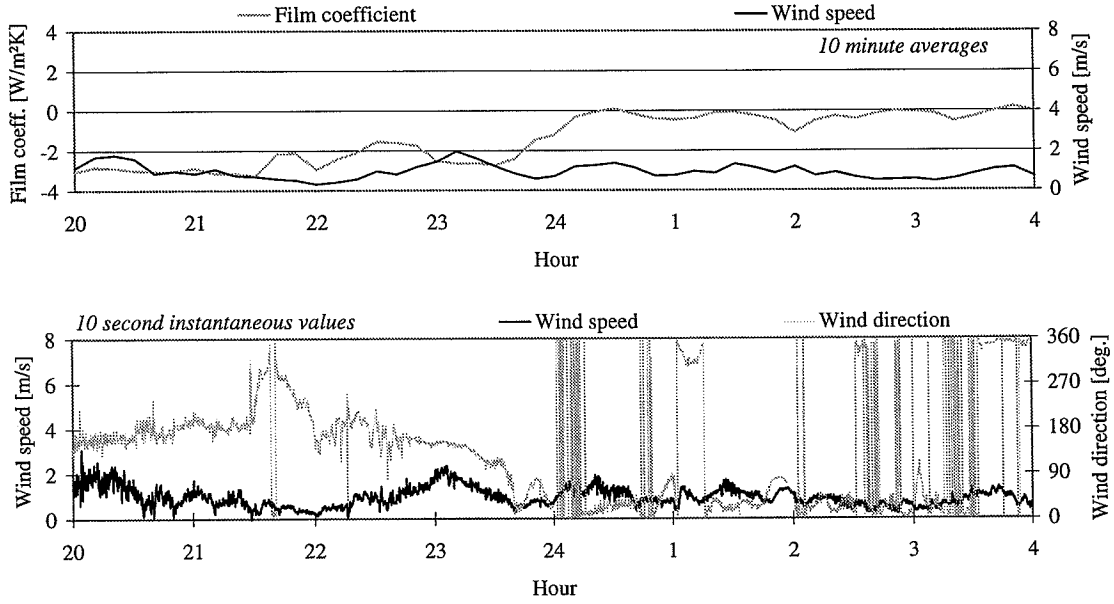

Figure 8.5 May 13th. Night-time variations of reference wind speed/direction and convective film coefficient. Top: film coefficient and wind speed, 10-minute averages. Bottom: wind speed and direction, 10-second instantaneous values. Lines across the diagram indicate changes past north (0° ~ 360°).

The convective film coefficient changes from being fairly constantly -3 W/m²K to being virtually zero from around 24hrs. Mean value: $h_{c,\,average}$ = -1.4 W/m²K.

Findings, May 13th

The model gives erroneous results in this case. Negative values for the convective film coefficient are in disagreement with the physical temperature distribution. The results have been presented in order to assess possible error sources. The temperature differences are virtually constant (Mean values: ΔT_g = 7.0 K; ΔT_a = 2.2 K). The convection heat flux is found to be inverted (Mean value: -3 W/m²). Magnitude of the other heat transfer quantities: Glazing heat flux: 39 W/m²; Long-wave irradiation: 265 W/m²; Long-wave radiosity: 307 W/m²; Thus, net radiation loss: 307 - 265 = 42 W/m². Note that the uncertainty of the long-wave radiation quantities (±6W/m²) exceeds the experimentally determined value of the convection heat transfer. The accuracy aspects are subject to discussion later in this chapter.

8.4.3 *CASE 2.* May 21st

A night with a relatively constant wind; average wind speed 3 m/s; wind direction around 320°.

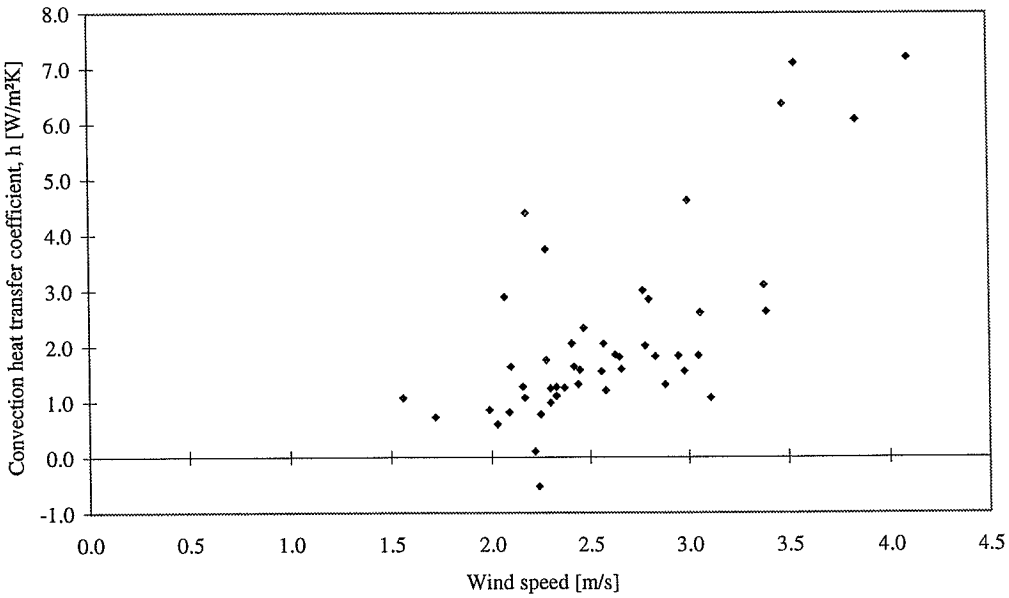

Figure 8.6 May 21st. Convective film coefficient as a function of reference wind speed.

The data show no apparent correlation, although a vague indication of a linear relationship can be seen. The convective film coefficient is found to have limited values, $h_c < 7.2$ W/m²K.

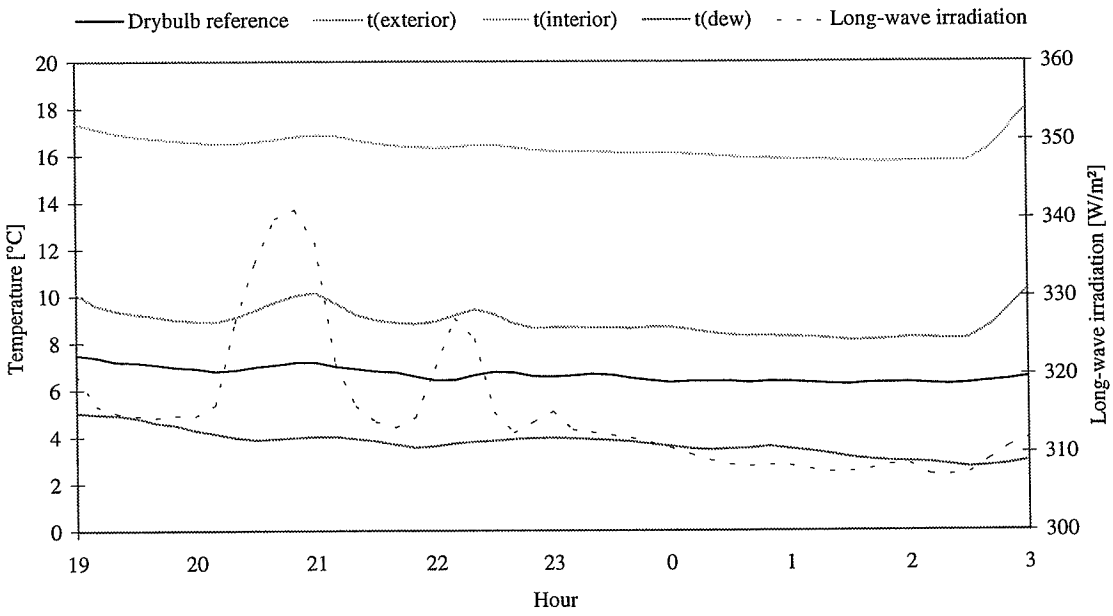

Figure 8.7 May 21st. Night-time variations of temperatures and long-wave irradiation. Dew point temperature has been calculated from measured values of ambient air temperature and relative humidity.

The temperatures are decreasing slightly during the night. The incident long-wave radiation is fluctuating with two maxima between 20 and 23hrs. Such maxima are typically due to cloud passages. The long-wave irradiation has an average value of 315 W/m².

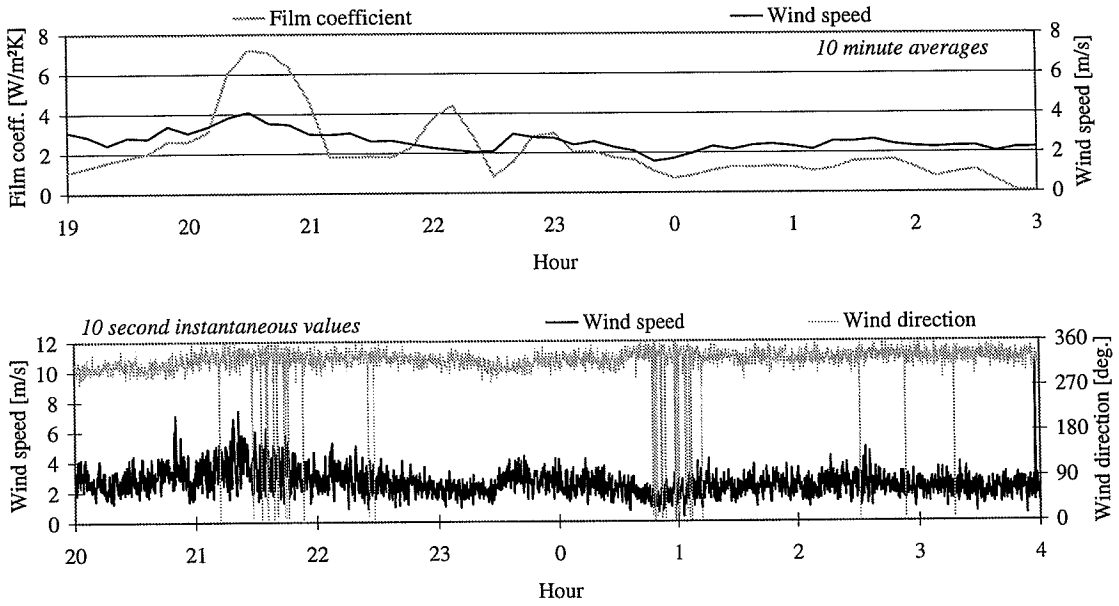

Figure 8.8 May 21st. Night-time variations of reference wind speed/direction and convective film coefficient. Top: film coefficient and wind speed, 10-minute averages. Bottom: wind speed and direction, 10-second instantaneous values.

The wind is quite constant, with an average wind speed of 2.5 m/s, and a wind direction around 320°. The convective film coefficient exhibits a variation very similar to the variation of the incident long-wave radiation in the previous figure.

The mean value of the film coefficient is 2.1 W/m²K. The film coefficient appears to be following the variations of the incident long-wave radiation. Consequently, the relation between incident long-wave radiation and the film coefficient is investigated.

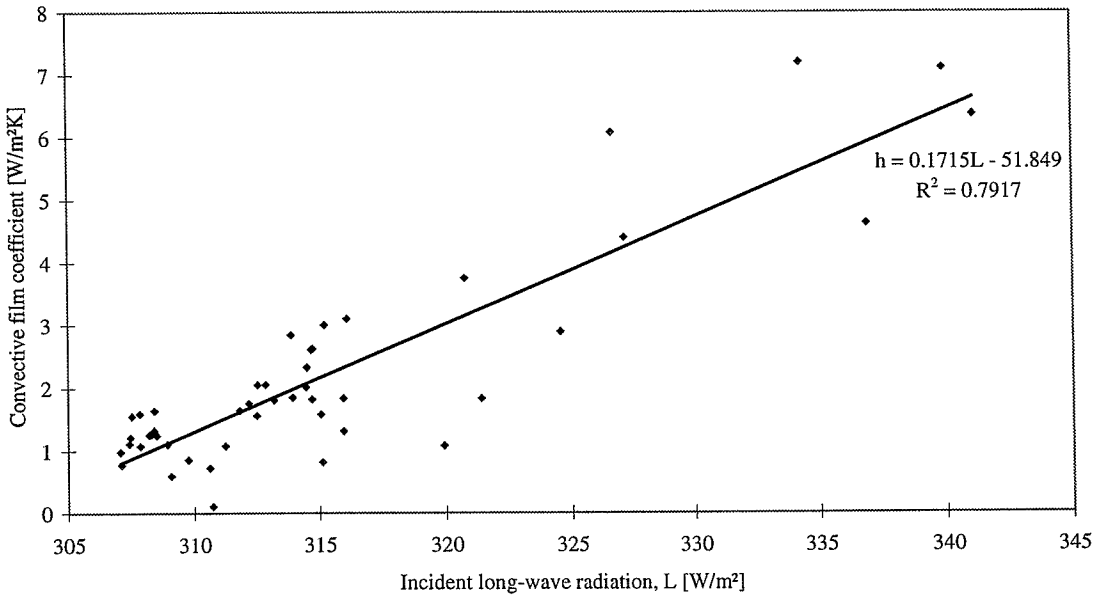

Figure 8.9 May 21st. Convective film coefficient and incident long-wave radiation.

The figure shows a linear correlation (least squares) between the two parameters. The correlation illustrates the significance of the radiation measurement accuracy on the determination of the film coefficient.

Findings, May 21st

The temperature differences are virtually constant (Mean values: ΔT_g = 7.5 K; ΔT_a = 2.2 K). The convection heat loss is limited (Mean value: 5 W/m²), compared to the other heat transfer quantities (Glazing heat flux: 41 W/m²; Long-wave irradiation: 265 W/m²; Long-wave radiosity: 301 W/m²; Thus, net radiation loss: 301 - 265 = 36 W/m²). The incident long-wave radiation is found to significantly influence the magnitude of the film coefficient. This may be due to strictly physical phenomena - for instance, the external surface temperature of the window pane is rising with increasing irradiation - yet, the correlation may also demonstrate the significance of the long-wave radiation measurement precision.

8.4.4 *CASE 3*. June 5th

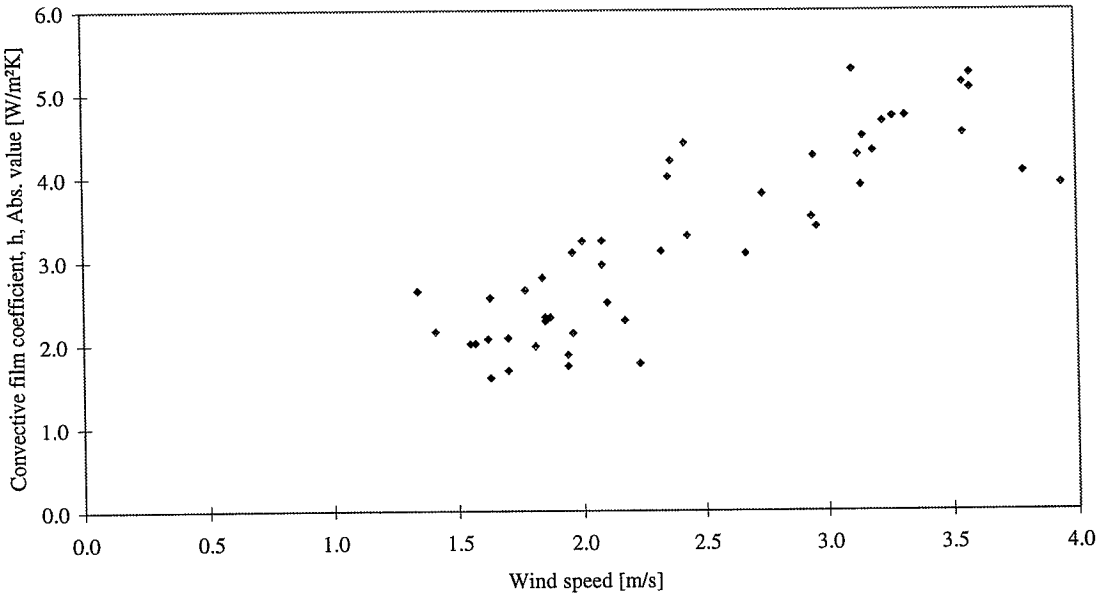

Figure 8.10 June 5th. Convective film coefficient as a function of reference wind speed.

The data display an indication of a linear relationship. The convective film coefficient is found to have small values, $h_c < 5.3$ W/m²K. Only positive values are found for the convective film coefficient, signifying that heat is transferred from the glazing to the ambient air.

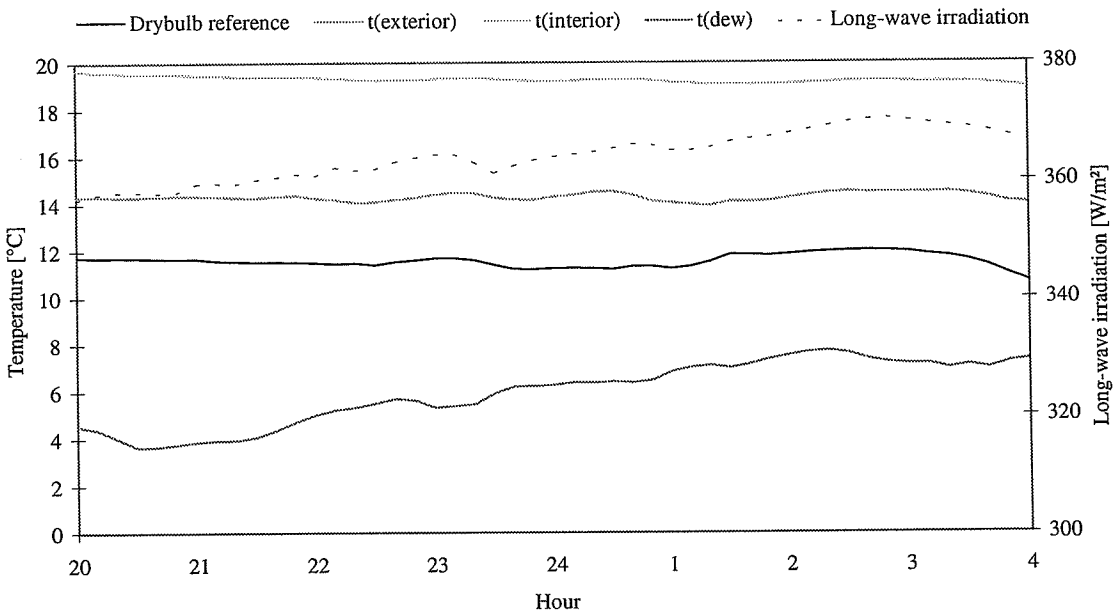

Figure 8.11 June 5th. Night-time variations of temperatures and long-wave irradiation. Dew point temperature has been calculated from measured values of ambient air temperature and relative humidity.

The temperatures are virtually constant throughout the night. The long-wave irradiation is increasing slightly from approximately 360 to 370 W/m². The increase in long-wave irradiation, and the steady temperature levels imply overcast conditions.

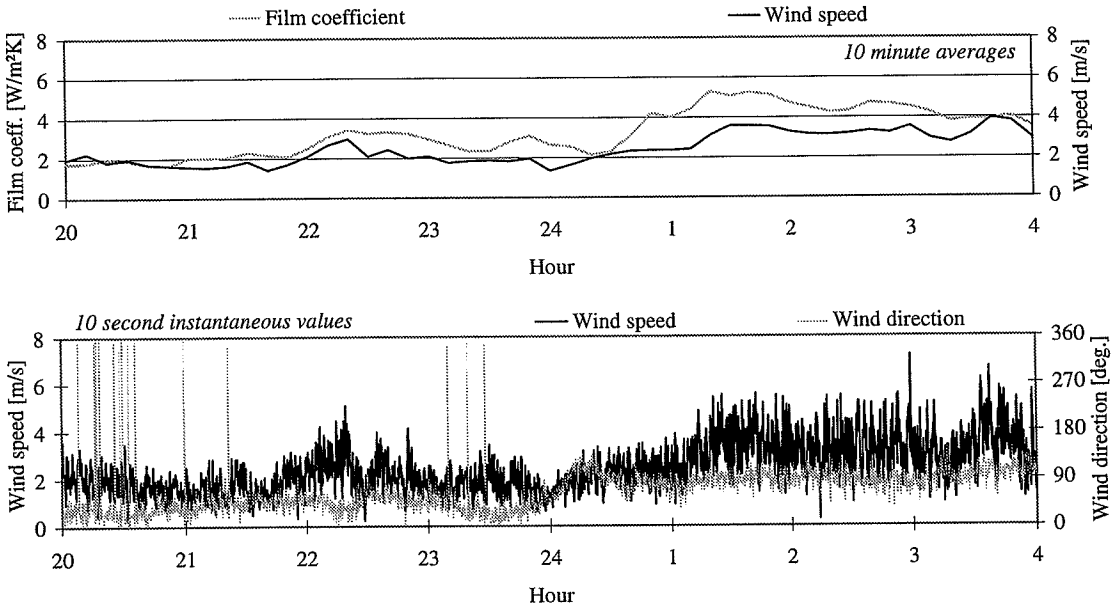

Figure 8.12 June 5th. Night-time variations of reference wind speed/direction and convective film coefficient. Top: film coefficient and wind speed, 10-minute averages. Bottom: wind speed and direction, 10-second instantaneous values.

The weather is relatively calm, with an average wind speed of 2.5 m/s. The wind direction changes from north-east to east around 24hrs. The convective film coefficient changes from being fairly constant around 2 W/m²K to be approximately 4 W/m²K from 24hrs. The mean value is 3.3 W/m²K.

Findings, June 5th

The temperature differences are virtually constant (Mean values: ΔT_g = 5.0 K; ΔT_a = 2.7 K). The convection heat loss is limited (Mean value: 9 W/m²), compared to the other heat transfer quantities (Glazing heat flux: 28 W/m²; Long-wave irradiation: 306 W/m²; Long-wave radiosity: 325 W/m²; Thus, net radiation loss: 325 - 306 = 19 W/m²).

8.4.5 *CASE 4.* June 6th

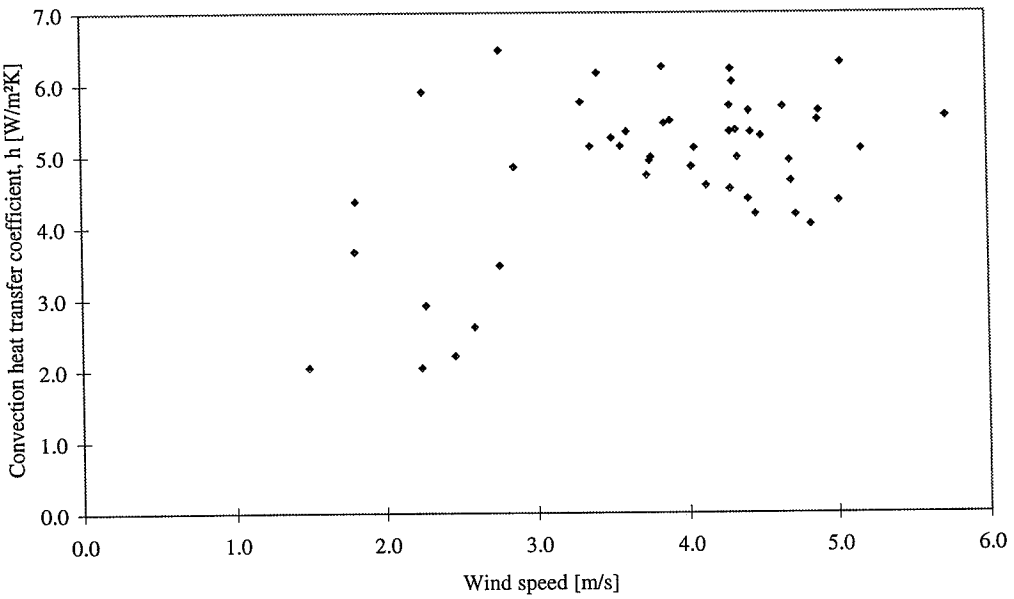

Figure 8.13 June 6th. Convective film coefficient as a function of reference wind speed.

The data are scattered, with a vague indication of a linear relationship. This particular night displays the largest value for the convective film coefficient, but the magnitude is still found to be limited, $h_c < 6.5$ W/m²K.

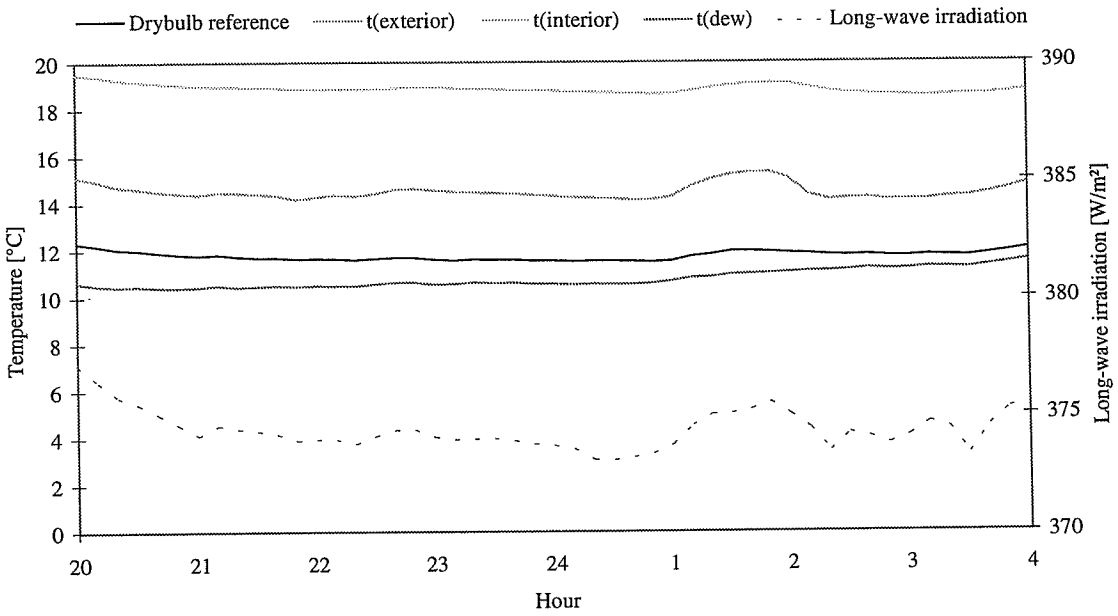

Figure 8.14 June 6th. Night-time variations of temperatures and long-wave irradiation. Dew point temperature has been calculated from measured values of ambient air temperature and relative humidity.

The temperatures are virtually constant. The long-wave irradiation is increasing slightly around 01hrs, leading to a corresponding increase in the temperatures of the glazing. Fluctuations in long-wave irradiation are insignificant. The relatively high level of incident long-wave radiation implies overcast conditions (Mean value: 374 W/m²). This is corroborated by small precipitation amounts (approximately 0.45 mm) collected between 19 and 04hrs. The humidity of the ambient air is high; the dew point temperature is gradually approaching the ambient air temperature.

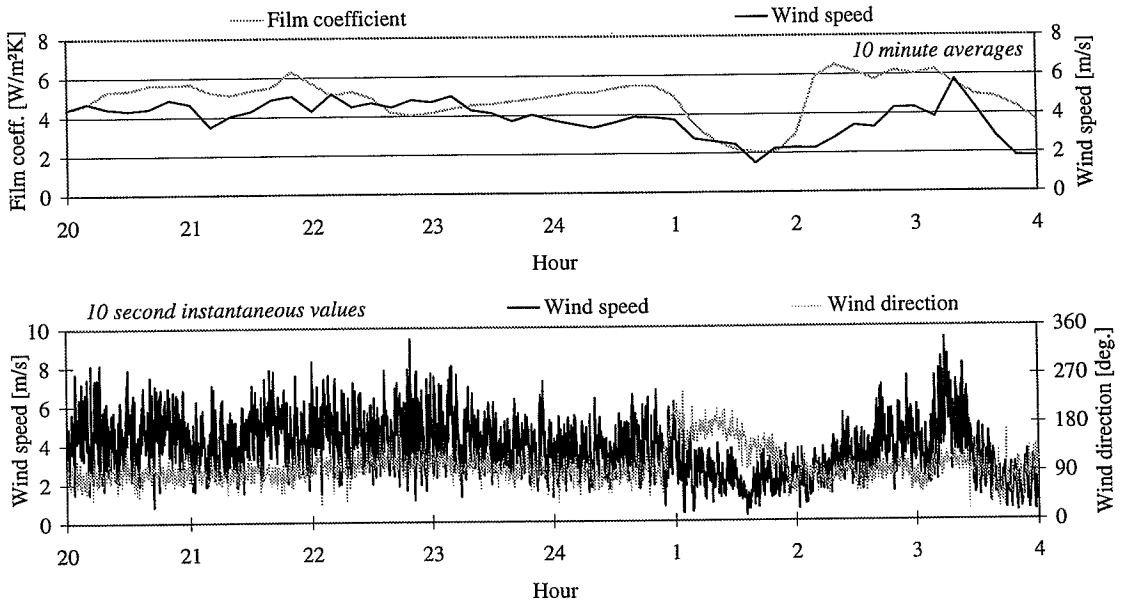

Figure 8.15 June 6th. Night-time variations of reference wind speed/direction and convective film coefficient. Top: film coefficient and wind speed, 10-minute averages. Bottom: wind speed and direction, 10-second instantaneous values.

The average wind speed is approximately 4 m/s. The wind direction is east, with a short change to south, between 01 and 02hrs. The convective film coefficient is fairly constant, approximately 5 W/m²K, only with small fluctuations, but changes to approximately 2 W/m²K between 01 and 02hrs. The mean value is 4.9 W/m²K.

Findings, June 6th

The temperature differences are virtually constant (Mean values: ΔT_g = 4.4 K; ΔT_a = 2.7 K). The convection heat loss is of the same order of magnitude (Mean value: 13 W/m²) as the other heat transfer quantities (Glazing heat flux: 24 W/m²; Long-wave irradiation: 314 W/m²; Long-wave radiosity: 326 W/m²; Thus, net radiation loss: 326 - 314 = 12 W/m²). The glazing is transferring heat to the ambient air by convection. The ambient air temperature is constantly below the external surface temperature of the glazing. The uncertainty of the long-wave radiation quantities no longer exceeds the experimentally determined average value of the convection heat transfer.

8.4.6 Rough calculation - natural convection

For comparison, a rough calculation of natural convection under similar conditions is given in the following. Only one case is considered, and the problem is simplified to consider only natural convection. The present example serves to yield an impression of the magnitudes found by use of the existing empirical relations rather than calculation of a specific situation. Numerous empirical relationships have been proposed; in this context an approach given by Bejan [1995] is adopted. In Chapter 4, a more detailed description of the convection formulae is given.

A fundamental problem pertaining to estimation of convection is the restrains on the model for validity. Can the surface under consideration be modelled as isothermal? In a building physical context, determination of a characteristic dimension is difficult, as this would imply knowledge of the flow distribution around the building geometry.

Consequently, in this context, a very simple approach is employed. The window is regarded as isolated from the rest of the facade, regardless that the flow may rise along the entire height of the facade. Effects of wind are neglected. The surface of the window pane is considered isothermal.

The average temperatures of the measuring period are used as realistic boundary conditions. These temperatures correspond to the conditions on both June 5th and 6th.

Ambient air *(~ 10°C) [Bejan, 1995]*

Thermal conductivity	λ	0.025 W/mK
Kinematic viscosity	ν	1.41×10^{-5} m²/s
Prandtl number	Pr	0.72 °C

Model data

Temperature difference, surface-ambient air	$\Delta T_a = t_s - t_a$	3 K
External surface temperature	t_s	14 °C
Ambient temperature	t_a	11 °C
Mean film temperature	T_m	286 K
Characteristic dimension (height)	L	2 m

For an isothermal, vertical wall, external convective heat transfer including turbulence effects can be calculated by means of the following formula (air, Pr = 0.72):

$$Nu_{average} = \left(0.825 + 0.325 Ra_L^{1/6}\right)^2$$

Where $Nu_{average}$ is the average Nusselt number over the height L [-]
Ra_L is the Rayleigh number [-]

The empirical relation is valid in the entire range of laminar-transition-turbulent ($10^{-1} < Ra < 10^{12}$). The fluid is air with Pr = 0.72, and the fluid properties are evaluated at the film temperature. In the laminar range ($Gr < 10^9$), more accurate results are achieved by means of the following equation (air, Pr = 0.72):

$$Nu_{average} = 0.68 + 0.515 Ra_L^{1/4}$$

The Grashof number is defined as follows:

$$Gr_L = \frac{\beta \Delta T g L^3}{\nu^2} = \frac{\Delta T g L^3}{T_m \nu^2}$$

Where	Gr_L	is the Grashof number (length or height, L)	[-]
	β	is the coefficient of thermal expansion	[K^{-1}]
	ΔT	is the temperature difference, T_s - T_a	[K]
	g	is the gravitational acceleration	[9.81 m/s²]
	L	is the characteristic length/height of the surface	[m]
	ν	is the kinematic viscosity (fluid)	[m²/s]
	T_m	is the mean film temperature	[K]

In the specific case, the Grashof number is

$$Gr_L = \frac{3\ K \times 9.81\ m/s^2 \times (2\ m)^3}{286\ K \times (1.41\ m^2/s)^2} \approx 0.41$$

Transition, or turbulence occurs, as $Gr > 10^9$. The formula for the laminar range is applied.

$$Ra_L = Gr_L\ Pr = 0.41 \times 0.72 \approx 0.3$$

Now the average Nusselt number can be determined.

$$Nu_{average} = 0.68 + 0.515 Ra_L^{1/4} = 0.68 + 0.515(0.3)^{1/4} \approx 1.1$$

The convective heat transfer coefficient for laminar, natural external convection is therefore

$$h_{c,average} = \lambda \frac{Nu_{average}}{L} = 0.025\ W/mK \frac{1.1}{2\ m} \approx 0.01\ W/m^2K$$

Note that wind and the full extension of the facade has been neglected.

8.5 Discussion

Data selection criteria

As discussed in the following, the accuracy of the method is depending closely on the temperature differences and the precision of the long-wave measurement. Some of the nights under consideration yield erroneous results, as mentioned earlier. Error sources and possible improvement of the method is discussed in the following. In order to base the system error estimation on realistic data, selection criteria has been defined to eliminate the most dubious cases. Nights with $\Delta T_a < 1$ K and/or $q_{conv} < 0$ W/m²K for $\Delta T_a > 0$ K have been neglected in the system error analysis. For the purpose of evaluating the overall system accuracy under the specific circumstances, average values have been generated for the data in compliance with these criteria.

Average values

Ambient temperature	t_a	11 °C
External surface temperature	t_s	14 °C
Internal surface temperature	$t_{s,i}$	19 °C
Temperature difference, glazing	$\Delta T_g = t_{s,i} - t_s$	5 K
Temperature difference, surface-ambient air	$\Delta T_a = t_s - t_a$	3 K
Glazing heat flux	q_g	28 W/m²
Incident long-wave radiance	L	356 W/m²
Net long-wave radiance/ε	$L - \sigma T_s^4$	-27 W/m²
Convection heat flux	q_{conv}	6 W/m²
Convective film coefficient	h_c	2.5 W/m²K

System error estimation

The convective film coefficient is determined on the basis of an array of component quantities. In the following, these quantities are commented in relation to precision aspects. Referral is made to the appendix for details regarding the system error estimation.

Convection heat flux

The convection heat flux, q_{conv}, is determined as the difference between the glazing heat flux, q_g, and the net long-wave radiation, $\varepsilon(L - \sigma T_s^4)$.

$$q_{conv} = q_c - \varepsilon\left(L - \sigma T_s^4\right)$$

Convective film coefficient, h_c

Given the convection heat flux, the convective film coefficient is determined as follows:

$$h_c = \frac{q_{conv}}{\Delta T_a}$$

The component estimated errors are given in the following table:

Quantity		**Average value**	**Absolute uncertainty**	**Relative uncertainty**
Glazing heat flux	q_g	28 W/m²	1 W/m²	0.05
Net long-wave radiance	$\varepsilon(L - \sigma T_s^4)$	-23 W/m²	5 W/m²	0.22
Temp. diff., surface - ambient air	ΔT_a	3 K	0.3 K	0.1
Convection heat flux	q_{conv}	6 W/m²	5 W/m²	0.8
Convective film coefficient	h_c	2.5 W/m²K	2 W/m²K	0.8

Table 8.2 Key figures. System error estimation.

The most significant source of uncertainty is seen to be the net long-wave radiance. This quantity consists of terms in L and T_s. The temperature term is found to be of minor significance, whereas the precision of the long-wave irradiance measurement is significant. Moreover, the temperature difference is encumbered with a considerable uncertainty. This could be readily reduced to one third by employing thermopiles instead of the thermocouples applied in this study.

The relative uncertainty of the convective heat transfer coefficient (and the convection heat flux) is found to be in the order of 0.8. A relative uncertainty of 80% is not acceptable, and does not allow for general conclusions regarding the nature of the convective heat transfer. However, the measured quantities do allow for a discussion of the phenomena involved, as well as an evaluation of the adopted measurement principle. Regardless of the uncertainty, the experiment does also provide information in terms of the temperature variations and the relative magnitude of the different heat flows.

The cases
Four cases (nights) are studied in detail:

May 13th
- Calm weather ('no wind')
- Ambient air temperature, $t_a \sim 8°C$
- Clear sky
- Average fluxes:
  - Net long-wave radiation loss: 42 W/m²
  - Glazing heat flux: 39 W/m²
  - Convection: -3 W/m² (erroneous)

May 21st
- 'Constant wind'
- Ambient air temperature, $t_a \sim 7°C$
- Fluctuating long-wave irradiation
- Average fluxes:
  - Net long-wave radiation loss: 36 W/m²
  - Glazing heat flux: 41 W/m²
  - Convection: 5 W/m²

June 5th
- Average wind speed 2 m/s
- Ambient air temperature, $t_a \sim 12°C$
- Wind direction: First *windward*, then *parallel flow*
- Overcast
- Average fluxes:
  - Net long-wave radiation loss: 19 W/m²
  - Glazing heat flux: 28 W/m²
  - Convection: 9 W/m²

June 6th
- Average wind speed 4 m/s
- Ambient air temperature, $t_a \sim 12°C$
- Wind direction: *Parallel* with a short change to *leeward*
- Overcast
- Average fluxes:
  - Net long-wave radiation loss: 12 W/m²
  - Glazing heat flux: 24 W/m²
  - Convection: 13 W/m²

Convective film coefficient, h_c
June 5th and 6th exhibit limited values for the convective film coefficient. A maximum value of 6.5 W/m²K is recorded, and the average values are 3.3 W/m²K and 4.9 W/m²K respectively.

Jonsson [1995] suggests the following linear relationship between the wind and the convective film coefficient at the external surface of a window pane:

$$h_c = 5.0 + 2.7u$$

Where	h_c	is the convective film coefficient	[W/m²K]
	u	is the reference wind speed	[m/s]

Thus, a *zero-wind situation* would yield a coefficient of h_c = 5 W/m²K.

Wallentén studied the energy transfer at the internal surface of a window exposed to ambient climate. He found the following expression for determination of the convective film coefficient as a function of window height, H, and temperature difference, ΔT_a:

$$h_c = 0.7 \times \left(\left(1.33 \Delta T_a^{1/3}\right) - \frac{0.474}{H} \right)$$

- valid for $\Delta T_a H^3 > 9.5$

In the specific case, the expression yields the following:

$$h_c = 0.7 \times \left(1.33 \times 3^{1/3} - \frac{0.474}{2} \right) \approx 1.2 \text{ W / m}^2\text{K}$$

From the literature, Wallentén reports values of h_c < 4.5 W/mK corresponding to temperature differences ΔT_a < 8 K.

The Danish standard *DS 418* [1986] states the values of the thermal surface resistance as follows:

External surface: $R_{s,e} = 0.04 \text{ mK / W} \Rightarrow h_c = 25 \text{ W / m}^2\text{K}$

Internal surface: $R_{s,i} = 0.13 \text{ mK / W} \Rightarrow h_c \approx 8 \text{ W / m}^2\text{K}$

Where	h_c	is the convective film coefficient	[W/m²K]
	$R_{s,e}$	is the thermal *external* surface resistance	[mK/W]
	$R_{s,i}$	is the thermal *internal* surface resistance	[mK/W]

The external surface coefficients in calm weather is seen to correspond to a situation between standard indoor conditions (or outdoor conditions with no wind) and experimental results obtained for internal surfaces.

Erroneous results

In the specific cases, only small temperature differences are observed. This is normal for the time of year. Calm weather situations, and consequently limited convection quantities, lead to erroneous results. Negative values are found for the convective film coefficient, h_c, in spite of positive temperature differences ΔT_a (for example May 13th). Situations with wind yield more significant/detectable convection quantities and positive values of h_c in accordance with the recorded positive values of ΔT_a (for example June 6th).

The influence of the limited temperature differences can be reduced, employing thermopile measurement between surface and ambient air. Wallentén [1998] studied the *Mayer ladder technique* for measurement and determination of the temperature profile in the vicinity of the surface. The attention of the study was focused on the internal surface of the window pane, but

since calm weather situations represent the highest condensation risk, the Mayer ladder technique constitutes a potential method to be investigated in future studies.

Influence of long-wave radiation
A study shows a correlation between incident long-wave radiation and the convective film coefficient (May 21st). This may to some extent be due to physical aspects such as the rising surface temperature, but also points at the significance of the radiation measurement precision.

Both June 5th and 6th are cloudy, whereas May 13th is a clear night with a more significant net long-wave radiation loss. In between, May 21st is a clear night with cloud passages and thus fluctuating long-wave irradiation. Seen in context with the erroneous data from May 13th, this corroborates the thesis, that the accuracy of the long-wave measurements may be the reason for the negative values for the convective film coefficient, as the absolute error will increase with increasing net radiation heat loss.

The precision of the long-wave measurement can be improved by means of a more accurate instrument. The Eppley PIR (Precision Infrared Radiometer) was under contemplation when the measurements were planned, but the Kipp & Zonen CG 1 pyranometer was chosen as a less costly alternative.

The long-wave radiation can be eliminated by shielding. A radiation shield, mounted in front of the window pane would have a temperature close to the ambient air temperature. Measurement of the shield surface temperature would make calculation of the long-wave radiation exchange possible. This would, however, change the conditions and make the set-up differ from the conditions at the real window.

Natural convection
Note that natural convection is included in the measured quantities. The natural convection will yield some sort of damping effect on the wind-convection correlation, as natural convection will dominate in 'no wind' situations and be less significant in situations with more wind. In this perspective, the magnitude of the temperature differences become important. The detail of the relation natural/forced convection is beyond the scope of this case study. For comparison, a rough calculation is made, estimating the natural convection heat transfer under ideal circumstances. A temperature difference of 3K and a characteristic dimension of 2 m (the window height) yield an average convective film coefficient of 0.01 W/m^2K. In calm weather situations, natural convection will prevail. The exact magnitude will be strongly dependent on position on the building geometry and the features of the specific surface.

Wind induced effects
June 5th (Figures 8.11 and 8.12). The temperatures are practically constant. Changes in the value of the film coefficient may thus be due to changes in the long-wave irradiation and/or wind speed and wind direction. The film coefficient is seen to follow the changes in the wind parameters. Around 24hrs, the wind speed increases slightly and, at the same time, the direction changes from ~30° to ~90° (*~windward* to *~parallel flow*). The film coefficient is seen to increase correspondingly.

June 6th (Figure 8.15). The film coefficient is following the changes of the wind parameters closely. In particular, the change in wind direction from east to south shows on the film coefficient (a change from flow parallel to the facade to a situation in which the window is leeward).

Average *all-night* values are interesting as a means to compare results of the nights and for rough estimation of the correlation between film coefficient and wind. However, it should be kept in mind that the main objective is to assess the condensation risk. In this perspective, focus should be kept on extreme situations rather than averages.

Furler [1988] found that the convective film coefficient depends closely on the wind direction. Moreover, the character of the air flow (laminar/turbulent) is important. Turbulent air flow gives rise to increasing convective heat transfer. In a building physical context, wind around buildings will usually be turbulent, whereas laminar flow may occur in calm weather situations with prevailing natural convection.

Although a linear relationship shows vaguely, the recorded data are too scattered to yield any correlation between the film coefficient and the reference wind velocity (figures 8.2, 8.6, 8.10 and 8.14). Surface air velocities have not been measured; it has not been practicable within the framework of the project. The wind speed and wind direction have been measured at the reference mast. These reference quantities should be conceived as measures to characterize the weather rather than expressions of the conditions at the particular position. Further detail has been neglected in this context, since the purpose of the present study is mainly estimation of magnitudes, relative significance of the parameters and evaluation of measurement technique.

Condensation modelling
There is a need for methods of modelling the condensation phenomena at the external surface of LE-window glazing. The complex nature of the problem dictates experimental investigation in order to determine empirically based correlations. Jonsson [1995] employed a simple moisture sensor. The sensor performed satisfactorily, but was found to be sensitive to disturbances such as depositions on the surface. It is crucial for the studies that measurements are carried out *in situ*, as precisely the function of 'real windows' is the subject. The necessity of maintaining realistic conditions imposes a range of demands on the model and the measurement set-up. For the purpose of condensation studies, different LE-window panes should be observed, and measurements should be carried out to characterize condensation events. This type of information may be used as a basis for estimation of the convective heat transfer quantities.

8.6 Findings

Studies of the convection processes at the external surface of window panes becomes increasingly important, as it becomes possible to manufacture windows with still lower thermal transmissivity. The improved thermal performance leads to lower temperatures at the external surface of the window pane. As a result, the condensation risk is augmenting, and condensation may turn out to represent a problem to the user of the window. The performance is not conceived as satisfactory if the glazing is not transparent in longer periods of time during daytime.

The complex heat transfer phenomena taking place at the external surface of the building envelope in general, and at a window pane in particular, is sparsely described. In a strictly thermal perspective, design guidelines yield adequate approximations for estimation of energy consumption and indoor thermal comfort. With respect to condensation phenomena, however, a considerably more detailed knowledge is a prerequisite for the establishing of applicable models and calculation tools.

In the present case study, an elementary set-up was established; partly to attempt to measure the relative magnitude of component heat fluxes, partly to acquire insight regarding the demands on an experimental set-up.

The measured convection quantities have been compared to the standards and to experiments reported in the literature. In general, low values have been determined for the convective film coefficient. The values determined in relatively calm weather situations are between the results found for internal surfaces and external surfaces with no wind. Note that this implies that the design guidelines overestimate the convective heat transfer; this is reasonable when calculating energy consumption, whereas condensation calculations should be based on more precise measures, or possibly underestimation.

The convective film coefficient is found to depend closely on wind direction. Moreover, the convective heat transfer depends on wind speed and turbulence. Local surface air velocity has not been recorded in this context, and the wind data should consequently be regarded as measures of the wind situation rather than measures of the microclimatic conditions.

Surface temperatures were measured on an ordinary double pane glazing with a centre part thermal resistance of 0.18 mK/W. Reference measurements comprised ambient air temperature, ambient air humidity, wind speed and wind direction - all taken from a reference mast above the roof of the building. Adjacent to the window, incident long-wave radiation was measured by means of a pyrgeometer. In order to eliminate the influence of solar radiation, only night-time observations were considered. This choice is justified by the fact that night-time situations represent the greatest condensation risk.

In certain cases the method yields erroneous results. This is ascribed to the combination of limited temperature differences and uncertainty of the long-wave measurements. Therefore, data has been subject to a selection criterion in order to filter out dubious information.

The measurement series was carried out in the months of May and June, 1998. In this period, the temperature differences, both across the glazing and from external surface to the ambient air, are limited. This leads to an uncertainty of an estimated 10% on the measurement of the temperature differences. The temperature difference, surface - ambient air, was determined by means of two thermocouples. It is recommended that the temperature difference be measured employing thermopiles from the surface to the ambient air. This would improve accuracy, especially in periods with limited temperature differences. As calm weather situations are of particular interest in relation to condensation studies, a Mayer ladder technique as described by Wallentén [1998] is a potential method of determining the temperature distribution in the boundary layer at the glazing surface.

An important source of uncertainty is the measurement of long-wave irradiation. The net long-wave radiation is found to be the main reason for the overall uncertainty of the results. The uncertainty can be reduced by means of a more accurate instrument. Another way to eliminate the influence of the long-wave radiation, is to shield the window surface and measure the shield temperature. However, since maintaining realistic conditions is quintessential to the condensation studies, this solution is not recommended.
In an appendix to this dissertation, a novel design for a convection measurement apparatus is described. It has not been possible to realize the design within the framework of the present project.

Observation of real LE-window panes mounted in different positions would yield valuable information in terms of characterizing situations with formation of condensation. Such a set-up should comprise measurement of reference surface temperatures employing a number of thermocouples, temperature differences by means of a number of thermopiles (possibly a Mayer ladder technique) and long-wave irradiation by means of a precision pyrgeometer. Moreover, general climate parameters such as wind, ambient air temperature and humidity as well as long-wave sky radiation should be recorded.

Chapter 9

METEOROLOGICAL TEST REFERENCE CASE

9.1 Background

With increasing computer capacity, it has been possible to develop detailed models of coupled heat and moisture transfer in building constructions. An example of such a model is the MATCH program, developed by Carsten Rode, Department of Buildings and Energy. Part of the input for such programs is climatic information, used as boundary conditions, typically in the shape of a design reference year or measured data.

The Danish Design Reference Year (DRY) is a compilation of weather data representing a typical Danish year, arranged as hourly simultaneous parameters. Precipitation is given as 3-hour values. No information regarding driving rain is given, owing to the intrinsic dependence on local characteristics.

As driving rain is an important moisture source in a climate such as the Danish, with frequent wind and precipitation, there is a need for driving rain data as input for hygrothermal models.

As part of the present work, a set of meteorological data has been compiled in the DRY-format. Three years of statistically unmodified, meteorological weather data, including hourly precipitation values, have been prepared in order to make calculations with *real weather situations* possible. The data should be thought of as *Meteorological Test Reference Cases of Copenhagen - METREC.*

Since no other generally applicable methods have been developed, driving rain data can be determined on the basis of guidelines given in the British Standard BS8104 [BSI, 1992]. The METREC-work is carried out, aiming at combining the BSI guidelines and hourly meteorological data; the principles of the British Driving Rain Index is consequently described briefly in the following. Referral is made to the BSI [1992] for an elaborate description and specifics regarding values of constants et cetera.

9.2 Danish Design Reference Year - DRY

The Danish Design Reference Year constitutes a valuable weather data input for calculations of indoor thermal climate, energy consumption of buildings and performance of solar energy systems. The DRY contains the following hourly data: dry-bulb and dew point temperature; global, diffuse and beam irradiance; wind speed and direction; cloud information; global, diffuse and beam illuminance and long-wave downward sky radiation. The DRY furthermore contains 5-minute values of beam irradiance.

The DRY has been compiled from 12 months of measured data for a given location, in true sequences within each month. After the selection of 12 months, an adjustment procedure has given each month true mean values and variances for the most important parameters, corresponding to the multi-year period from which the DRY-months have been selected, or corresponding to meteorological normals [Jensen and Lund, 1995].

9.3 Airfield Driving Rain - Lacy's Equation

Driving rain is defined as rain droplets with a horizontal velocity component due to simultaneous wind. The *driving rain intensity* is the rate of these drops impinging onto a plane, for instance the surface of a building. The airfield driving rain is described in Chapter 4 of the present dissertation. The *airfield driving rain*[1] is defined as the rain striking a vertical plane, always facing the wind, with standard meteorological wind exposure[2].

Lacy [1965] proposed the following relationship, describing the airfield driving rain:

$$r_v = 0.222 u r_h^{0.88}$$

Where	r_v	is the driving rain intensity	[mm]
	r_h	is the rain intensity in the horizontal plane	[mm]
	u	is the wind speed	[m/s]

Lacy's work has lead to the British Driving Rain Index, described in the following section.

9.4 Driving Rain Index - DRI

In recognition of the complex nature of the driving rain problem, a qualitative measure has been introduced. The Driving Rain Index characterizes a given location, relatively to other locations, in terms of driving rain quantities. The first extensive works in this field were carried out by Hoppestad [1955] in Norway. Hoppestad based his work on the hypothesis, that the amount of driving rain is proportional to the product of precipitation and wind speed.

During the years 1962-1977 Lacy worked on characterizing the climate of the British Isles. Lacy [1977] developed the Driving Rain Index, DRI, which, in an elaborated form was later implemented as a British Standard entitled: *British Standard BS 8104 : 1992. Code of Practice for Assessing the exposure of walls to wind-driven rain* [BSI, 1992]. The guidelines of the BS 8104 have recently been proposed as a working draft by the CEN/TC 89 in a slightly edited version [CEN/TC 89, 1998]. In the following, the basic principles of the British DRI are described briefly.

BS 8104 states two distinct aspects of exposure to wind-driven rain, as follows:

a) average moisture content of masonry, for which the local annual index is the most significant factor;
b) rain penetration through the masonry, for which the local spell index is the most significant factor.

In 1976, the BRE (Building Research Establishment in the UK) published the report *Driving Rain Index*, in which it was stated that the amount of driving rain striking a facade is proportional to the normal precipitation and a local wind speed. On this basis, maps of the British Isles yielding a number of zones and, respectively, DRIs, were produced. These DRIs

[1] The airfield driving rain is sometimes referred to as the *free driving rain.*
[2] The standard exposure of wind instruments over level, open terrain is 10 metres above the ground. Open terrain is defined as an area where the distance between the anemometer and any obstruction is at least ten times the height of the obstruction [WMO, 1983]

are given as the product of average wind speed and average amount of precipitation - both on an annual basis. Recently, the BRE has published the standard BS 8104, giving a corresponding index, in which the observations have been split into direction intervals of 30°, giving a *Directional DRI* as opposed to the superseded *Omnidirectional DRI*. The standard makes calculation of the *worst likely spell in any 3 year period* possible, and yields a number of correctional factors for local conditions, such as terrain roughness, topography, obstructions and the design of the proposed building. Referral is made to BS 8104 for details. In the following, a brief introduction to the concepts and nomenclature of the standard is given.

Definitions [BSI, 1992]

Spell
A period, or sequence of periods, of wind-driven rain on a vertical surface of given orientation. A spell is of variable length and can include several periods of wind-driven rain interspersed with periods of up to 96 h without appreciable wind-driven rain.

Airfield index
The quantity of driving rain that would occur 10 m above the ground level in the middle of an airfield, at the geographical location of the proposed wall.

Airfield annual index, D_A
The average annual airfield index for a given direction, in litres per square metre per year.

Airfield spell index, D_S
The airfield index for a given direction during the worst spell likely to occur in any 3 year period, in litres per square metre per spell.

Wall annual index, D_{WA}
The quantity of wind-driven rain in litres per square metre per year at a point on a given wall, based on the airfield annual index and corrections for roughness, topography, obstruction and wall factors.

Wall spell index, D_{WS}
The quantity of wind driven rain in litres per square metre per spell at a point on a given wall, based on the airfield spell index and corrections for roughness, topography, obstruction and wall factors.

Terrain roughness factor, R
A factor which allows for the general conditioning of the wind speed by the roughness of the terrain upwind of a wall.

Topography factor, T
A factor which allows for the effect of local topography on wind speed.

Obstruction factor, O
A factor which relates to shelter from the very local environment, and allows for obstructions, such as buildings, fences or trees , close to and upwind of the wall.

Wall factor, W
A factor which allows for the characteristics of the proposed wall. It is the ratio between the quantity of water falling on the wall and the quantity falling in equivalent unobstructed space[3].

The method [BSI, 1992]
The method is based on six steps, as follows:

a) Using the *wind-driven rain maps* given in the standard, values can be determined for different zones of the British Isles. The values are split into geographical and directional indices. Thus, a map value corresponding to a location and an orientation of a proposed wall is found.

b) Terrain roughness factor, R, is chosen.

c) Topography factor, T, is chosen.

d) Obstruction factor, O, is chosen.

e) Wall factor, W, is chosen.

f) The airfield index (annual or spell) is now combined with factors R, T, O and W to give the annual or spell wall indices as follows:

$$D_{WA} = D_A \times R \times T \times O \times W$$

$$D_{WS} = D_S \times R \times T \times O \times W$$

The driving rain index gives an estimate of the annual (or spell) driving rain amount based on local weather statistics.

Since no general method of generating driving rain data on the basis of meteorological observations exists, the intention of the METREC-work was to combine the above guidelines with weather data recorded by the Danish Meteorological Institute and at the Solar Measurement Station.

9.5 Data Material

Meteorological data
It would have been preferable to deal with data registered at a single weather station. Nevertheless, data have been acquired at three different locations due to circumstances explained in the following.

In the course of recent years, the DMI has initiated short time scale measurements of precipitation in the Copenhagen area. Unfortunately, these measurements are not combined with wind observations. Such combined observations would be of great value to driving rain research. Data has kindly been made available by the DMI, although for the purpose of the

[3] The wall factor is equivalent to the *catch ratio*, a more usual term in related literature.

present study only. Future employment of the data in commercial context will be subject to negotiation with the DMI.

It has been necessary to combine observations from two different DMI stations in order to obtain accurate precipitation information as well as a comprehensive set of parameters for hygrothermal calculations. The stations have been chosen as close to university as possible. Since the DMI data material does not contain information about beam and diffuse irradiation, solar data have been acquired from the Solar Measuring Station (SMS) at the Department of Buildings and Energy [Lund, 1994].

When recording the precipitation amounts, the *tipping bucket* principle have been employed (every time a volume corresponding to 0.2 mm precipitation is collected, a pulse is registered. Each minute, the number of pulses is recorded).

As part of the data processing, precipitation has been neglected in periods with air temperatures below +2°C. The instrumentation is not suited for measurements at lower temperatures. Snow would have to be melted to be measured. Measuring snow is a complex matter and it is not considered essential to hygrothermal simulations.

Unfortunately, wind data are only available as hourly values. The precipitation data have consequently been converted into corresponding hourly values. The thus introduced loss of information is unfortunate, but must be seen as an acceptable approximation, bearing in mind that the precipitation and the wind are recorded at different locations.

At some point, the detailed precipitation data may be used as a basis for studies of the rain event progress, in search for systematic variations.

The solar radiation is given as hourly averages based on 2-minute values.

METREC files

Three years of data have been compiled, namely the years 1991, 1992 and 1993. The files are referred to as *METRECxx*, *'xx'* designating the year. The files should be seen as realistic instances rather than typical years. The contents of the files will be described in the following.

DRY no.	Parameter	Unit	Log interval	Format	Column
1	Station identification		h	A5	1-5
2	Time indicator, Local- or True solar time		h	A1	6
3	Dry-bulb temperature	0.1°C	h	I4	7-10
4	Dew point temperature	0.1°C	h	I4	11-14
5	Global radiation	Wm^{-2}	h	I4	15-18
6	Diffuse radiation	Wm^{-2}	h	I4	19-22
7	Direct radiation	Wm^{-2}	h	I4	23-26
8			h		
9			h		
10			h		
11			h		
12			h		
13			h		
14			h		
15	Wind direction	deca deg.	h	I2	53-54
16	Wind speed	0.1 ms^{-1}	h	I3	55-57
17			h		
18-29	Special data		h		
18			h		
19			h		
20			h		
21	Precipitation	0.1 mm	h	I4	72-75
22			h		
23			h		
24			h		
25-27	Airfield driving rain	0.1 mm	h	I3	82-84
28	Relative humidity	%	h	I3	85-87
29					
30	Year		h	I2	92-93
31	Month	1 .. 12	h	I2	94-95
32	Day	1 .. 31	h	I2	96-97
33	Hour	1 .. 24	h	I2	98-99
34	Continuation	0	h	I1	100

Table 9.1 Format of the METREC-files. The structure is adopted from the Danish Design Reference Year, DRY.

Parameters
Below, a brief explanation is given for each parameter.

Station identification
All of the data, though recorded at different stations, are collected north of Copenhagen. The locations are listed below. Here, as is the case for the DRY, the identification is *COP* for Copenhagen.

Time indicator
Local time is given since the data apply for a specific area, namely northern Copenhagen. This choice is indicated with the code L.

Dry-bulb temperature
Recorded by the DMI at Sjælsmark.

Dew point temperature
The dew point temperature is calculated as a function of air temperature and relative humidity.

Global, diffuse and direct radiation
Recorded at SMS/IBE/DTU Lyngby. Global and diffuse radiation are measured at a horizontal surface. The values are hourly averages based on measurements every 2 minutes.

Wind direction
Recorded by the DMI at Sjælsmark in the altitude of 10 metres. The values are averages of 10 minutes before every change of hour. Data supplied from the DMI in degrees are rounded to deca degrees. Convention: 09 ~ east; 18 ~ south; 27 ~ west; 36 ~ north.

Wind speed
Recorded by the DMI at Sjælsmark in the height of 10 metres. As above, the values are averages of 10 minutes before every change of hour.

Precipitation
Recorded by the DMI at Virum. The measurements are carried out employing the *tipping bucket* principle. A signal is registered every time an amount of liquid corresponding to 0.2 mm of precipitation has been collected. The DMI has recorded tips per minute, but the data has been added into hourly values due to insufficient wind data. In recognition of problems related to recording of snow, e.g. limited accuracy of the equipment, low temperature precipitation has been neglected. Precipitation recorded with air temperatures below +2°C have been neglected.

Airfield driving rain
The airfield driving rain is calculated as a function of precipitation and wind speed.

Relative humidity
Recorded by the DMI at Sjælsmark. The values do not exceed a maximum of approximately 96%RH due to the equipment used. Measurements of RH in the high range is associated with inaccuracies in the order of 3%. When establishing the DRY, this problem has been dealt with by adjusting the maximum values to 100% (or by setting the dew point temperature equal to the dry-bulb temperature). Such an adjustment has not been performed in the METREC material - the present data represent the measured values.

Continuation
The DRY yields synthesized 5-minute values for radiation data. In the DRY, the *continue* parameter is used to indicate if the following line contains such data. The METREC files do not contain 5-minute values, hence the continue parameter is set constantly equal to zero.

Locations
The weather data have been recorded at the following three stations:

DTU/IBE/SMS Lyngby, north of Copenhagen.
Parameters: Global radiation; Diffuse radiation.

DMI/30188 Sjælsmark, north of Copenhagen.
Parameters: Wind direction; Wind speed; Air temperature; Relative humidity.

DMI/20221 Virum, north of Copenhagen.
Parameters: Precipitation.

Reservations, limitations and profile
The original data material covered 10 years, namely the period 86.05.22 - 95.05.21, chosen because high resolution (short time-scale) precipitation data were available from the DMI in this interval. In the course of processing, the data quality has been assessed in terms of missing and erroneous data. This assessment is fundamentally subjective. After having treated all of the data, three years have been found satisfactory and suited for the task, namely the years 1991, 1992 and 1993. Other files could have been established, employing extra efforts in data correction, but three years were found to be sufficient at this stage of the work.

As a means to compare data of the different METREC-files, a few key parameters have been computed for each file. These characteristics together constitute a so-called *ProFile* for each METREC-file. The annual ProFile is given below, whereas the monthly values are given in connection with the METREC-files.

** Airfield Driving Rain. ** Helbo, 1997, Master Thesis at the IBE*

ProFile				
File Year	**METREC 91** 1991	**METREC 92** 1992	**METREC 93** 1993	**DRY** '1975-1989'
Precipitation [mm]	*683*	*607*	*644*	*720*
Driving Rain* [mm]	*629*	*617*	*679*	
Number of hours with precipitation	*784*	*724*	*735*	*2089***
Number of freeze/thaw cycles	*59*	*70*	*77*	

Table 9.2 ProFile: characterization of the METREC-files, and comparison with the DRY.

Note that the DRY contains precipitation data for every 3 hours, and that Helbo consequently distributed the precipitation equally over the corresponding 3 hours. Thus, it seems only reasonable to expect approximately 3 times as many hours with precipitation.

In the METREC-files, precipitation has been neglected for air temperatures below 2°C. This may explain the annual totals below average as given in the DRY.

The number of freeze/thaw cycles should be understood as the number of times that the temperature has been below the freezing point for a period of time, not considering the length of the time interval.

The weather data have been observed in the northern Copenhagen and must be regarded as regional data. Validity in other areas must be evaluated carefully, taking local characteristics into consideration.

Calculation of driving rain data
When modelling the hygrothermal behaviour of a specific construction, the impinging driving rain can be estimated on the basis of the airfield driving rain, adopting the correctional factors of the BS 8104.

Wind factor
Apart from the correctional factors, attention should be directed to the dependence on the wind direction relative to the proposed surface. The driving rain can, as a reasonable approximation, be reduced by simple projection of the wind component onto the normal of the surface. The correctional factor is the given as the cosine to the angle between the wind direction and the normal to the proposed surface - This correction is recommended by Newman [1987] and used when generating the driving rain indices.

The angle of attack (horizontal plane) between the wind and the normal to the exposed surface is given as

ξ = wind direction - surface orientation

Projection of the wind onto the normal of the surface yields a wind factor given by the cosine to the angle of attack:

$$F = \cos(\xi) \qquad \text{for} \qquad F > 0$$

Otherwise: $F \equiv 0$

Where	ξ	is the angle of attack	[°]
	F	is the wind factor	[-]

Note that it is assumed that driving rain only strikes windward surfaces. Turbulent conditions at the edges of the leeward surfaces are not considered in this type of approximation. To some extent, driving rain will strike leeward surfaces of a structure under natural conditions with complex turbulent airflow. This effect has not been dealt with in the present work, but should be included in future studies.

The estimated driving rain can be calculated by Lacy's equation, the DRI correctional factors and the wind factor as follows:

$$r_{wall} = r_v \times R \times T \times O \times W \times F$$

Where	r_{wall}	is the estimated driving rain impinging on the wall	[mm]
	r_v	is the airfield driving rain intensity	[mm]
	R	is the terrain roughness factor [BSI, 1992]	[-]
	T	is the topography factor [BSI, 1992]	[-]
	O	is the obstruction factor [BSI, 1992]	[-]
	W	is the wall factor [BSI, 1992]	[-]
	F	is the wind factor	[-]

9.6 Applications

The METREC-files contain instances of climatic situations; actual meteorological events as recorded by the DMI and at the SMS. The data should be thought of as test reference cases - hence the appellation. Intentionally, the material serves as input for hygrothermal calculations encompassing driving rain on built structures.

It must be kept in mind, that the driving rain given in the files is only valid as an *airfield* parameter. Adjustments accounting for local exposure should be carried out by the user, for instance as part of the hygrothermal calculation routine.

One application of the material could be selection of moisture critical periods for dimensioning. The Design Reference Year has been established primarily for energy calculations. It is adjusted to yield typical situations with a representative share of extreme situations. However, critical situations for moisture calculations may differ from those chosen from an energy point of view.

Including driving rain, and simulating a well-known structure exposed to selected critical meteorological events, may yield a reference in terms of hygrothermal performance.

Chapter 10

CONCLUSION

Findings

In the following, the main findings are briefly summarized for each main area of the project.

Microclimate definition

In a building physical perspective, the (exterior) microclimate is defined as the conditions affecting transfer of heat and moisture in the immediate vicinity of the external surface of the building envelope. The microclimate results from a combination of meteorological factors and local characteristics.

Methodological problems

The project, and the complex problems under consideration, have been discussed in a philosophical context, and methodological problems are identified. In particular, the problems pertaining to the processes of preparation and interpretation are discussed - the preparation process being the delimitation of a well-defined object of a given investigation. The combination of complex climatic phenomena and the need for information, in terms of applicable guidelines, dictates a pragmatic approach, which, as a matter of fact, is also the case for engineering science in general. Adoption of parameter definitions and assumptions regarding the relative significance of parameters may to some extent predetermine the outcome of the research. Such assumptions and parameter definitions should thus be introduced consciously and with possible consequences in mind.

Driving rain

One of the main tasks has been to investigate and develop methods of measuring driving rain on buildings. A traditional driving rain collector (DRC), consisting of a tray mounted onto a vertical building surface and drained to a commercially available pluviometer, has been produced. In order to improve the performance of the collector, a new design has been developed. A collector plate equipped with a self-siphoning reservoir is suspended from a load cell, thus permitting detection of droplets staying on the collector. Moreover, a net with a mesh size of 1 mm is fixed inside the collector tray, in order to minimize reflection of the impinging droplets by dispersion. The new design is referred to as the *load cell DRC*.

The set-up is exposed to wind pulsation leading to a fluctuating output. However, the fluctuations are not significant compared to the changes of load level caused by driving rain.

The data processing has not yet been fully developed; the load cell output is logged as 10-second instantaneous values, giving the cumulative driving rain load. This cumulative output has to be converted into driving rain amounts over specific periods. The wind fluctuations have to be smoothened out by means of averaging. As the data processing has not been fully developed, preliminary studies are based on a *10-minute averaging approach*. In general, this method yields adequate approximations, although it will result in underestimation in extreme cases with frequent siphoning of the load cell DRC reservoir.

Evaporation from the collectors is detected by the load cell DRC, even in periods of high ambient air humidity in connection with precipitation events. It is expected, that precipitation may also progress during precipitation, leading to underestimation of the driving rain load.

The traditional DRC and the novel load cell DRC were mounted side-by-side for comparative studies. Preliminary results indicate that the load cell DRC detects substantially more driving rain than the traditional one. During the measurement series, the traditional DRC detected approximately 60 per cent of the driving rain detected by means of the load cell DRC. The discrepancy is ascribed to evaporation from the traditional collector. Three different DRC designs are currently being tested side-by-side on the facade of a high-rise building at Eindhoven University of Technology (load cell DRC, DRC with a wiper and a traditional tipping-bucket DRC). Results will be published during 1999.

The spatial distribution over a three storey, west facing gable has been found to be in agreement with the qualitative guidelines of present standards. Along the upper edge of the three storey gable, the catch ratios were found to be up to twice the catch ratio found around the centre. The data material is yet too limited to yield a basis for quantitative comparison. As present standards are based on results obtained by means of traditional driving rain collectors, findings regarding evaporation from the collectors, and subsequent underestimation, may lead to future reconsideration of the guidelines.

The relation between the observed reference precipitation, and precipitation observed under standard meteorological conditions, is a complex issue. Reduced amounts will be recorded with increasing height, owing to aerodynamic effects around the pluviometer. Future measurements should, if at all possible, include additional precipitation measurements under standard conditions.

Computational fluid dynamics methods
Computational fluid dynamics methods represent an interesting alternative to costly wind tunnel testing of air flow around buildings. During recent years, methods of simulating driving rain have been developed, but the work is still at a relatively early stage. Depending on the specific CFD-code, gridding is cumbersome, and in some cases even impossible. Increasing computer capacity and the developing of codes are facilitating the solving of still more complex problems - the true difficulty remains the validation of the results.

The models and the results are difficult to validate - both in terms of driving rain and air flow. The fact that programs are developed, and user interfaces are improved should not divert attention from the fact that the problem is a complicated fluid dynamics task. Assumptions regarding boundary conditions are quintessential, and design of computational grid will affect the results. Future applications may comprise calculation of driving rain catch ratios depending on weather type, local features, building geometry and position on a given building. For validation of such routines there is a pronounced need for comprehensive driving rain measurements and methods of comparing results obtained with different types of collectors.

Long-wave radiation
Short duration measurements of long-wave irradiation have been carried out from horizontal and vertical surfaces, in order to compare with selected empirical formulae from the literature.

The atmospheric component clearly constitutes the most uncertain part, when estimating the irradiation. This is reflected in large discrepancies between the measured and the theoretically determined values. The determination is more accurate for vertical than for horizontal surfaces, as the atmospheric component becomes less significant. The best fit to the measured data was achieved by means of Cole's formulae for long-wave radiation incident upon inclined building surfaces.

The common assumption of the surroundings acting as a black-body radiator at ambient air temperature appears to yield an adequate approximation under the considered conditions - particularly considering the uncertainty of the atmospheric component.

The long-wave data of the design reference year can be used, keeping the uncertainty in mind. The ground component can be calculated, assuming the surroundings to act as a black-body radiator at ambient air temperature. However, whenever possible, the incident long-wave radiation should be measured - preferably by means of a precision pyrgeometer.

Window convection heat transfer
The improved thermal performance of windows results in lower external surface temperatures on the window pane, and consequently in condensation risk. In terms of energy calculations, the convection heat loss is not considered significant. A more detailed description of the complex phenomena is a prerequisite for the establishing of applicable models for assessment of condensation risk. Consequently, night-time measurements were carried out on a north facing window pane.

The convective heat transfer coefficient determined in calm weather situations were found to have values between the results found for internal surfaces and external surfaces with no wind. This implies that the design guidelines overestimate the convective heat transfer, which appears reasonable for energy calculations, but is not adequate for assessment of condensation risk and condensation duration. Such calculations should be based on more detailed measures, or possibly underestimation.

The convective film coefficient is found to depend closely on wind direction. Moreover, the convective heat transfer depends on wind speed and turbulence. Local surface air velocity has not been recorded in this context, and the wind data should consequently be regarded as measures of the wind situation rather than measures of the microclimatic conditions.

Observation of in situ low-ε window panes mounted in different positions would yield valuable information in terms of characterizing situations with formation of condensation. Such a set-up should comprise measurement of reference surface temperatures employing a number of thermocouples, temperature differences by means of a number of thermopiles (possibly a Mayer ladder technique) and long-wave irradiation by means of a precision pyrgeometer. Moreover, general climate parameters such as wind, ambient air temperature and humidity as well as long-wave sky radiation should be recorded.

Meteorological data for hygrothermal simulations
Three years of meteorological data have been compiled in the format of the Danish Design Reference Year (DRY). The material is referred to as Meteorological Test Reference Case, Copenhagen (METREC), and the specific years are 1991, 1992 and 1993. The files provide a basis for hygrothermal calculations with climatic situations differing from those of the DRY. Precipitation is given as hourly values, as opposed to the 3 hour values of the DRY. The data can be combined with the guidelines for estimation of driving rain as given in the British standard BS 8104, in order to include driving rain data in hygrothermal simulations.

Recommendations for future activities

In general, there is a pronounced need for a better understanding of the microclimatic conditions at the external surface of buildings envelopes. Driving rain data are needed for the validation of theoretical estimation of driving rain loads. The driving rain measurement technique has to be developed in order to establish a basis for exchange of results, and the relation between reference precipitation and meteorological precipitation should be investigated.

Driving rain

- Comparative testing of DRC types
- Studies of evaporation during rain
- Long duration measurements - preferably in more locations and more orientations
- Checking of reference precipitation measurement
- CFD estimation of driving rain

Long-wave radiation

- Simultaneous pyrgeometer measurement from vertical and horizontal surfaces

Window convection heat transfer and condensation phenomena

- In situ measurements on low-ε windows encompassing observation of condensation and precision measurement of long-wave irradiation. Long duration measurements allowing for observation of seasonal variations

The complex convection phenomena at the external surface of the building envelope should be investigated in order to provide information for the modelling of, for instance, condensation phenomena.

NOMENCLATURE

List of symbols

A	Area	[m²]
C	Cloudiness	[-]
c	Fractional cloud cover	[-]
c_p	Specific heat at constant pressure	[J/kgK]
D	Depth;	[m];
	Driving rain amount;	[kg];
	Driving rain index	[l/m²year]
d	diameter	[m]
F	View factor	[-]
G	Solar irradiance	[W/m²]
g	Gravitational acceleration	[9.81 m/s²]
Gr	Grashof number	[-]
H	Height	[m]
h_c	Convective film coefficient (convective heat transfer coefficient)	[W/m²K]
J	Radiosity	[W/m²]
K	Calibration factor, pyrgeometer	[μV/Wm^{-2}]
L	Characteristic length;	[m];
	Long-wave irradiance	[W/m²]
n	Number	[-]
N	Cloud cover	[Okta]
Nu	Nusselt number	[-]
O	Obstruction factor	[-]
p	Pressure	[Pa]
Pr	Prandtl number	[-]
Q	Heat transfer	[W]
q	Heat flux	[W/m²]
R	Terrain roughness factor;	[-];
	Thermal resistance	[m²K/W]
r	Radius;	[m];
	Roughness height	[m]
Ra	Rayleigh number	[-]
r_h	Normal precipitation intensity	[mm]
r_v	Driving rain intensity	[mm]
t	Temperature	[°C]
T	Absolute temperature;	[K];
	Topography factor	[-]
u	Wind speed	[m/s]
U	Thermal transmittance	[W/m²K]
u	Wind speed	[m/s]
u(z)	Wind speed at height z	[m/s]
u_{10}	Reference wind speed in the height of 10 m	[m/s]
V	Voltage	[V]

W	Wall factor;	[-];
	Width	[m]
w	Vertical wind speed component	[m/s]
z	Height/altitude	[m]

Greek letters

α	Absorptivity	[-]
	Thermal diffusivity	[m^2/s]
β	Coefficient of thermal expansion	[K^{-1}]
γ	Surface tilt angle	[°]
δ	Estimated error/uncertainty	
ε	Emissivity	[-]
κ	Von Karman constant	[0.4]
λ	Thermal conductivity	[W/mK]
μ	Viscosity (dynamic)	[kg/ms]
ν	Kinematic viscosity	[m^2/s]
ρ	Reflectivity	[-]
φ	Relative humidity	[-]
σ	Stefan-Boltzmann constant	[5.67×10^{-8} W/m^2K^4]
τ	Transmissivity	[-]
ξ	Angle of attack;	[°];
	Wind elevation angle	[°]
ψ	Auxiliary quantity	
Ω	Cross-sectional area	[m^2]

Subscripts

A	Atmospheric
a	Ambient air
c	Centre;
	Convection
conv	Convection
dp	Dew point
e	External
eq	Equivalent
f	Forced
G	Ground
g	glazing
h	Horizontal
i	Indoor;
	Internal
L	Characteristic length
m	mean
n	Natural;
	Normal
R	Resulting
r	Radiation
s	Saturation;
	Solar;
	Surface

t	Terminal
tr	Transition
v	Vapour;
	Vertical
*	Friction (velocity)

Chief Abbreviations

CFD	Computational Fluid Dynamics
DMI	Danish Meteorological Institute
DRC	Driving Rain Collector
DRI	Driving Rain Index
DRY	Design Reference Year
IBE	Department of Buildings and Energy
LE	Low emissivity
METREC	Meteorological Test Reference Case
RH	Relative Humidity
SMS	Solar Measurement Station

REFERENCES

ASHRAE. 1995. Heating, Ventilating, and Air-Conditioning - Applications. 1995 ASHRAE handbook. USA.

Beijer, Oscar and Johansson, Arne 1976. Slagregn mot betongfasader. Rapport 7:76. CBI, Swedish Cement and Concrete Research Institute at the Institute of Technology. Stockholm. Sweden.

Bejan, Adrian. 1995. Convection Heat Transfer. Second edition. John Wiley & Sons. USA.

Berdahl, Paul and Fromberg, Richard. 1982. The Thermal Radiance of Clear Skies. *Solar Energy*. Vol.29. No.4. pp.299-314.

Berdahl, Paul and Martin, Marlo. 1984. Emissivity of Clear Skies. Technical Note. *Solar Energy*. Vol.32. No.5. pp.663-664.

Best, A.C. 1950. The size distribution of raindrops. *Quarterly journal of the Royal Meteorological Society*. Vol.76. 1950. pp.16-36.

Borlinger, Anneli. 1996. The Heat Exchange between Building Surfaces and Their Environment. Proceedings of the 4th Symposium on Building Physics in the Nordic Countries: Building Physics '96. VTT Building Technology. Espoo. Finland.

Bottema, Marcel. 1992. Wind Climate and Urban Geometry. Rapport nr. 92.63.K. Technische Universiteit Eindhoven. Faculteit Bouwkunde. Vakgroep FAGO. The Netherlands.

BSI. 1992. Code of practice for Assessing exposure of walls to wind-driven rain. BS 8104. British Standard. BSI. Milton Keynes. England.

CEN/TC 89. 1998. Hygrothermal performance of buildings - Climatic data - Part 3: Calculation of a driving rain index for vertical surfaces from hourly wind and rain data. CEN/TC 89 WI 46.3. Working draft.

Choi, E.C.C. 1993. Simulation of wind-driven-rain around a building. *Journal of Wind Engineering and Industrial Aerodynamics*. Vol.46 & 47. 1993. pp.721-729.

Choi, E.C.C. 1994a. Determination of wind-driven-rain intensity on building faces. *Journal of Wind Engineering and Industrial Aerodynamics*. Vol.51. 1994. pp.55-69.

Choi, Edmund C.C. 1994b. Parameters affecting the intensity of wind-driven rain on the front face of a building. *Journal of Wind Engineering and Industrial Aerodynamics*. Vol.53. 1994. pp.1-17.

Choi, E.C.C. 1997. Numerical modelling of gust effect on wind driven rain. *Journal of Wind Engineering and Industrial Aerodynamics*. Vol.72. 1994. pp.107-116.

CIBS Guide. 1982. A2 Weather & Solar Data. The Chartered Institution of Building Services. London. UK.

Cole, R.J. 1976. The Longwave Radiation Incident upon the External Surface of Buildings. *The Building Services Engineer.* Vol.44. December 1976. pp.195-206.

Cole, R.J. 1979. The longwave radiation incident upon inclined surfaces. Technical Note. *Solar Energy.* Vol.22. pp.459-462.

Cole, R.J. and Sturrock N.S. 1977. The Convective Heat Exchange at the External Surface of Buildings. Review Paper. *Building and Environment.* Vol.12. pp.207-214.

Dascalaki, E. et al. 1994. Natural convection heat transfer coefficients from vertical and horizontal surfaces for building applications. *Energy and Buildings.* Vol.20 (1994). pp.243-249.

Doebelin, Ernest O. 1990. Measurement systems: application and design. 4th Edition. McGraw-Hill Publishing Company. USA.

DS 418. 1986. Beregning af bygningers varmetab. 5. udgave. Dansk Standard DS 418. Dansk Ingeniørforening. Denmark.

Duffie, John A. and Beckman, William A. 1991. Solar Engineering of Thermal Processes. Second Edition. John Wiley & Sons Inc. N.Y. New York. USA.

Flori, Jean-Paul. 1988. Conditions de mouillage et de sechage des facades verticales - Etude bibliographique. Rapport CSTB EN-CLI 88.17 L. CSTB. Nantes. France.

Furler, Reto. 1988. Experimental and Theoretical Studies on the Energy Balance of Windows. Dissertation. Swiss Federal Institute of Technology. Zurich. Switzerland.

Geving, Stig. 1997. Moisture design of building constructions - Hygrothermal analysis using simulation models. Norwegian University of Science and Technology. Trondheim. Norway.

Hansen, H.E.; Kjerulf-Jensen, P. and Stampe, Ole B. (ed.) 1992. Varme- og Klimateknik. Grundbog. Danvak. Teknisk Forlag A/S, København. Denmark.

Hoppestad, Sverre. 1955. Slagregn i Norge. Norges Byggeforskningsinstitut. Rapport Nr. 13. Norway.

IEA. 1980. An introduction to meteorological measurements and data handling for solar energy applications. International Energy Agency. Programme to develop and test solar heating and cooling systems. Task IV - Development of an Insolation Handbook and Instrument Package. U.S. Department of Energy. DOE/ER-0084. USA.

Ito, N.; Kimura, K. and Oka, J. 1972. A Field Experiment Study on the Convective Heat Transfer Coefficient on Exterior Surface of a Building. Paper presented at the ASHRAE Semi-annual Meeting, New Orleans, LA, January 23-27, 1972. ASHRAE Transactions. Vol. 78. Part I. pp.184-191. USA.

Jakobsen, Arne and Pedersen, Stig A. 1997. Engineering Science and the Reality. Article used as course literature. Technical University of Denmark.

Jayamaha, S.E.G.; Wijeysundera, N.E. and Chou, S.K. 1996. Measurement of the Heat Transfer Coefficient for Walls. *Building and Environment.* Vol.31. No.5. pp.399-407.

Jensen, J.M. and Lund, H. 1995. Design Reference Year, DRY - Et nyt dansk referenceår. Laboratoriet for Varmeisolering. Meddelelse Nr. 281. Technical University of Denmark.

Jonsson, Bertil. 1995. Utvändig kondens på fönster - Mätningar i Borås 1994. SP Report 1995:1. Swedish National Testing and Research Institute. Sweden.

Karagiozis, Achilles and Hadjisophocleous, George. 1995. Wind-Driven Rain on High-Rise Buildings. Paper presented at Thermal Performance of the Exterior Envelopes of Buildings VI. December 1995. Florida. ASHRAE Special Publication. USA.

Kipp and Zonen. 1992. Instruction manual CG 1/2 Pyrgeometer. Kipp & Zonen. Delft. The Netherlands.

Kobysheva, N.V. 1992. Guidance Material on the Calculation of Climatic Parameters used for Building Purposes. World Meteorological Organization. Technical Note No. 187. Geneva. Switzerland.

Lacy, R.E. 1965. Driving Rain and the Onslaught of Rain on Buildings. Proceedings of the RILEM/CIB Symposium on Moisture in Buildings. Helsinki. Finland.

Lacy, R.E. 1977. Climate and building in Britain. Building Research Establishment Report. Department of the Environment. Building Research Establishment. Her Majesty's Stationary Office. London. UK.

Laws, J. Otis and Parsons, Donald A. 1944. Paper presented at The Twenty-Fourth Annual Meeting. American Geophysical Union. Transactions of 1943. Part II. National Research Council. Washington D.C. USA.

Lund, Hans. 1994. Solmålestationen. Rapport nr. 94-18. Laboratoriet for Varmeisolering. Technical University of Denmark.

Lyberg, Mats Douglas. 1977. Driving Rain Measurements on a Tall Building. The National Swedish Institute for Building Research. 1977-08-25. Sweden.

Lyberg, Mats Douglas. 1979. Review of Micro- and Buildingphysical Properties of Driving Rain. The National Swedish Institute for Building Research. Bulletin M79:13E. Sweden.

Mautner, Thomas (ed.) 1997. Dictionary of Philosophy. Penguin Books. UK.

Mills, Anthony F. 1992. Heat Transfer. University of California at Los Angeles. Richard D. Irwin, INC. USA.

Mook, Fabien J.R. van; Wit, M.H. de and Wisse, J.A. 1997. Computer simulation of driving rain on building envelopes. Proceedings of the 2nd EACWE in Genova, June 22-26, 1997. Eindhoven University of Technology. The Netherlands.

Mook, Fabien J.R. van. 1998. Description of the measurement set-up for wind and driving rain at the TUE. FAGO-report 98.04.K. Eindhoven. The Netherlands.

Nevander, Lars Erik and Elmarsson, Bengt. 1994. FUKT handbok - praktik och teori. AB Svensk Byggtjänst. Stockholm. Sweden.

Newman, A.J. 1987. Microclimate and its Effects on Durability. Paper presented at a meeting of the Road and Building Materials Group of the SCI, held in London on 17 April 1986. Chemistry & Industry. Issue No.7. 7. September 1987. pp.583-593. London. UK.

Nicol, Keith. 1977. The Energy Balance of an Exterior Window Surface, Inuvik, N.W.T., Canada. Review Paper. *Building and Environment.* Vol.12. pp.215-219.

Plate, Erich J. (ed.) 1982. Engineering Meteorology: Studies in Wind Engineering and Industrial Aerodynamics. Elsevier Scientific Publishing Company. The Netherlands.

prEN 673. 1996. Glass in building - Determination of thermal transmittance (U-value) - Calculation method. Final Draft. European Standard. CEN. Brussels. Belgium.

Prior, M.J. 1985. Directional driving rain indices for the United Kingdom - computation and mapping. Background to BSI Draft for Development DD93. Building Research Establishment Report. Building Research Establishment. Garston. Watford. UK.

Quintela, D.A. and Viegas, D.X. 1995. Convective Heat Losses from Buildings (ed. Cermak, Jack E. et al.) Wind Climate in Cities. NATO ASI Series. Series E: Applied Sciences - Vol. 277. Kluwer Academic Publishers. The Netherlands.

Rasmussen, R.E.H. 1956. Elementær maaleteori. Anden udgave. Jul. Gjellerups Forlag. Copenhagen. Denmark.

Rauhala, Kari. 1984. The Impact of Town Planning on the Microclimatic Conditions and Energy Consumptions of Residential Buildings. *Energy and Buildings.* Vol.7 (1984). pp.229-241.

Rodgers, G.G.; Poots, G.; Page, J.K. and Pickering, W.M. 1974. Theoretical Predictions of Raindrop Impaction on a Slap Type Building. *Building Science.* Vol.9. pp.181-190.

Sandin, Kenneth. 1987. Fukttilstånd i Autoklaverede Lättbetongväggar - Fältmätning av slagregnets och ytskiktets inverkan. Rapport TVBM - 3026. Avdelningen för Byggnadsmaterialära. Tekniska Högskolan i Lund. Lund. Sweden.

Sankaran, R and Paterson, D.A. 1997. Computation of rain falling on a tall rectangular building. *Journal of Wind Engineering and Industrial Aerodynamics.* Vol.72. 1994. pp.127-136.

Schwarz, B. and Frank, W. 1973. Schlagregen. Meβmethoden - Beanspruchung - Auswirkung. Berichte aus der Bauforschung. Heft 86. Wilhelm Ernst & Sohn. Berlin. Germany.

Sharples, S. 1984. Full-scale Measurements of Convective Energy Losses from Exterior Building Surfaces. *Building and Environment.* Vol.19, No.1. pp.31-39.

Sneyers, R.; Meert, E.; Soubrier, D. and Van Ackere, G. 1979. Intensite de la pluie battante et pression du vent sur les facades - Calculs basés sur les mesures de la pluie et du vent à l'air libre. *C.S.T.C. - Revue.* No.2. June 1979.

Wallentén, Petter. 1998. Heat flows in a Full Scale Room Exposed to Natural Climate. Report TABK--98/3051. Department of Building Science. Lund Institute of Technology. Lund University. Sweden.

WINDOW. 1994. WINDOW 4.1 Program description. Arasteh, D.K; Finlayson, E.U.and Huizenga, C. University of California. USA.

WMO. 1983. Guide to Meteorological Instruments and Methods of Observation. Fifth edition. WMO - No. 8. World Meteorological Organization. Geneva. Switzerland.

Yazdanian, M. and Klems, J.H. 1994. Measurement of the exterior convective film coefficient for windows in low-rise buildings. Paper No. NO-94-14-4. ASHRAE Transactions 1994. Vol.100. Part I. pp.1087-1096. USA.

Zürcher, Ch.; Finger, G.; Kneubühl, F.K.; Thiébaud, F. and Vetsch, F. 1982. The influence of thermal and solar radiation on the energy consumption of buildings. Infrared Phys. Vol. 22. pp. 277-291. UK.

Window Convection: System Error Estimation

Data selection criteria

The method is depending closely on the temperature differences and the precision of the long-wave measurement. In order to base the system error estimation on realistic data, selection criteria has been defined to eliminate the most dubious cases. Nights with $\Delta T_a < 1$ K and/or $q_{conv} < 0$ W/m²K for $\Delta T_a > 0$ K have been neglected in the system error analysis. The latter are apparently erroneous data. As the following system accuracy estimation will show, these erroneous results may be caused by the combination of limited temperature differences and limitations of long-wave radiation measurement accuracy. For the purpose of evaluating the overall system accuracy, under the specific circumstances, average values have been generated for the data in compliance with these criteria.

Average values

Ambient air temperature	t_a	11	[°C]
External surface temperature	t_s	14	[°C]
Internal surface temperature	$t_{s,i}$	19	[°C]
Temperature difference, glazing	$\Delta T_g = t_{s,i} - t_s$	5	[K]
Temperature difference, surface - ambient air	$\Delta T_a = t_s - t_a$	3	[K]
Glazing heat flux	q_g	28	[W/m²]
Incident long-wave radiance	L	356	[W/m²]
Net longwave radiance/ε	$L - \sigma T_s^4$	-27	[W/m²]
Convective heat flux	q_{conv}	6	[W/m²]
Convective film coefficient	h_c	2.5	[W/m²K]

The convective film coefficient is determined on the basis of an array of component quantities. In the following, these quantities are commented in relation to precision aspects.

Pyrgeometer

The instrument is described in detail in Chapter 5. The pyrgeometer output is a current, V. K is a calibration constant. V/K expresses the net long-wave radiation balance. Measured values: Average: $(V/K)_{average}$ = -27 W/m². Maximum: $(V/K)_{max}$ = -63 W/m². During daytime, solar irradiation gives rise to a window heating offset and reduced precision. During the present measurements, no window heating offset occurs since only night-time data are studied. The manufacturer states an accuracy of ±10% on the quantity V/K. Neglecting window heating offset, the maximum error is estimated to be $\delta L \approx \pm 6$ W/m². Thus, the estimated relative uncertainty is:

$$\frac{\delta L}{L} = \frac{6}{356} \approx 0.02$$

Emissivity

From the literature ε is found to be between 0.84 [Window, 1994] and 0.86 [Zürcher et al., 1982]. These references obviously consider the material properties of clean glazing, whereas the specific pane may be not completely clean. Moreover, the temperature sensors are fixed to the glazing using tape with slightly differing characteristics, compared to the glass. The error is estimated to be in the order of 0.02, giving a relative uncertainty of

$$\frac{\delta\varepsilon}{\varepsilon} = \frac{0.02}{0.84} \approx 0.02$$

Thermal resistance, double pane centre part

The thermal resistance of the centre part of the glazing is calculated theoretically, employing the programme 'WINDOW 4.1'. The average temperatures are used as environmental boundaries, representing the relevant temperature interval. The thermal resistance is found to be $R_c = 0.18$ m²K/W. The absolute uncertainty is estimated to be in the order of 0.01 m²K/W. Hence, the relative uncertainty is estimated as

$$\frac{\delta R_c}{R_c} = \frac{0.01}{0.18} \approx 0.05$$

Temperature difference, thermopile measurement

The temperature difference across the glazing is measured by means of a thin copper-constantan (Cu/Cu-Ni) thermopile with an accuracy better than ±0.1 K (at approximately 20°C). The thin wire thermocouple and thermopile were calibrated against a precision temperature meter[1], and were found to have an accuracy of 0.1 K. The calibration was performed in air, in connection with the set-up. The type TT thermocouple used for ambient air temperature measurements were found to have an accuracy of 0.2 K. The relative uncertainty is calculated, using the average value of the temperature difference $\Delta T_{g,\,average} = 5$ K.

$$\frac{\delta(\Delta T_g)}{\Delta T_g} = \frac{0.1}{5} = 0.02$$

Temperature measurement, thermocouple

Interior surface temperature and exterior ambient air temperature are measured employing copper-constantan thermocouples. The accuracy is determined by calibration with a precision thermometer in the relevant temperature interval (20°C). Physical calibration has been chosen since the overall accuracy depends on data-logger and conversion expressions. The calibration was carried out as described above. The thermocouple was found to have an accuracy better than ±0.2 K (at approximately 20°C). Relative uncertainties:

$$\frac{\delta T}{T} = \frac{0.2}{283} \approx 0.0007$$

$$\frac{\delta t_a}{t_a} = \frac{0.2}{11} \approx 0.02$$

[1] S 1220 Series High Precision Digital Temperature Meter. Systemteknik AB. Sweden.

$$\frac{\delta t_{s,i}}{t_{s,i}} = \frac{0.2}{19} \approx 0.01$$

Note that the ambient air temperature is recorded at the reference mast placed above the roof of the building. An arrangement encompassing a thermopile in the immediate vicinity of the window, yielding the temperature difference between exterior glazing temperature and ambient air temperature, would have been easily established. However, in this series only the standard reference air temperature has been recorded.

Combined errors, component quantities

The absolute uncertainty of a sum, a + b + c, is given by the root-sum square (rss) formula

$$\delta(a+b+c) = \sqrt{\delta(a)^2 + \delta(b)^2 + \delta(c)^2}$$

The relative uncertainty of a product, a × b × c, is given by

$$\frac{\delta(a \times b \times c)}{a \times b \times c} = \sqrt{\left(\frac{\delta a}{a}\right)^2 + \left(\frac{\delta b}{b}\right)^2 + \left(\frac{\delta c}{c}\right)^2}$$

In case of an exponential product, $C \times a^{\alpha} \times b^{\beta} \times c^{\gamma}$, the relative uncertainty is

$$\frac{\delta\left(C \times a^{\alpha} \times b^{\beta} \times c^{\gamma}\right)}{C \times a^{\alpha} \times b^{\beta} \times c^{\gamma}} = \sqrt{\left(\alpha\frac{\delta a}{a}\right)^2 + \left(\beta\frac{\delta b}{b}\right)^2 + \left(\gamma\frac{\delta c}{c}\right)^2}$$

[Rasmussen, 1956; Doebelin, 1990]

When determining the uncertainty of a quantity based on sums of products, first the absolute, hence the relative, uncertainty of the component products are determined. Absolute uncertainties can be estimated from knowledge of measurement precision and typical values of the quantities.

The convective film coefficient is determined experimentally by use of the equation

$$h_c = \frac{1}{\Delta T_a}\left(\frac{\Delta T_g}{R_c} + \varepsilon\left(L - \sigma T_s^4\right)\right)$$

The overall system uncertainty is given by the component uncertainties as calculated in the following.

Glazing heat flux, q_g

The glazing heat flux is expressed by the thermal resistance of the glazing and the temperature difference across the glazing.

$$q_g = \frac{\Delta T_g}{R_c}$$

Hence, applying the *rss formula*:

$$\frac{\delta q_g}{q_g} = \sqrt{\left(\frac{\delta(\Delta T_g)}{\Delta T_g}\right)^2 + \left(\frac{\delta R_c}{R_c}\right)^2} = \sqrt{0.02^2 + 0.05^2} \approx 0.05$$

$$\delta q_g \approx \frac{\delta q_g}{q_g} \times q_{g,average} = 0.05 \times 28 \approx 1 \text{ W/m}^2$$

The remaining quantities are treated analogously.

External surface temperature, t_s

$$t_s = t_{s,i} + \Delta T_g$$

Hence

$$\delta t_s = \delta T_s = \sqrt{\delta t_{s,i}^2 + \delta(\Delta T_g)^2} = \sqrt{0.2^2 + 0.1^2} \approx 0.2 \text{ K}$$

thus

$$\frac{\delta t_s}{t_s} \approx \frac{\delta t_s}{t_{s,average}} = \frac{0.2}{14} \approx 0.01$$

$$\frac{\delta T_s}{T_s} \approx \frac{\delta T_s}{t_{s,average} + 273} = \frac{0.2}{14 + 273} \approx 0.0007$$

Exterior temperature difference, ΔT_a

$$\Delta T_a = t_s - t_a$$

Hence

$$\delta(\Delta T_a) = \sqrt{\delta t_s^2 + \delta t_a^2} = \sqrt{0.2^2 + 0.2^2} \approx 0.3\text{K}$$

thus

$$\frac{\delta(\Delta T_a)}{\Delta T_a} \approx \frac{\delta(\Delta T_a)}{\Delta T_{a,average}} = \frac{0.3}{3} = 0.1$$

This significant relative error is owing to the limited temperature differences occurring in May - June.

Net long-wave radiance, $\varepsilon(L - \sigma T_s^4)$
Exponential rss formula:

$$\frac{\delta(\sigma T_s^4)}{\sigma T_s^4} = 4\frac{\delta T_s}{T_s} = 4 \times 0.0007 \approx 0.003$$

$$\delta(\sigma T_s^4) \approx \frac{\delta(\sigma T_s^4)}{\sigma T_s^4} \times \sigma T_{s,average}^4 = 0.003 \times 0.84 \times 5.67 \times 10^{-8} \times (14+273)^4 \approx 1 \text{ W/m}^2$$

Summation rss formula:

$$\delta(L - \sigma T_s^4) = \sqrt{\delta L^2 + \delta(\sigma T_s^4)^2} = \sqrt{6^2 + 1^2} \approx 6 \text{ W/m}^2$$

$$\frac{\delta(L - \sigma T_s^4)}{L - \sigma T_s^4} \approx \left| \frac{\delta(L - \sigma T_s^4)}{(L - \sigma T_s^4)_{average}} \right| = \left| \frac{6}{-27} \right| \approx 0.22$$

$$\frac{\delta(\varepsilon(L - \sigma T_s^4))}{\varepsilon(L - \sigma T_s^4)} = \sqrt{\left(\frac{\delta\varepsilon}{\varepsilon}\right)^2 + \left(\frac{\delta(L - \sigma T_s^4)}{L - \sigma T_s^4}\right)^2} = \sqrt{0.02^2 + 0.22^2} \approx 0.22$$

Which is a significant relative uncertainty.

$$\delta(\varepsilon(L - \sigma T_s^4)) \approx \frac{\delta(\varepsilon(L - \sigma T_s^4))}{\varepsilon(L - \sigma T_s^4)} \times \varepsilon\left|(L - \sigma T_s^4)_{average}\right| = 0.22 \times 0.84 \times 27 \approx 5 \text{ W/m}^2$$

Convective heat flux, $q_{conv} = q_g + \varepsilon(L - \sigma T_s^4)$
Now, the uncertainty of the full energy balance can be calculated.

$$\delta q_{conv} = \delta(q_g + \varepsilon(L - \sigma T_s^4)) = \sqrt{\left(\frac{\delta q_g}{q_g}\right)^2 + \left(\frac{\delta(\varepsilon(L - \sigma T_s^4))}{\varepsilon(L - \sigma T_s^4)}\right)^2} = \sqrt{1^2 + 5^2} \approx 5 \text{ W/m}^2$$

The uncertainty is significant compared to the magnitude of the convective heat transfer itself.

With an average heat transfer by convection of 6 W/m², the relative uncertainty is

$$\frac{\delta q_{conv}}{q_{conv}} \approx \frac{\delta q_{conv}}{q_{conv,average}} = \frac{5}{6} \approx 0.8$$

Convective film coefficient, h_c
The last calculation yields the relative uncertainty of the convective film coefficient.

$$h_c = \frac{q_{conv}}{\Delta T_a}$$

The *summation rss formula* yields

$$\frac{\delta h_c}{h_c} = \sqrt{\left(\frac{\delta q_{conv}}{q_{conv}}\right)^2 + \left(\frac{\delta(\Delta T_a)}{\Delta T_a}\right)^2} = \sqrt{0.8^2 + 0.1^2} \approx 0.8$$

The absolute uncertainty is thus

$$\delta h_c \approx \frac{\delta h_c}{h_c} \times h_{c,average} = 0.8 \times 3 \approx 2 \text{ W/m}^2\text{K}$$

A relative uncertainty of 80% is not acceptable, and does not allow for general conclusions regarding the nature of the convective heat transfer. However, the measured quantities do allow for a discussion of the phenomena involved as well as an evaluation of the adopted measurement principle. Regardless of the uncertainty, the experiment does also provide information in terms of the temperature variations and the relative magnitude of the various heat flows.

Full-Scale Experimental Determination of the External Convective Film Coefficient

The objective of this section is to convey some thoughts on a method for measuring the convective film coefficient, full-scale, at the exterior of the building envelope. An elementary case study on window convection heat transfer is presented elsewhere in the present report. In conclusion of the case study, it was found that small convection quantities, in combination with considerable uncertainty of long-wave radiation measurements, do not make up an acceptable basis for fundamental conclusions.

The novel apparatus, as described in the following, have been in contemplation before the window case study, but, unfortunately it has not been possible to carry out the experiment described in the following within the framework of the present project. However, since the phenomena is of importance to building physics in general, and to window technology research in particular, these notes and sketches may hopefully serve as a contribution to subsequent activities.

The problem is complex, and the pitfalls are numerous, when an apparatus is designed to assimilate the characteristics of the building envelope, and yet yield meaningful statements about convection quantities that are essentially limited.

The design is aiming at a flexible, manageable system, facilitating mobile measurement activities. The development is described successively in order to cast light on the many facets of the problem. The outcome is a proposal for a full set-up encompassing both a novel test-plate system and commercially available reference measurement equipment. The main preoccupation is reduction of disturbance of local conditions, in the pursuit of a *Fly-on-the-Wall Principle.*

Background

Typically, the convection at the exterior surface of the building envelope is *mixed*, i.e. both forced and natural convection will occur simultaneously. The extent of turbulence is a result of both wind speed, wind direction and local features in general, whereas natural convection depends on the temperature difference between the proposed surface and the ambient air as well as on the geometry of the surface.

When measuring the convective heat transfer, it is desirable to limit the effect of radiation exchange between surface and surroundings as well as solar irradiation. This is in order to operate with significant and detectable convection quantities, and thus expose the processes more unambiguously. Thus, there exists an inconsistency with the desire to operate with conditions equivalent to the conditions at the surface of a 'real' building envelope.

The following parameters have a direct influence on the magnitude of the convective heat transfer: Surface temperature (in relation to temperature of surroundings and temperature of the ambient air; These are often assumed to be identical); Air velocity across the surface; Surface geometry (vertical extent in particular); Surface roughness (significant to the air flow in the boundary layer).

It would be interesting to base the studies on measurement of surface temperatures on a real building envelope. This is problematic because of the complex hygrothermal processes taking place at the surface; Processes that involve both moisture and material. Moreover, it is not possible to isolate the convection quantities distinctly in such 'real' situations.

A method for measuring the convective heat transfer consists in maintaining an over-temperature on a test-plate. In periods where this over-temperature is established by supplying an electrical effect to the plate, the 'natural' state is changed or disturbed. The thus established over-temperature will, in itself, increase both the natural convection and the long-wave radiosity.

The test-plate temperature depends on the thermal capacity of the material. The thermal capacity of a given test-plate should be compared to the thermal capacity of 'normal' building materials and 'normal' built structures in order to evaluate possible effects.

The effect of radiation exchange can be limited by operation with test-plates having low long-wave emissivity and, at the same time, low solar absorptivity. Once again, the conditions are changed, compared to the 'real' building envelope.

If electrical effect is consequently supplied to maintain an over-temperature, the conditions at the end of the night will not reflect the 'reality'. The set-up will not display the undercooling phenomena occurring owing to night-time long-wave heat loss to the sky. However, it should be noted, that the direction of the convective heat transfer obviously does not influence the magnitude of the convective film coefficient.

Theory

Energy balance for the exterior surface of the building envelope:

$$q_c + \alpha G + \varepsilon L = \varepsilon\sigma T_s^4 + h_c(T_s - T_a) \qquad (1)$$

where	q_c	is the conduction energy flux (from the inside)	[W/m²]
	G	is the solar irradiance	[W/m²]
	L	is the incident long-wave radiance	[W/m²]
	α	is the solar absorptivity	[-]
	ε	is the long-wave emissivity of the surface	[-]
	σ	is the Stefan-Boltzmann constant	[5.67 x 10^{-8} W/m²K⁴]
	h_c	is the convection heat transfer coefficient	[W/m²K]
	T_s	is the temperature of the exterior surface	[K]
	T_a	is the reference temperature of the ambient air	[K]

Note that the thermal capacity of the building envelope has been neglected, as the balance is studied for small time steps and thin material layers. A schematic representation of the balance is shown in the figure below. The figure has been adopted from the window convection case study and depicts a double pane glazing. The mechanisms at the external surface are the same for any other type of building envelope component.

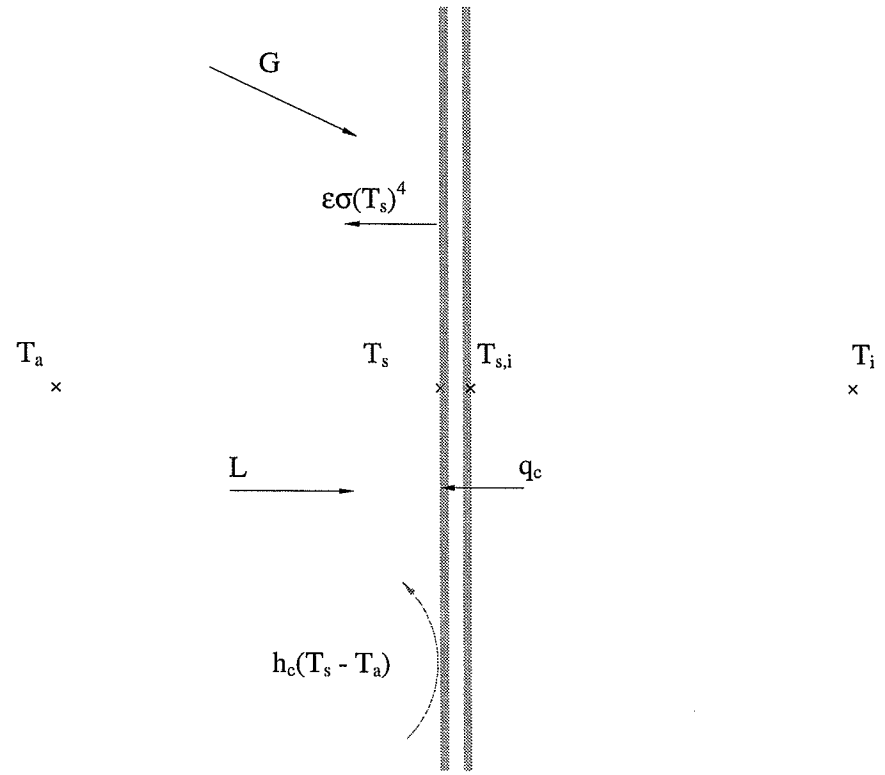

Figure A.1 Energy balance at the exterior surface of a double pane glazing. Thermal capacity of the glazing is neglected.

Comments on the design of a measurement set-up:

ε Should be minimized in order to limit the significance of radiation exchange - not least the night-time long-wave radiosity - and furthermore to limit over-temperatures in relation to the surroundings owing to solar irradiation.

G Can be eliminated by nocturnal measurements. Shielding can eliminate direct radiation. Measured with a pyranometer.

L Less significant during daytime, when solar irradiation is predominant. Important during night-time, when undercooling is taking place. Measured with a pyrgeometer.

q_c Can be measured in terms of supplied electrical effect and temperature difference across a reference material on the inside.

A method for measuring the film coefficient is based on application of Equation 1. By employing two similar elements/test-plates with differing over-temperature $\Delta T_a = T_s - T_a$, the film coefficient is determined experimentally [Sharples, 1984].

If the elements/test-plates are nominated A and B, the following equations are obtained analogously to Equation 1.

$$q_{cA} + \alpha_A G + \varepsilon_A L = \varepsilon_A \sigma T_{sA}^4 + h_{cA}(T_{sA} - T_a) \quad (2)$$

$$q_{cB} + \alpha_B G + \varepsilon_B L = \varepsilon_B \sigma T_{sB}^4 + h_{cB}(T_{sB} - T_a) \quad (3)$$

Conditions $T_{sA} \sim T_{sB}$ yield:

$$h_{cA} = h_{cB} = h_c$$

Clearly, if test-plates A and B are similar, i.e. made from the same materials, they will have the same radiation properties:

$$\varepsilon_A = \varepsilon_B = \varepsilon$$

and

$$\alpha_A = \alpha_B = \alpha$$

Subtraction of equations 2 and 3 yields

$$h = \frac{q_{cA} - q_{cB} - \varepsilon\sigma(T_{sA}^4 - T_{sB}^4)}{T_{sA} - T_{sB}} \quad (4)$$

This expression can cause great errors, if the difference between T_{sA} and T_{sB} is too small. Ito et al. [1972] state the following criteria:

$$0.7 < \frac{T_{sA} - T_a}{T_{sB} - T_a} < 0.9 \quad (5)$$

The convective film coefficient can thus be determined experimentally by measurement of two temperatures and the supplied effect for each of the two test-plates together with the ambient air temperature.

Set-up

Two (or more) test-plates are mount on/in a wall. The convective film coefficient, h_c, is determined experimentally, by supplying different levels of electrical effect to the plates and record the thus supplied effect, surface temperatures and the ambient temperature plus the conduction heat transfer towards the building envelope. This principle gives rise to the following comments:

Night-time
No solar irradiation - The long-wave radiation exchange becomes significant. The surface temperature may be lower than the temperature of the ambient air. Night-time undercooling may reverse the convective heat transfer.

Daytime
Solar irradiation is reducing the significance of the long-wave radiation exchange. The surface temperature is higher than the temperature of the ambient air.

Problems
- A set up based on test-plates with over-temperatures will not reflect situations with reverse convective heat transfer, when the plates are cooling in the course of the night.
- Solar irradiation may give rise to natural convection owing to high surface temperatures.

Unheated plates
Operation with unheated test-plates is an option; This would make radiation measurements necessary, and test-plates with different radiation properties should be employed in order to evaluate the influence. Only materials with well-known or measurable radiation properties can be applied. In this context, it is relevant to evaluate the accuracy of such radiation properties and radiation measurements. Due to the absence of heating, periods with minimal temperature differences will prevail, leading to a pronounced risk of errors of similar order of magnitude as the convection heat transfer itself. Moreover, heating of the test-plates has a spin-off in terms of preventing condensation; Unheated plates may experience condensation during night-time undercooling, leading to erroneous or, at least, distorted results.

Parameter identification
The parameters are divided into three levels pertaining to the physical lay out of the problem.

Climate (Reference/meteorological)
- Ambient air temperature
- Wind speed
- Wind direction
- Long-wave irradiation
- Solar irradiation

Microclimate
- Surface air velocity
- Surface temperature
- Air temperature near the surface

Material properties
- Long-wave emissivity
- Solar absorptivity
- Thermal capacity
- Roughness

Note that the emissivity can be measured, but will vary owing to deposits of water and pollutants et cetera.

Wind measurements
In the literature, the reference wind speed is first correlated with the surface air velocity at the building, then the surface air velocity is correlated with the convective heat transfer coefficient [e.g. Sharples, 1984]. Such studies will suffer from underdetermination, but may serve as a basis for evaluation of existing calculation methods. The aim is usually rough guidelines for the applications.

Test-plate design notes
The principle of the test-plate is shown in the following figures.

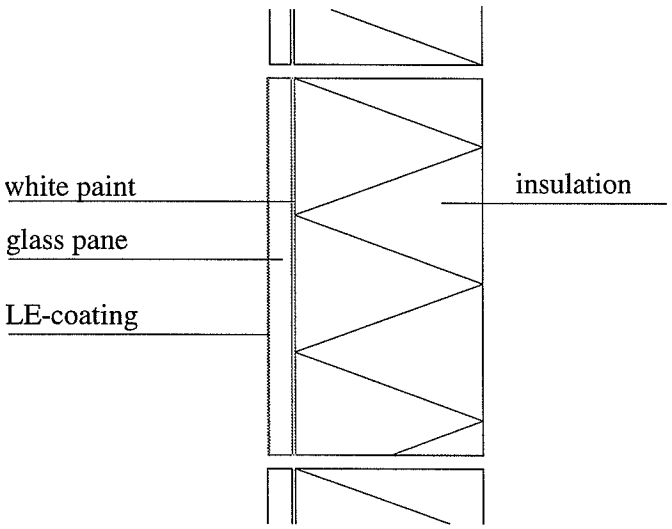

Figure A.2 Sketched test-plate principle. Glass pane.

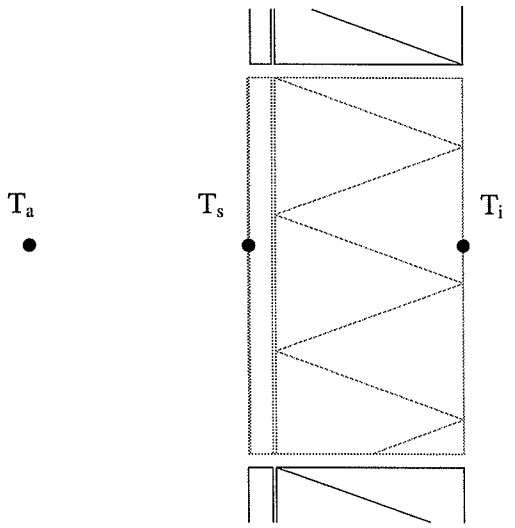

Figure A.3 Test-plate principle. Schematic of the measured temperatures.

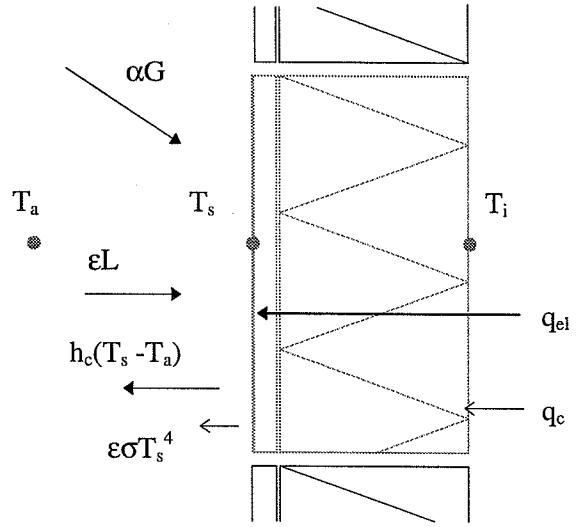

Figure A.4 Test-plate principle. Schematic of the energy balance. Thermal capacity neglected.

Version I.

- The test-plate consists of one layer of glass painted white on the back and with a hard low-emissivity (LE) coating on the outside. A layer of insulating material is placed behind the glass.
- The White paint reduces the effect of solar irradiation.
- The LE-coating reduces the effect of long-wave radiation.
- The insulation reduces the conduction heat loss, and provide a thermal resistance reference.
- The thermal capacity and the solar absorptivity of the glass should be taken into account.
- The surrounding plate/casing should have properties comparable to the properties of the glass.
- Relatively small over-temperatures should be maintained. The temperatures thus remain comparable to the temperature of the building envelope surface, but still condensation is avoided.

Version II.

The first sketches were based on relatively large[1] test-plates (e.g. 0.5 m × 0.5 m, or 1 m × 1 m) in an attempt to limit edge-effects, and in order to operate with dimensions, comparable to the dimensions of the building envelope.

The first design proposal consisted of such 6 test-plates, 4 made of glass and 2 made of aluminium (2 LE-coated glass plates supplied with different effects; 2 unheated glass plates, with and without LE-coating; 2 aluminium plates, painted black and white respectively). Such a set-up would cover a large area on the proposed surface - Incidentally, cf. one of the reasons for the design. Owing to the large area thus covered, it would not be possible to obtain similar flow conditions for the six plates. This would imply that, in any case, the air flow should be recorded in the immediate vicinity of each of the six plates. A serious problem, apart from the obvious financial aspect, is that comparison between the plates would consequently be dubious - or at least problematic.

[1] In this context, measures are generally compared to dimensions of the building envelope.

"Fly-on-the-Wall approach"
Another approach to the problem is based on a wish for 1) The set-up should influence the local conditions to the least possible extent, and 2) The proposed test-plates should be placed within a relatively small area with uniform flow conditions.

Test-plates of LE-coated glass can be supplied with an electrical effect through the LE-coating. The influence of radiation effects is limited by painting the plate white on the back, and by having the LE-coating on the outside. Nevertheless, it is cumbersome to compensate for the actual absorption, as it is depending on numerous parameters.

Stainless steel plates
Subsequently, as an alternative, stainless steel is proposed as the test-plate material. Stainless steel is weather resistant, which is a basic criterion. The dimensions are reduced to 0.1 m × 0.1 m. To compensate for edge-effects, the test-plates are supplied with guard-rings. Four such plates can be mount against a thin slice of insulating material and make up a total measurement area of approximately 0.5 m × 0.5 m, allowing for virtually uniform flow conditions. The insulation is phased off against the wall to minimize disturbance of the local conditions. Sketches of the design are shown in the figures below.

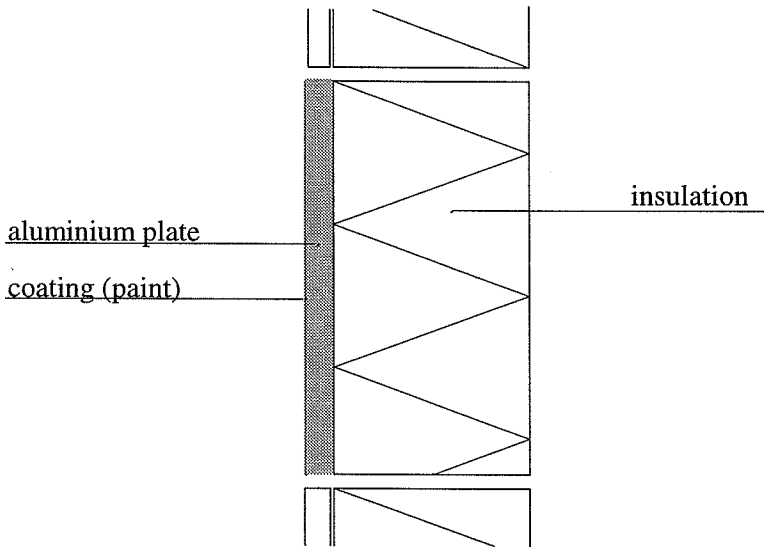

Figure A.5 Sketched test-plate principle. Painted aluminium plate instead of glass pane.

Figure A.6 Sketched test-plate principle. Elevation and cross-section of the four-plate set-up.

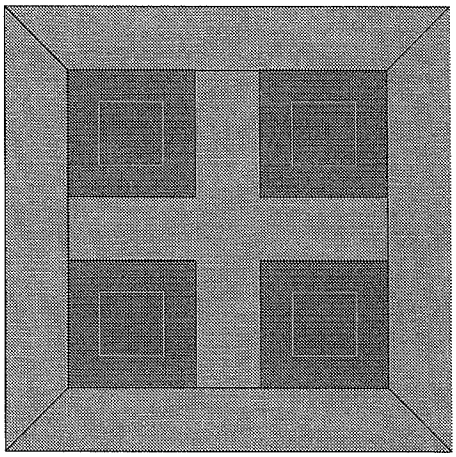

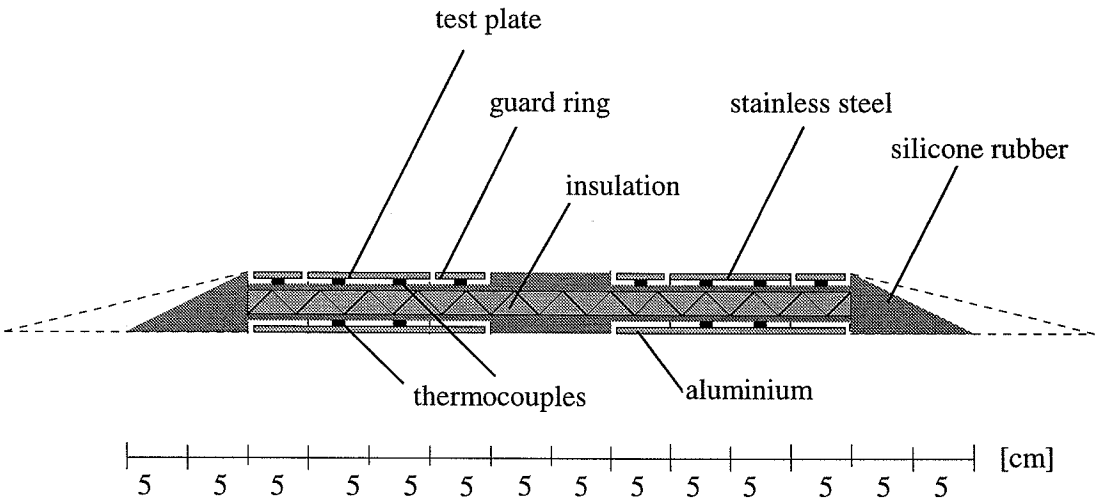

Figure A.7 Sketched principle of apparatus for measurement of convective heat transfer. Vertical cross-section. Insulation protected by cast silicone rubber.

Clearly, the system can be mount in various ways. Below, one proposal is shown. A steel frame will provide a stiff and more solid system.

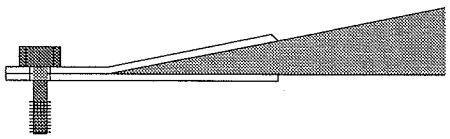

Figure A.8 Sketched principle of proposal for wall-mount steel frame. Vertical cross section.

Comments on the specific design

- Temperatures on the back of the test-plates are measured on aluminium plates to obtain better definition. As the four areas should be kept isolated from each other, four separate aluminium plates should be used.
- The set-up should be sealed to be weather resistant. Water run-off may occur, but measurements will not be valid during rain. Precautions are thus primarily intended to protect the equipment.
- An aspect of weatherproofing pertains to the thermal properties of the reference insulation material. The material should either be kept dry or be insensitive to changes in relative humidity or wetting. Two models have been considered 1) Insensitive material: Foamglass is an option. The problem is that it is fragile, thus making operations difficult. Another option is a more solid material such as acrylic, but it is found to be ineffective in terms of thermal resistance. 2) A polyurethane foam, cast in a silicone rubber casing. This would make up a solid, manageable unit; An advantage if the set-up is expected to be transferred, and mount in various locations. Another, less elegant, solution is to coat the full set-up after assembly.
- After mounting the test-plates and guard rings onto the insulation plate, edges are sealed with silicone.
- A version could consist of 4 stainless steel plates. Three plates are polished and one is painted black. Two of the polished plates are heated to different over-temperatures compared to the temperature of the surroundings, and the third is unheated as a reference. The black plate is heated and will reach higher temperatures when exposed to solar irradiation. When constructing the set-up, the unheated plate is prepared for heating to accommodate possible future modifications.
- A set-up with glass plates would be relevant to studies of condensation risk aspects. A version could consist of 2 heated LE-coated plates, 1 unheated LE-coated plate and 1 unheated plate without LE-coating.
- The steel plates are wound with wires allowing both temperature measurement and effect supply.
- A system that can be dismantled would be preferable, but since cold bridges should be avoided, it is necessary to glue the components together.
- The thickness of the steel plates is not important to the mechanical stability of the system, since the plates are fastened to the insulation material. Thickness can be chosen based on demands to the ability to transfer the necessary effect.
- A thickness of approximately 1 mm is proposed for both aluminium and steel plates.
- The temperature of the guard-ring is governed by the temperature of the matching test-plate. The temperature of the (active) test-plate is governed relative to the temperature of the

surroundings. The system can be made simple by employing a system developed for the thermal mannequins at the institute. The guard ring and the test-plate can possibly be made as one integral steel plate. However, this option should be subject to laboratory testing.

- Over-temperatures of 8 K and 10 K are proposed.
- An important aspect of the system is the ability to record the supplied effect. This imposes demands upon the data acquisition system. Two alternative solutions have been formulated. One is to employ a commercially available power supply, maybe even comprising a temperature control system. The other is to employ micro-controllers and develop the necessary software. The ability to operate with exact currents and record the intervals may offer greater accuracy.
- For comparison, the temperature of the wall is recorded simultaneously.
- Air velocity, ambient air temperature, solar irradiation and long-wave irradiation are measured in the immediate vicinity of the test-plate.
- Air velocity is measured, preferably by means of an ultra-sonic anemometer.
- Ambient air temperature is measured by means of both a thermocouple and thermopiles from the test-plates.
- Solar irradiation is measured by means of a pyranometer mount next to the test-plates.
- Long-wave irradiation is measured by means of a pyrgeometer mount next to the test-plates.

Literature

Selected studies on convective heat transfer from buildings:

[1972]	Ito et al.	*Full-scale measurements.*
[1977]	Nicol	*Full-scale measurements. Window.*
[1977]	Cole and Sturrock	*Review paper.*
[1984]	Sharples	*Full-scale measurements.*
[1988]	Furler	*Wind tunnel measurements. Comparison with literature.*
[1994]	Dascalaki et al.	*Review. Heat transfer inside buildings. Pascool-programme. Heat transfer form building elements to the indoor air.*
[1994]	Yazdanian and Klems	*Full-scale measurements. Low-rise buildings. Comparison with ASHRAE standard and literature.*
[1995]	Quintela and Viegas	*Wind tunnel measurements. Comparison with literature.*
[1996]	Jayamaha et al.	*Full-scale measurements.*
[1998]	Wallentén	*Full-scale measurements. Window. Indoor.*

Dew Point Temperature

Determination of the ambient dew point temperature on the basis of ambient air temperature and relative humidity. Formulae adopted from Kjerulf-Jensen in [Hansen et al., 1992].

Partial water vapour pressure for saturated air at dry-bulb temperature T_a (accuracy ± 0.15%):

$$p_{v,sat} = \exp\left[23.5771 - \frac{4042.9}{T_a - 37.58}\right] = \exp\left[23.5771 - \frac{4042.9}{t_a + 235.57}\right]$$

Where	$p_{v,sat}$	is the partial water vapour pressure, saturated air	[Pa]
	T_a	is the ambient air temperature	[K]
	t_a	is the ambient air temperature	[°C]

Actual partial water vapour pressure of the ambient air, p_v:

$$p_v = \varphi p_{v,sat}$$

Where	p_v	is the partial water vapour pressure	[Pa]
	φ	is the ambient relative humidity	[-]

Dew point temperature of the ambient air with water vapour pressure p_v (accuracy ± 0.02 K):

$$T_{dp} = 37.58 - \frac{4042.9}{\ln(p_v) - 23.5771}$$

or

$$t_{dp} = \frac{4042.9}{23.5771 - \ln(p_v)} - 235.57$$

Where	T_{dp}	is the ambient dew point temperature	[K]
	t_{dp}	is the ambient dew point temperature	[°C]
	p_v	is the partial water vapour pressure	[Pa]

Combining the above equations yields the following expression:

$$t_{dp} = \frac{4042.9}{23.5771 - \ln\left(\frac{RH}{100} \cdot \exp\left[23.5771 - \frac{4042.9}{t_a + 235.57}\right]\right)} - 235.57$$

Where	t_{dp}	is the ambient dew point temperature	[°C]
	t_a	is the ambient air temperature	[°C]
	RH	is the ambient relative humidity	[%]